SEPTEMBER 2018 Ph.D. in Civil Engineering ALAA A. MOHAMMEDAMEEN

UNIVERSITY OF GAZİANTEP
GRADUATE SCHOOL OF
NATURAL & APPLIED SCIENCES

MECHANICAL BEHAVIOR AND DURABILITY OF CONFINED AND UNCONFINED ENGINEERED CEMENTITIOUS COMPOSITE EXPOSED TO CHEMICAL ATTACK

Ph.D. THESIS

IN

CIVIL ENGINEERING

BY

ALAA ABDULHAMEED MOHAMMEDAMEEN

SEPTEMBER 2018

Mechanical Behavior and Durability of Confined and Unconfined Engineered Cementitious Composite Exposed to Chemical Attack

Ph.D. Thesis

in

Civil Engineering

University of Gaziantep

Supervisor
Prof. Dr. Abdulkadir ÇEVİK
Co. Supervisor
Assist. Prof. Dr. Mehmet Eren GÜLŞAN

by

Alaa Abdulhameed MOHAMMEDAMEEN

September 2018

REPUBLIC OF TURKEY
UNIVERSITY OF GAZİANTEP
GRADUATE SCHOOL OF NATURAL & APPLIED SCIENCES
CIVIL ENGINEERING DEPARTMENT

Name of the thesis: Mechanical Behavior and Durability of Confined and Unconfined Engineered Cementitious Composite Exposed to Chemical Attack

Name of the student: Alaa Abdulhameed MOHAMMEDAMEEN

Exam date: September 28, 2018

Approval of the Graduate School of Natural and Applied Sciences.

Prof. Dr. A. Necmeddin YAZICI
Director

I certify that this thesis satisfies all the requirements as a thesis for the degree of Doctor of Philosophy.

Prof. Dr. Hanifi ÇANAKCI
Head of Department

This is to certify that we have read this thesis and that in our opinion it is fully adequate, in scope and quality, as a thesis for the degree of Doctor of Philosophy.

Assist. Prof. Dr. Mehmet Eren GÜLŞAN
Co. Supervisor

Prof. Dr. Abdulkadir ÇEVİK
Supervisor

Examining Committee Members:	Signature
Prof. Dr. Abdulkadir ÇEVİK	....
Assoc. Prof. Dr. Nildem TAYŞİ	....
Assist. Prof. Dr. M. Tolga GÖĞÜŞ	....
Assist. Prof. Dr. Ahmet Emin KURTOĞLU	....
Assist. Prof. Dr. Anıl NİŞ	....

I hereby declare that all information in this document has been obtained and presented in accordance with academic rules and ethical conduct. I also declare that, as required by these rules and conduct, I have fully cited and referenced all material and results that are not original to this work.

Alaa A. MOHAMMEDAMEEN

ABSTRACT

MECHANICAL BEHAVIOR AND DURABILITY OF CONFINED AND UNCONFINED ENGINEERED CEMENTITIOUS COMPOSITE EXPOSED TO CHEMICAL ATTACK

MOHAMMEDAMEEN, Alaa
Ph.D. Thesis in Civil Engineering
Supervisor: Prof. Dr. Abdulkadir ÇEVİK
Co-Supervisor: Assist. Prof. Dr. Mehmet Eren GÜLŞAN
Sebtember 2018
153 pages

In this thesis, the mechanical performance and the durability of Engineered Cementitious Composites (ECC) specimens under chemical attacks were investigated. Static and cyclic loading tests were carried out for confined and unconfined ECC specimens in order to research the performance after chemical attack. Carbon fiber reinforced polymer (CFRP) and basalt fiber reinforced polymer (BFRP) fabrics were used to achieve the confinement of the specimens. In addition, the use of CFRP/BFRP fabrics as a rehabilitation technique was also studied for the specimens exposed to the chemical environments. Unconfined ECC specimens were also produced as a reference specimens and all specimens were continuously immersed in chemical solutions. The mechanical performance and the durability of specimens were evaluated by means of the visual inspection, weight change, static and cyclic loading tests, failure mode and microscale analysis by scanning electron microscopy (SEM). Results indicated that ECC specimens produced with low lime fly ash (LCFA) showed superior performance than the specimens produced with high lime fly ash (HCFA) in the chemical environments. In addition, confinement of ECC specimens with BFRP/CFRP fabrics significantly improved compressive strength, ductility, and durability of the specimens. Both fiber reinforced polymer (FRP) can be used as a rehabilitation material in the chemical environment.

Keywords: Engineering Cementitious Composite (ECC); Carbon Fiber; Basalt Fiber, Polyvinyl Alcohol Fiber, Chemical Attacks.

ÖZET

KİMYASAL ATAĞA MARUZ KALMIŞ SARGILI VE SARGISIZ TASARLANMIŞ ÇİMENTO ESALI KOMPOZİTLERİN MEKANİK DAVRANIŞI VE DURABİLİTESİ

MOHAMMEDAMEEN, Alaa
Doktora Tezi, İnşaat Mühendisliği
Tez Danışmanı: Prof. Dr. Abdulkadir ÇEVİK
Yardımcı Tez Danışmanı: Dr. Öğr. Üyesi Mehmet Eren GÜLŞAN
Eylül 2018
153 sayfa

Bu tezde, tasarlanmış çimento esaslı kompozit numulerinin kimyasal ataklar altındaki mekanik performansları ve durabiliteleri araştırılmıştır. Kimyasal ataktan sonraki performansı araştırabilmek için sargılı ve sargısız çimento esaslı kompozit numuler üzerinde statik ve döngüsel yükleme testleri gerçekleştirilmiştir. Numulerin sargısını yapmak için karbon lif takviyeli ve bazalt lif takviyeli kumaşlar kullanılmıştır. Ayrıca, karbon/bazalt lif takviyeli polimer kumaşların bir rehabilitasyon tekniği olarak kimyasal çevrelere maruz kalmış çimento esaslı kompozit numunelerinde kullanımı çalışılmıştır. Sargısız çimento esaslı kompozit numuleri aynı zamanda referans numuleri olarak üretilmişlerdir ve bütün numuneler sürekli olarak kimyasal çözeltilerde bekletilmişlerdir. Numunelerin mekanik performansları ve durabiliteleri gözlemleme, ağırlık değişimi, statik ve döngüsel yükleme testleri, göçme türleri ve mikro ölçekli analiz vasıtaları ile değerlendirilmiştir. Sonuçlar düşük kireçli uçucu külden üretilmiş çimento esaslı kompozit numunelerinin yüksek kireçli uçucu külden üretilenlerine göre kimyasal çevrelerde daha iyi performans sergilediğini göstermiştir. Ayrıca, çimento esaslı kompozitlerin karbon/bazalt lif takviyeli kumaşlarda sargılanması, bu numunelerin basınç mukavemetlerini, sünekliklerini ve durabilitelerini önemli derecede arttırmıştır. Her iki lif takviyeli polimer kumaş türü de kimyasal çevrelerde rehabilitasyon malzemesi olarak kullanılabilir.

Anahtar Kelimeler: Tasarlanmış çimento esaslı kompozir; Karbon Lif; Bazalt Lif; Polivinil Alkol Elyafı; Kimyasal Ataklar.

To my Mother and Father

ACKNOWLEDGMENTS

Firstly, I would like to express my sincere gratitude to my advisor **Prof. Dr. Abdulkadir ÇEVİK** for the continuous support of my PhD study and related research, for his patience, motivation, and immense knowledge. His guidance helped me in all the time of research and writing of this thesis. I am thankful to God for blessing me with a teacher like you.

I would like also to thank my Co-Supervisor **Assist. Prof. Dr. Mehmet Eren Gülşan** for his continuous help that facilitate the experimental works, I also thank him as a close friend of mine. Besides my advisors, I would like to thank the rest of my thesis committee, **Assoc. Prof. Dr. Nildem TAYŞİ, Assist. Prof. Dr. M. Tolga GÖĞÜŞ, Assist. Prof. Dr. Ahmet Emin KURTOĞLU** and **Assist. Prof. Dr. Anil NİŞ** for their important comments and suggestions.

My sincere thanks also go to the **Instructors of the civil engineering department** and all my friends whose helped me in all stages of my study.

Sincere thanks to **Kurdistan Ministry of Higher Education and Scientific Research** and **Duhok Polytechnic University** for their support which was the main motivation to complete my study. Thanks to **Gaziantep University** to provide me the opportunity to obtain a doctorate degree.

I am very grateful for my parents, brothers and sister. Their understanding and their love encouraged me to work hard and to continue pursuing a Ph.D. project abroad. Their firm and kind-hearted personality has affected me to be steadfast and never bend to difficulty. They always let me know that they are proud of me, which motivates me to work harder and do my best.

I am greatly indebted to my devoted husband Radhwan ALZEEBAREE, my sweet children Tara ALZEEBAREE, Sidra ALZEEBAREE and Kinan ALZEEBAREE. They form the backbone and origin of my happiness. Their love and support without any complaint or regret has enabled me to complete this Ph.D. project.

Finally, I would like to thank to those who took part in completion of this thesis.

TABLE OF CONTENTS

Page

LIST OF TABLES

Page

LIST OF FIGURES

Page

LIST OF SYMBOLS

ECC	Engineered Cementitious Composite
FRP	Fiber Reinforced Polymer
CFRP	Carbon Fiber Reinforced Polymer
BFRP	Basalt Fiber Reinforced Polymer
SEM	Scanning Electron Microscopy
LCFA	Low Calcium Fly Ash
HCFA	High Calcium Fly Ash
PVA	Polyvinyl Alcohol Fiber
SP	Super-plasticizer
OPC	Ordinary Portland Cement
FA	Fly Ash
AFRP	Aramid Fiber Reinforced Polymer
GFRP	Glass Fiber Reinforced Polymer
HPFRCC	High Performance Fiber Reinforced Cementitious Concrete
NC	Normal Concrete
HRWRA	High Rang Water Reducing Admixture
A/B	Total Aggregate to Binder Ratio
$Ca(OH)_2$	Calcium Hydroxide
GGBFS	Ground Granulated Blast Furnace Slag
SF	Silica Fume
MK	Meta-Kaolin
RHA	Risk Husk Ash
ASTM	American society for testing and materials
C-S-H	Calcium silicate hydrate
KSO_4	Potassium Sulfate
LOI	Loss of ignition
CaO	Calcium Oxide
HVFA	High Volume Fly Ash

$Mg(OH)_2$	Magnesium Hydroxide
C_2S	Di-Calcium-Silicate-Hydrated
C_3S	Tri-Calcium-Silicate-Hydrated
M_4SH_8	Non-Cementitious Product
SH	Silica Hydrated
FeS_2	Oxidation of pyrite
SO_2	sulfur dioxide
NaCl	Sodium Chloride
H_2SO_4	Sulphuric Acid
$MgSO_4$	Magnesium Sulfate
LVDT	Linear Variable Displacement Transducers
W/C	Water to Cement Ratio
SNF	Sulphonated naphthalene formaldehyde
CFRP-ECC	ECC specimen wrapped by CFRP
BFRP-ECC	ECC specimen wrapped by BFRP
HC	High Calcium Fly Ash Specimens
LC	Low Calcium Fly Ash Specimens
U	Unwrapped specimens
CF	Specimens Wrapped by CFRP
BF	Specimens Wrapped by BFRP
Co	Control Specimens
Sw	Specimens exposed to Seawater Attack
Ac	Specimens exposed to Acid Attack
Su	Specimens exposed to Sulfate Attack
W28	Specimens Wrapped at age of 28days
W90	Specimens Wrapped at age of 90days
T28	Specimens Tested at age of 28days
T90	Specimens Tested at age of 90days
GLM-ANOVA	General Linear Model Analysis of Variance
HCFA-ECC	High Calcium Fly Ash ECC specimens
LCFA-ECC	Low Calcium Fly Ash ECC specimens
U-LCFA	Unwrapped Low Calcium Fly Ash Specimens

U-HCFA	Unwrapped High Calcium Fly Ash Specimens
CF-LCFA	Low Calcium Fly Ash Specimens Wrapped by CFRP
BF-LCFA	Low Calcium Fly Ash Specimens Wrapped by BFRP
CF-HCFA	High Calcium Fly Ash Specimens Wrapped by CFRP
BF-HCFA	High Calcium Fly Ash Specimens Wrapped by BFRP

CHAPTER 1
INTRODUCTION

1.1 General

The durability of the structures under various chemical attacks becomes significant especially in urban areas due to increased population, high number of factories and hazardous wastes. Ordinary concrete degradation under chemical attacks is a well-known problem and research continue to prevent the deterioration of concrete under chemical attacks. As well as chemical attacks, structures exposed to axial and shear loads and bending moments, especially in earthquake zones. In such a situation, structures may experience seismic loads after the loss of mechanical strength due to chemical attack and the failure of the structures becomes inevitable.

Today many older buildings are required for strengthening their current civil engineer infrastructure. As a result of deterioration by corrosion or ageing caused by environmental concerns, structures cannot meet the current more severe design purposes, especially in earthquake regions. The high cost of structural rehabilitation and low probability of main seismic occurrences make it hard to validate economically. To minimize the risk of structural collapse, the rehabilitation technique is considered to be the most suitable solutions by improving the critical structural elements. Retrofitting or strengthening of older constructions in order to increase ductility or resist higher design loads has been done with traditional materials like steel jackets and externally bonded steel plates since 1960s (ACI Committee 440, 2002). One of the most important structural parts are the columns which are susceptible of exceptional loads. Columns in older structures, often have inadequate diagonal reinforcement, therefore columns are vulnerable to buckling of the longitudinal reinforcement, which can lead to undesirable early strength degradation. Confinement is requisite to prolong the softening of concrete exposed to ultimate load states and to permit a ductile response of the concrete member. Strengthening of the column members have been developed by a numbers of retrofit techniques for which have led to enhancement in both ductility and axial strength capacity and to avoid buckling of the longitudinal reinforcement. Confinement techniques with old-style materials like reinforced concrete jackets or steel jackets were stated in an earlier study (Priestley *et al.*, 1996). Recently, fiber reinforced polymer (FRP) is a novel technique as external confinement by wrapping FRP sheets around columns (concrete member) to produce an external reinforced jacket. Specifications and international design codes for the strengthening of concrete structures by externally bonded FRP jacket systems have been published (International Code Council-Evaluation Service (ICC-ES), 1997; FBI, 2001; ACI Committee 440, 2002; TR 55., 2004; Bank, 2006). The preference of FRP fabrics for the repair and strengthening aims can be attributed to low thermal conductivity, lightweight, high resistance to corrosion and chemical attacks (Nanni and Bradford, 1995; Hamilton *et al.*, 2009; Halliwell, 2010). This strengthening method is of practical activity for given its rapid performance and low labor costs. In this technique a passive confinement to the concrete core is provided by the sheet and resisted the lateral expansion of the column due to axial compression so that both strength and ductility properties of the concrete member improved (Nanni and Bradford, 1995). The mostly common FRP materials on the constructional in-situ applications are carbon (CFRP), aramid (AFRP) and glass (GFRP) fibers. CFRP is the most commonly used and the more expensive one among them despite the lower costs of AFRP and GFRP since CFRP fibers showed superior mechanical performance than the others (Fardis and Khalili, 1981; Saadatmanesh, Ehsani and Li, 1994; Saatcioglu and Grira, 1999; Pessiki *et al.*, 2001; Matthys *et al.*, 2005; Wu and Wang, 2009; Turgay *et al.*, 2010). Fardis and Khalili (Fardis and Khalili, 1982) were among the first researchers who wrapped the concrete cylinders with FRP materials. They indicated that the cylinder specimens confined with GFRP jacket exhibited strength gain from 1,5 to 5 times than the compressive strength of unconfined specimens depending on the jacket thickness. They developed an analytical model using their results to model the behavior of FRP confined specimens with increasing axial compressions (Fardis and Khalili, 1982). Saadatmanesh et al. (Saadatmanesh and Li, 1994) studied both circular and rectangular cross-sections of reinforced columns and they wrapped the columns with clear spacing of (152-305) mm of FRP straps. The results indicated that the ultimate compressive strength and ductility were increased with an increase in strap thickness. The results also indicated that the ductility was decreased with an increase in the strap spacing. An analytical model for confined concrete was exploited with the same stress versus strain relationships as suggested by Mander *et al* (Mander *et* *al.*1988). Information regarding the use of FRP materials have been provided by a several published Sstudies on the design guidelines (ACI Committee 440, 2002; Concrete Society, 2004). A quite well confinement strength was predicted using a derived analytical models for cylinder specimens. In addition, the distribution of the confining stress is influenced by the corner sharpness of non-circular columns (square and rectangular cross-sections) which decreases the compressive strength of the columns and makes a definite uncertainty in calculating the compressive strength of non-circular members. In addition, basalt fiber (BFRP) is a new fabric material used in civil engineering applications and has revealed to be an efficient material for strengthening purposes of the infrastructure. The basalt fibers are produced through melting process from basalt rocks and no other additives are included in the forming process, which creates benefits in cost. Sim (2005) reported that basalt fibers (BFRP) exhibited good mechanical properties at lower costs and showed good resistance to high temperature and chemical exposure compared to glass fibers (GFRP) (Sim, 2005). The ultimate strain of basalt fiber is higher than that of the other common FRP fabrics and thus basalt FRP fabrics can be used in order to improve strength and ductility of the column members.

Engineered Cementitious Composite (ECC) is one of the most familiar and effective strain-hardening cementitious composite types. ECC enables high level of ductility and the formation of multiple micro-cracks instead of a single macro crack under uniaxial tensile and flexural loadings, which makes ECC significantly more durable under static and cyclic (earthquake) loadings compared to ordinary concrete. The tensile strain capacity of the ECC concrete can be approximately 300-500 times bigger than that of the ordinary concrete. In addition, the crack width remains smaller than 60 μm, which prevents or slows down the deterioration rate due to chemical attacks and improves the service life of the structures (Liu *et al.*, 2017). ECC also provides higher fatigue strength due to the controlled crack propagation of fiber bridging effect (Qiu and Yang, 2017).

The usage of fly ash has started to increase due to its environmental nature. Fly ash can be utilized as an aluminosilicate source (Nazari *et al.*, 2015) and depending on the source, fly ash can be termed as F type (including low calcium) and C type (including more than 20wt.% calcium). Both types of fly ashes are naturally low reactive materials and their use improves the durability of the structures (Nazari and Sanjayan, 2015). In addition, the durability of the structures depends on the environmental effects. The most common environmental attacks for structures are temperature fluctuations, wetting-drying, and wind effects (Reis and Ferreira, 2006). In addition, the sulphuric acid is one of the most hazardous environmental attacks. The acid attacks can arise from different sources, like acid rain, marine environments, or from the soil. Basalt FRP and carbon FRP fabrics showed greater resistance against these environmental attacks (Al-Tamimia, Abed and Al-Rahmani, 2014; Cai and Zhou, 2017; Wu and Li, 2017). However, the effect of chemical attack on FRP composites can emerge by a relocation of fluids or moisture. Researchers showed that the chemical solutions can react with the polymer fabrics and they change the chemical composition of FRP. Therefore, deterioration of interfacial transition zone between fibers and matrix is realized, which results in a loss of mechanical performance. Stress corrosion is another common failure type due to chemical attack, and it is realized when the internal strength of the material is reduced by chemical penetration under sustained internal stress (Kumar and Ray, 2007; Triangle, 2009).

Although there are few studies investigating the chemical attack on ECC specimens, there is limited or lack of study regarding the influence of the chemical attack on ECC specimens wrapped with basalt and carbon FRP fabrics under static and cyclic loading. In addition, the use of FRP materials as a rehabilitation technique in chemical environments is also investigated. SEM analysis was conducted to clarify the influence of the chemical attack on wrapped and unwrapped ECC specimens in micro-scale. The results of the study can be significant for structures subjected to chemical attack and FRP materials can be used to improve the service life of structures.

1.2 Objectives and Aim of this Research

The main objective of this thesis is to improve knowledge on strengthening of the concrete columns by FRP jackets and investigate the influence of various types of fiber sheets as a retrofit material under different chemical environments. The aims of the research are:

1. Investigation and review of the mechanical and durability performance of ECC with different types of fly ash and FRP materials.
2. Research of the ultimate compressive strength and axial strain capacity of axially loaded ECC cylinders confined with different types of fiber jackets.

3. Study of the cyclic loading behavior of the different types of FRP materials on confined ECC under different chemical attack.
4. Examination of the influence of the chemical attacks on confined and unconfined ECC specimens in micro-scale using scanning electron microscopy (SEM) analysis.

1.3 Outline of the Thesis

In this PhD thesis, the whole work is demonstrated via seven chapters;

Chapter 1 Introduction: A general introduction and the significant of the thesis are given.

Chapter 2 Literature Review and Background: A literature review was conducted on the ECC concretes, FRP materials, application of FRP fabrics, mechanical and durability performance of ECC and FRP fabrics.

Chapter 3 Experimental Study: this chapter covers highlights of the experimental test carried out in this study. The properties of the materials used, mixing procedures, the preparation of samples, and testing procedures are mentioned.

Chapter 4 Acid Attack: The experimental results and a detailed discussion of the mechanical and durability performance of FRP confined and unconfined ECC subjected to sulphuric acid attack

Chapter 5 Sulfate Attack: The test results and discussion regarding the mechanical and durability performance of FRP confined and unconfined ECC exposed to magnesium sulfate attack

Chapter 6 Seawater Attack: The experimental results and a detailed discussion of the mechanical and durability performance of FRP confined and unconfined ECC under seawater (sodium chloride) attack

Chapter 7 Conclusions: a key to the main conclusions drawn from the results of the present study are concluded.

CHAPTER 2
LITERATURE REVIEW

This chapter presents the history and recent development of ECC concretes and FRP fabrics, Types of FRP materials and their application, used materials in ECC, fly ash, polyvinyl-alcohol (PVA) fiber and its influence on mechanical properties of ECC concrete. In addition, the durability performance of ECC and FRP materials under chemical attack also investigated as well.

2.1 Introduction

In the last decades, an extensive request has been conducted for alternative strengthening techniques for the improvement in terms of strength and ductility performances of the structure. Nowadays, the most consistent material utilized for the strengthening of the structures are the FRP composites due to ease of installation, less weight, and resistance to corrosion. Researches is still continuing on such materials; however, there is a limited or no study investigating the strength and ductility performance of FRP materials when applied on ECC concretes with different binder materials. This chapter provides a literature background on the performance of different FRP structural members subjected to axial load and chemical attacks, as well as the behavior of engineered cementitious composite and the materials used in the production of ECC concretes for some of the recent investigations.

2.2 Engineered Cementitious Composites (ECC)

2.2.1 Introduction and Mix Design of ECC

Engineered Cementitious Composite (ECC), as a new type of High Performance Fiber Reinforced Cementitious Composite (HPFRCC) materials, is a micromechanically designed ductile fiber reinforced cementitious composite to attain high durability under normal service environments (Li and Kanda, 1998; Li *et al.*, 2001; Li, 2003). The range of the ultimate tensile strain capacity of ECC matrix varies between 3% to 5%, depending on the ECC mixture. This considered the most individual property separating ECC from fiber reinforced (FRC) and ordinary concretes (NC). The strain capacity of ECC concrete is over 300 times that of normal concrete which achieved through the creation of many closely spaced micro-cracks. The ECC concrete exhibited improved post-peak performance and showed strain hardening characteristic. Though the components of ECC concrete may be similar to FRC, the strain hardening characteristic of ECC within micro-cracking is realized via micromechanical tailoring of the matrix components (i.e. cement, aggregate, and fibers) (Li and Kanda, 1998; Lin and Li, 1999; Li *et al.*, 2001; Li, 2003). The strain hardening performance can be obtained using different ECC mix ratios. Fiber properties like aspect ratio, modulus of elasticity, and strength have been tailored in ECC matrix. Table 2.1 presents the standard mix proportions of Engineered Cementitious Composite (ECC) utilizing a polyvinyl-alcohol fiber (PVA).

Table 2.1 Typical mix design of ECC material (Yang *et al.*, 2009)

Cement	Water	Microsilica sand	Fly ash	HRWRA*	Fiber (%)
1.00	0.56	0.8	1.2	0.013	2.00

*HRWRA = High range water reducing admixture; all ingredients proportion by weight except for fiber.

In addition, ECC contains low amounts of short and discontinuous fiber (2% by volume), whereas high fiber fractions were used for the high strength fiber reinforced concretes. Therefore, ECC allows flexibility in construction performance through low amount of fiber volume. To date, ECC concretes have been used for extrusion (Stang, 1999), self-consolidation casting (Kim and Li, 2003), shotcreting (Kim and Li, 2003), and conventional mixing (Lepech *et al.*, 2008).

2.2.2 ECC Mixtures

ECC utilizes similar ingredients with FRC and generally, the used materials are cement, fine aggregate, water, fibers and some common chemical additives to attain desired workability. Discussion of each of these materials has been discussed below.

2.2.2.1 Cement

ECC can be produced utilizing ordinary Portland cement (OPC). ECC contains cement content considerably higher than the ordinary concrete; normally two or three times higher than ordinary concrete (Wang and Li, 2007). Table 2.1 illustrates a typical mixture proportions of PVA-ECC. The reasons of the high cement in ECCs are to obtain higher rheology of the mixes for controlled fiber distribution and also to obtain the desired matrix toughness for strain-hardening behavior.

2.2.2.2 Aggregates

Aggregates usually occupy a significant volume fraction in normal concrete, and hence have significant influences on different parts of material characteristic. In addition, aggregates considered to be a significant economic filler in cement-based materials, and also has an importance role for dimensional stability of cement-based composites. In addition, aggregates reduce the shrinkage of the concrete. However, the incorporation of aggregates with a bigger grain sizes results in clumping and therefore, it becomes difficult to realize a uniform dispersion of fibers as particle size increased. The greater the size and volume of aggregates, the more interaction of fibers and clumping would appear. Therefore, the size and amount of the aggregates can have a substantial effect on the characteristic of composite and aggregates can cause problems with fresh mix workability, fiber distribution, and toughness of matrix. For this reason, typical ECC materials contains fine aggregate (micro-silica sand) with an aggregate to total binder ratio (A/B) of 0.36 to claim acceptable volume stability and stiffness (Li and Wu, 1995). The maximum grain size of micro-silica sand is 250 μm with a mean size of 110 μm. In addition, fine silica sand should be used to achieve the best gradation of components to obtain suitable workability (Fischer and Li, 2002)

2.2.2.3 Fiber

ECC has not require large amounts of fibers as in the case of high strength fiber reinforced concretes. In general, the volume of discontinuous fiber becomes 2% for the purpose of structural applications. The mixing procedure of ECC is similar to ordinary concrete due to the fiber chopped nature and the relatively small volume of fibers. In addition, there are some studies regarding the economic utilization of ECC in structural applications by reducing the amount of fibers (Li, 2003).

2.2.3 Pozzolanic Materials

In order to obtain strain hardening behavior, the fracture toughness of matrix has to be controlled such that before reaching the maximum stress via fiber bridging, multiple cracks could appear. Due to the lack of large aggregate particles in the ECC mixture, a higher cement content used as compared to conventional concrete. In general, ECC typically have cement content around 830 to 1200 kg/m^3 (Lepech *et al.*, 2008) amd due to the high cement content, high heat of hydration occurred during production. Additionally, such amount of cement can be responsible for 3% of global greenhouse gas emissions to the environment (Lepech *et al.*, 2008). The utilization of industrial byproducts as a replacement of cement is one of the crucial approach to reduce the environmental problems. Pozzolanic materials can be partially used instead of ordinary cement in concrete production.

Pozzolan is defined by ACI Committee 116R-94 (ACI Committee 116R, 1994) as "a siliceous and aluminous material or siliceous, which in itself owns low or no cementitious amounts but will, in finely separated process and in the existence of humidity, chemically reacts with calcium hydroxide (CaOH) at normal temperatures to create compounds having cementitious characteristic." The most common pozzolanic materials used are fly ash (FA), condensed silica fume (SF), ground granulated blast furnace slag (GGBFS), volcanic materials, meta-kaolin (MK) and rice husk ash (RHA). These pozzolanic materials can enhance the fresh and hardened state performance of concrete (Hossain, 2003, 2005; Hossain and Lachemi, 2004; Anwar Hossain, 2012; Hossain *et al.,* 2012; Karahan *et al.*, 2012). Although several types of supplementary cementitious materials exist, the focus of this review will be on the fly ash used in this study. A brief overview of the history, properties, production, and utilization of fly ash in concrete is described below.

2.2.3.1 Fly Ash

Fly ash can be considered as the most common mineral admixture utilized for concrete production. It is a by-product of burning pulverized coal of electric power stations. During combustion, most of the carbon and volatile matter is burned off, leaving the coal's mineral impurities (clay, quartz, feldspar, and shale) behind and then fuse together while in suspension. The fused particles are carried away by the exhaust by electrostatic precipitators or bag filters. During this process, the fused material cools down and solidifies to form the spherical fly ash particles. Typical particle size is around 20 microns but it may range from one micron to as large as 100 microns. Surface areas may change from 200 to 700 m^2/kg but typically are between 300 - 500 m^2/kg (Kosmatka *et al.,* 2011). Fly ash consists primarily of silica, aluminum, iron, and calcium in a silicate glass form. Minor constituents can be found in the form of sodium, potassium, magnesium, sulfur, and carbon. American Society for Testing and Materials (ASTM) classified the fly ash in two classes as shown in Table 2.2. Class C is typically manufactured from lignite or sub-bituminous coals and Class F is typically manufactured from bituminous coals (ASTM C618, 2012).

Table 2.2 Specifications for fly ash (ASTM C618, 2012)

Class of Ash	ASTM Specification
Class C	$SiO_2 + Al_2O_3 + Fe_2O_3 > 50\%$
Class F	$SiO_2 + Al_2O_3 + Fe_2O_3 > 70\%$

Utilization of fly ash in the production of ECC can result in improved ductility, micro-cracking behavior, durability properties and sustainability. (Bisaillon *et al.*, 1994; Kuroda *et al.*, 2000; Lepech *et al.*, 2008).

2.2.3.2 Production of fly ash

The term of FA can be defined according to ASTM (ASTM C618, 2012). "The finely separated residue that results from the process of combustion of powdered coal or ground and that is transferred by flue gasses". FA is usually manufactured by the steam generating plants and coal-fired electric. Characteristically, coal is pulverized and blown with air into the boiler's burning chamber where it directly ignites, creating heat and generating a molten mineral remainder. Boiler tubes take heat from the boiler, refrigerating the flue gas and causing the molten mineral remainder to harden and form ash. The lighter fine ash particles term as fly ash, and stay suspended in the flue gas. While coarse ash particles term as bottom ash, fall to the bottom of the combustion chamber as shown in Figure 2.1.

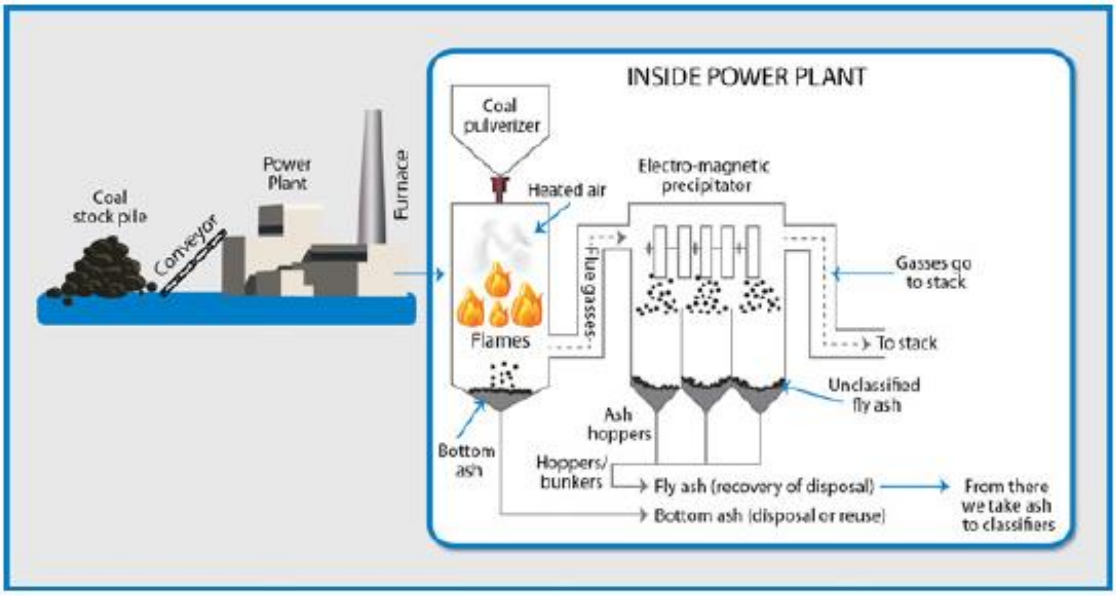

Figure 2.1 The process of manufacturing of fly ash (FA) in a power plant (Sephaku Ash's facility, 2013)

FA particles are naturally spherical, finer than lime OPC, the diameter of particles ranging from 1 μm to 150 μm (Figure 2.2). ASTM 618-12 (ASTM C618, 2012) specified two major classes of FA depending on chemical composition resulting from the kind of coal burned; class C and F. F type FA usually manufactured from bituminous coal or burning anthracite, while C type FA generally obtained from the burning of sub-bituminous coal and lignite (Halstead, 1986).

According to ASTM, the main difference between class F and C is the amount of silica, calcium, alumina, and iron content in the FA. The amount of calcium in class F fly ash is less than 10% while in C type FA the calcium content is higher than 10 %. The influence of high CaO normally leads to increase in the rate of reaction. Moreover, the high amount of calcium caused a rapid reaction and may not be appropriate for applications that needed longer setting time or workability. In addition to chemical composition on FA, the other characteristics of FA are uniformity, fineness, and loss of ignition (LOI) (Deb, 2013).

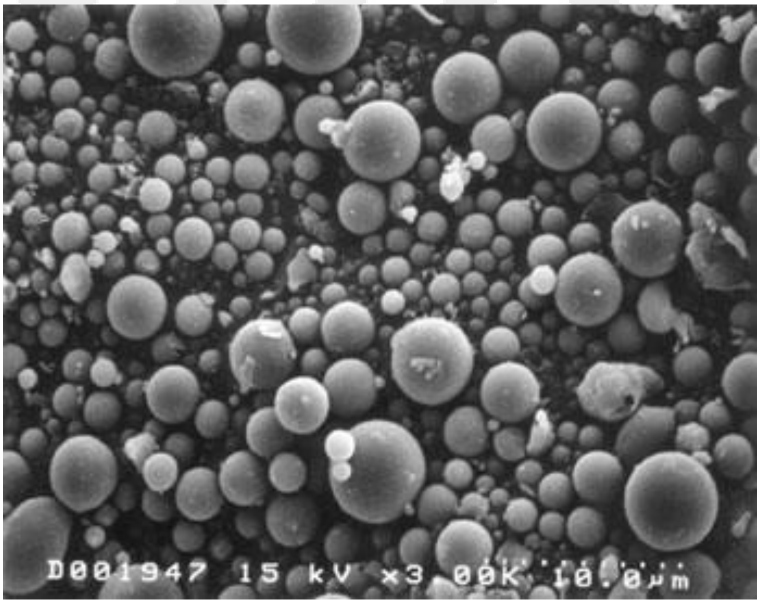

Figure 2.2 Fly ash particles enlargement (Deb, 2013)

2.2.3.3 Use of fly ash in concrete

The spherical shape of FA often supports to develop the workability of the fresh concrete, whereas the small FA particles plays an important role as a filler of voids in the mixture, and make dense and durable concrete. The use of FA can enhance workability, durability, ultimate strength and cohesiveness. In addition, the fine particles in fly ash can reduce bleeding and segregation in concrete.

Use of FA in concrete can be useful to decrease permeability of water and aggressive agents. A significant achievement in the utilization of FA instead of OPC is realized up to 60% with improved strength and durability performance. High volume of FA can be more resource-efficient and durable than the OPC concrete (Mehta, 2004). The HVFA technology has been started to use in structural applications, for example, 50% OPC is replaced with FA in the construction of highways in India

2.3 Confined and Unconfined Concrete

Kent and Park offered a stress-strain equation for both confined and unconfined concrete (Kent and Park, 1971). In their model, they simplified Hognestad's equation (Hognestad, 1951) to more fully define the post-peak stress-strain performance. The ascending branch in this model is characterized by revising the Hognestad 2nd degree parabola by replacing ε_{C0} by 0.002 and 0.85 f_c' by f_c'.

$$f_c = f_c'\left[\frac{2\varepsilon_c}{\varepsilon_{co}} - \left(\frac{\varepsilon_c}{\varepsilon_{co}}\right)^2\right] \quad (1)$$

The post-peak part of the curve was expected to be a straight line whose slope was described mainly as a function of the strength of concrete.

$$f_c = f_c'[1 - Z(\varepsilon_c - \varepsilon_{co})] \quad (2)$$

Where

$$Z = \frac{0.5}{\varepsilon_{50u} - \varepsilon_{co}} \quad (3)$$

Where ε_{50u} refers to the strains matching the stress equal to 50% of the maximum strength of unconfined concrete.

$$\varepsilon_{50u} = \frac{3 + 0.29f_c'}{145f_c' - 1000} \ (f_c' \ in \ MPa)$$
$$\varepsilon_{50u} = \frac{3 + 0.002f_c'}{f_c' - 1000} \ (f_c' \ in \ Psi) \quad (4)$$

Figure 2.3 presented the Kent and Park model.

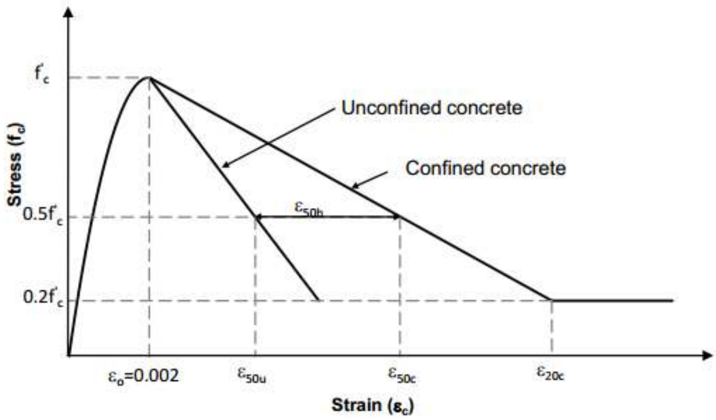

a) The stress-strain model proposed by Kent and Park (1971) for unconfined and confined concrete.

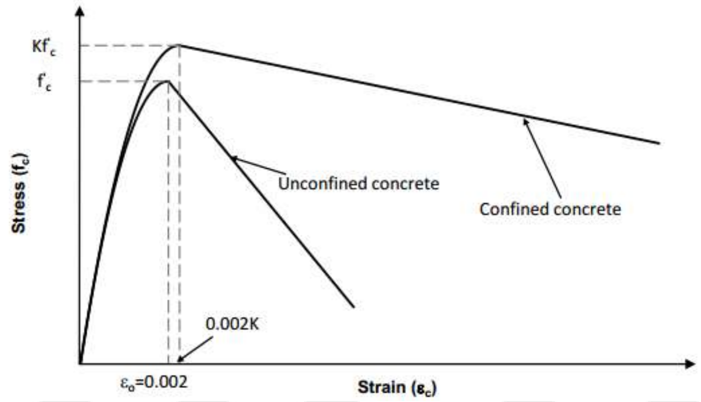

b) The stress-strain behavior of compressed concrete confined by rectangular steel hoops - Improved by Kent and Park (1982).

Figure 2.3 The stress-strain behavior for confined and unconfined concrete

2.4 Mechanical Behavior of Concrete

Concrete is a composite material, consisting of coarse and fine aggregates and cement matrix. Due to the differential shrinkage and thermal mismatch between aggregate and matrix, tensile stress and initial de-bonding cracks have been observed in concrete as reported by earlier (Hsu *et al.*, 1963). The mechanical behavior of concrete depends on the development of micro cracking inside concrete.

2.5 Uniaxial Compression Loading and Stress Strain Behavior

Typical stress-strain curves for concrete under compression loadings are given in Figure 2.4 (Wischers, 1978). The stress strain curve of concrete can be divided into three stages. In the first stage, the stress-strain curve has a nearly linear elastic behavior until 30% of maximum stress point of fc'. The existing cracks in the concrete before loading remain nearly unchanged. Based on thermodynamics, the available internal energy is less than the energy required for crack-release energy.

From the stress at above 30% of peak stress, the second stage, the nonlinear response is observed. During this stage, the micro-crack propagation is constant. During the third stage, the stress-strain curve presents a regular increase in curve up to about 75% to 90% of f_c'. In this stage, an unstable crack developing is observed during loading. If the load is kept constant, the cracks will continue to propagate with a decreasing rate up to the failure. The stress level of about 75% of f_c' is termed the start of unsteady fracture propagation of critical stress as it corresponds to the minimum amount of volumetric strain.

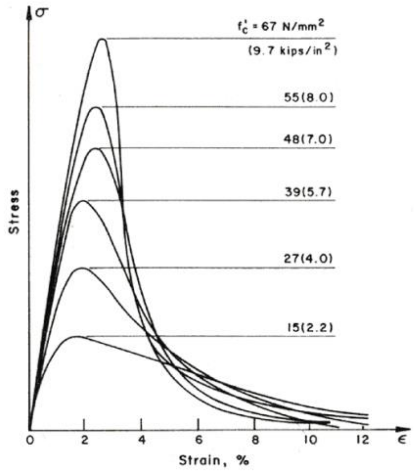

Figure 2.4 Complete compressive stress-strain curve (Wischers, 1978)

2.6 Durability of concrete and FRP fabrics to chemical attack

2.6.1 Durability of Concrete

The durability performance in field conditions of hydraulic concrete structures are usually called into question. Most concrete hydraulic structures are constructed depending on their individual application for a service life around 50 – 100 years (Schleiss and Boes, 2011). In addition, inadequate durability behavior of concrete material usually creates deterioration of structures even earlier to reach their expected service life (Ning, 2004).

The most well-known source of inadequate durability of concrete hydraulic structures in field conditions is the enlargement of cracks inside concrete (Han *et al.*, 2003; Li *et al.*, 2011). Various causes like chemical attack, mechanical loading, foundation settlement, shrinkage, and thermal contraction can affect the cracking in concrete for concrete dams (ACI Committee 224, 2001). In general, cracking in hydraulic structures accelerates chemical deterioration through providing easy access for harmful ions such as chloride and sulfate ions to progress into the core of the concrete hydraulic structure (Tsukamoto, 1990). Earlier investigations confirmed that the effect of cracks on the corrosion development is negligible if the cracks width are relatively narrow; yet, the rate of corrosion increases considerably as the cracks width exceed 100 μm. Therefore, the width of crack must be carefully organized to realize required durability performance of hydraulic structures (Tsukamoto, 1990; Li and Stang, 2004).

In addition, crack width control is considered a significant challenge for ordinary concrete. Great attempts have been realized to control crack initiation and propagation inside concrete, like proportioning and careful choice of the used material, and control the temperature during construction and utilizing steel reinforcement (Baoying *et al.*, 1994; Bo-Fang, 2006; Sun *et al.*, 2006). Moreover, concrete cracking is almost unavoidable due to the intrinsic brittleness of concrete under environmental and mechanical loadings (Li, Mo, 2011). Furthermore, it is usually accepted that crack width in concrete members is difficult to control; therefore, a material with inherent and regular crack width control ability is highly required.

2.6.2 Durability of Concrete to Seawater

The potentially aggressive constituents of seawater with respect to concrete are the sulfate, chloride, carbonate and bicarbonate as reported earlier by Prasad *et al.* (2006). In addition, Vicat (1812) conducted a studied and concluded that the chemical action of seawater on concrete is primarily due to harmful ions presented by magnesium sulfate ($MgSO_4$). This is deteriorated by the chloride existing in the seawater which results in spalling and cracking. The strength of the concrete in the beginning tends to increase during the early period of seawater attack, then followed by a reduction of strength as a results of produced expansion. Bryant investigated that the magnesium and potassium sulfates ($MgSO_4$, KSO_4) inside the seawater can produce sulfate attack in concrete when they quickly react with calcium hydroxide ($Ca(OH)_2$) existent in the cement within the hydration of C_2S and C_3S as illustrated below (Bryant, 1964).

$$S + CH + 2H\ CSh_2 + KH$$

$$S + CH + 2H - CSH_2 + MH$$

Where M – MgO and K – KO

The attack by magnesium sulfate ($MgSO_4$) is relatively severe as it creates simple soluble magnesium hydroxide ($Mg(OH)_2$) that accelerates the reaction by creating gypsum and $MgSO_4$ similarly reacts with the calcium sulfate gel (CSH). In addition, together with that formed by the reaction of $MgSO_4$, $Ca(OH)_2$ blend with silica hydrate (SH) created by the reaction with cementation gels to produce non-cementations form (M_4SH_8).

When ECC concrete is subjected to high chloride concentrations environments, like marine structures or bridge decks and for pavements exposed to de-icing salts, chloride ions may change the fiber/matrix interface. To study these influences, ECC coupon specimens were exposed to a 3% NaCl solution under preloaded uniaxial tension at different strain levels and under room temperature for 1, 2 and 3 months and hence later reloaded up to failure (Şahmaran and Li, 2007). They conducted that all reloaded specimens retained multiple micro-cracking performance and more than 3% tensile strain capacity, while the tensile strength was decreased around 10% and the average crack width expanded from 40 to 100 µm. The lower tensile strength and wider crack widths may be resulted from a reduction in chemical bonding at the interface between fiber/matrix, as concluded by pull-out test data of single fiber by Kabele *at al.* (2007) (Kabele *at el.* 2007).

Şahmaran and Li (2007a) (Şahmaran and Li, 2007) investigated the durability behavior of non-air-entrained ECC when exposed to freezing and thawing cycles under mechanical loading in the existence of de-icing salts. The surface condition after 50 exposure cycles, total mass, and visual evaluation of the climbing residue of ECC stayed within suitable forms according to ASTM C 672. This durability level sustained right even for the specimens pre-loaded to cracking at high levels of deformation. In addition, a reference non-air-entrained mortar specimens were produced for comparison. As expectable, these mortar prisms deteriorated severely under identical testing conditions. To determine the residual tensile performance of pre-loaded and no pre-loading (control) ECC coupon specimens, the specimens were subjected to freezing and thawing cycles for 25 and 50 cycles under de-icing salts. They concluded that the reloaded specimens exhibited negligible reduction of ductility, but retained a tensile strain ability of more than 3% and multiple micro-cracking performance. It was also realized that multiple micro-cracks due to mechanical loading restored satisfactorily in the presence of salt solutions under freezing and thawing cycles and healed the specimens to approximately the initial toughness. These outcomes approved that both micro-cracked and control ECC continued durable in the existing of deicing seawater under freezing and thawing cycles.

2.6.3 Durability of Concrete against Sulfate Attack

External sulfate attack is one of the durability issue related to concrete which was first recognized by the United States Breau of Reclamations in 1908 (BP, 1968). Since its recognition, it has been the issue of many investigations and remain not fully understood (Neville, 2004). The deterioration of concrete member by sulfates rely on numerous factors such as type of cement, water to cement (w/c) ratio, permeability, the environment, and exposure conditions (Marchand *et al.*, 2003). The two factors; the permeability of the concrete and the chemistry of the cement will tend to dominate the durability of concrete under sulfate attack.

Bonen and Cohen described previously the general reactions of external sulfate attack (Bonen and Cohen, 1992). Sulfate attack on concrete or cement mortars leads to the change of the hydration forms of cement to gypsum, ettringite, and other stages, and also to the deterioration of the principal strength representing calcium silicate hydrate gel (C-S-H). The production of gypsum and ettringite is critical in cementitious structures subjected to most types of sulfate attacks. The resulting expansion due to sulfate attack is usually attributed to the creation of gypsum and ettringite, although there is some disagreement about the exact mechanisms resulting the expansion (Cohen, 1983; Brown and Badger, 2000). Bonen and Cohen also observed that when the aggressive solution includes magnesium ion, which is available in magnesium sulfate ($MgSO_4$), the production of magnesium hydroxide (brucite) and sodium silicate hydrated gel (C-S-H) into magnesium silicate hydrate (M-S-H) (Bonen and Cohen, 1992). In addition, Diamond and Lee described the conversion of microstructure of sulfate deteriorated concrete in detail (Diamond, 2004). Scanning electron microscopy (SEM) have been also used by several researchers to clarify the inspection of new phases and the conversion of present phases of hydrated cement as a result of sulfate attack (Bonen, 1992; Portland *et al.*, 1992).

2.6.4 Durability of Concrete to Acid Attack

Sulphuric acid can be exist in various environments surrounding the concrete infrastructures. The effect of sulfuric acid on concrete is summarized below.

Groundwater generally includes free sulphuric acid and sulfates. Oxidation of pyrite (FeS_2) or other sulfides which may present in soils can produce free sulphuric acid with the help of air oxygen under weathering environments.

$$2FeS_2 + 7O_2 + 2H_2O \longrightarrow 2FeSO_4 + 2H_2SO_4$$
$$Or$$
$$4FeS_2 + 15O_2 + 2H_2O \longrightarrow 2Fe_2(SO_4)_3 + 2H_2SO_4$$

It should be stated that the level of the damage in concrete infrastructures near to groundwater depends on the amount of water and the concentration of the sulphuric acid. In addition, the permeability of the soil, which is closed with the concrete exhibits a significant role (Marchand *et al.*, 2003). A significant amount of sulphuric acid can be also exist in industrial wastes. For example, in the steel and iron industry, strong inorganic acids, like sulphuric and hydrochloric acids, are utilized to eliminate rust and organize the surface in the last treatment before the steel and iron are sold to builders. Therefore, the wastewater that is generally discharged into the system of underground sewage can present waste sulphuric acid which is considered one of a very hazardous acid for concrete pipes and may cause severe deterioration in the long or short term period.

Acid rain may also include sulphuric acid, which is created by oxidation of sulfur dioxide (SO_2), a creation of the burning of petroleum and coal or other industrial products. The acid rain can deteriorate the concrete infrastructures due to its pH value (~3) but it has a slightly weak influence on concrete in comparison to other acid damages.

Gypsum can be responsible for the expansion in the volume of the concrete structures and it is the primary products of the reaction between cement composites and sulphuric acid. Monteny *et al*. illustrated in details the creation of gypsum and other compounds, which produced from the reaction of sulphuric acid and concrete (Monteny *et al.*, 2000).

The volume increase as a result of expansion due to gypsum formation will produce internal tensile stresses in concrete and finally spalling of the surface of concrete. The ettringite occurs as a reaction of gypsum with calcium aluminate stages, resulting in an increase in the volume by a factor of around 7, which is considerably greater than the increase in volume due to gypsum. The previously mentioned internal stresses will ultimately lead to a significant amount of cracking in the microstructure of concrete member (Monteny *et al.*, 2000). The decalcification of C-S-H may also cause by sulphuric acid and will eventually alter the C-S-H into amorphous hydrous silica.

The white gypsum produced by sulphuric acid attacks covers the concrete surface and thereby it can work as a defending layer to avoid more deterioration of the matrix of concrete.

2.6.5 Durability of FRP to Acids Attack

Acid attacks on FRP constructions can originate from different sources like acid rain, marine environments, or from the soil below the construction (Kumar *et al.*, 2007; Guide, 2009). The typical process of an acid attack on FRP composites is via transportation of fluids or moisture (Kumar *et al.*, 2007). Acids cause a reaction between the polymer matrix and/or fibers, which alters the chemical composition and thus affect the mechanical properties of the material (Kumar *et al.*, 2007; Guide, 2009). These alterations cause debonding of the polymer matrix and fiber interface, which deteriorates the strength and stiffness of the material (Kumar *et al.*, 2007). The extent of damage to FRP composites due to acid attacks mainly depends on the possibility of interaction with the moisture in the surrounding environment (Kumar *et al.*, 2007). A common failure due to acid attack is stress corrosion when the internal strength of the material is reduced via acid degradation under sustained internal stress (Kumar *et al.*, 2007). In acid and moist environments, fillers in FRP composites are not recommended because they make the material more permeable and able to absorb the damaging substances easier (Guide, 2009; Zaman *et al.*, 2013). In civil engineering, all polymer matrices are considered to have sufficient resistance towards acid attacks. However, the commonly used polymer resins are sensitive to high concentrations of nitric and sulphuric acids (Guide, 2009; Hollaway, 2010; Zaman *et al.*, 2013). The most chemically stable resin is epoxy, which have better properties to withstand chemical attacks. However, epoxy is still susceptible to moisture absorption, which can transport acids into the material (Kumar *et al.*, 2007; Guide, 2009). Vinyl ester and polyester display satisfactory resistance towards chemical attack. If problems with high acid concentrations and temperatures, it is recommended to choose a more durable resin like epoxy (Guide, 2009). Acid attacks also affect the connections between components in FRP bridges. Adhesive connections are usually designed with epoxy-based adhesives, which means that they have good chemical durability (Guide, 2009; Sethi, 2014). However, mechanical (steel or other alloys) connections are susceptible to acid environments. The presence of moisture will further accelerate the corrosion rate of these connections (Guide, 2009).

2.6.7 Durability of FRP to Alkali Attack

Like acid attacks, alkali attacks also affect the polymer matrix and fibers, and alter their internal chemical composition, reducing the mechanical properties of the material (Hollaway, 2010). The degradation from alkali environments ultimately affects the internal bonds between polymer matrix and fibers due to the formation of micro cracks in the polymer matrix (Hollaway, 2010; Zaman *et al.*, 2013). Like acid attacks, the effects of alkali attacks can increase due to higher temperature and internal stress in the composite (Ceroni *et al.*, 2006). Some of the common alkali substances are sodium, calcium, and ammonium hydroxides (Guide, 2009). The best resistant fiber is the carbon due to low absorption of moisture and chemically stable nature (Ceroni *et al.*, 2006; Hollaway, 2010). Aramid fibers display satisfactory resistance towards alkali attacks. However, in combination with the absorption of moisture, alkali substances can have a damaging effect on aramid fibers and deteriorate the interface in the polymer matrix by altering the surface area of the fibers (Ceroni *et al.*, 2006). Glass fibers are susceptible to moisture absorption and together with alkali substances deterioration occurs on the mechanical properties. The reduction in strength is higher in glass fibers compared to other fibers under alkali environments (Ceroni *et al.*, 2006). The resin in the polymer matrix is sensitive to high concentrations of alkali substances in the surrounding environment (Hollaway, 2010; Zaman *et al.*, 2013). The resistance depends on the chemical stability and permeability of the polymer resin (Zaman *et al.*, 2013). Because of this, epoxy and vinyl ester resins are suitable in alkali environments. Vinyl ester resins display the best resistance in alkali environments due to low absorption rates, and epoxy resins have a stable chemical structure (Ceroni *et al.*, 2006). Polyester is sensitive to alkali attacks due to the less stable chemical structure than the other polymer resins and therefore it is not recommended in these environments (Friberg and Olsson, 2014). In general, FRP composites are not significantly affected by moderate concentrations of alkali substances in the surrounding environment (Ceroni *et al.*, 2006). When field-testing was conducted, FRP composites did not show significant degradation of the mechanical properties as a result of alkali attacks. The problem with alkali attacks mainly relates to concrete constructions with FRP composite rods are used as a reinforcement where concentration levels are high enough to cause degradation (Hollaway, 2010).

CHAPTER 3
EXPERIMENTAL DETAILS

3.1 Materials

3.1.1 Ordinary Portland Cement

Portland cement type CEM I 42.5 R having Blaine fineness of 326 m^2/kg and specific gravity of 3.14 was used for preparing the ECC cylinder test specimens to evaluate the mechanical properties. Physical properties and the chemical composition of OPC are illustrates in Table 3.1.

3.1.2 Fly ash

F type low calcium fly ash (LCFA) and C type high calcium fly ash (HCFA) conforming to ASTM C 618 (ASTM C618, 2012) was utilized in this study as a binder with OPC for preparing the ECC specimens as presented in Figure 3.1. It was supplied by thermal power plant, named Ceyhan Sugözü, placed in Turkey. Fly ash (FA) used in this study have specific surfaces of 387 and 306 m^2/kg and specific gravities of 2.30 and 2.27 for LCFA and HCFA, respectively. Physical properties and the chemical composition of both types of FA are illustrated in Table 3.1.

a) Fly ash class F (LCFA)

b) Fly ash class C (HCFA)

Figure 3.1 Fly ash used in the production of ECC specimens

Table 3.1 Chemical compositions and physical properties of OPC and FA

Mat.	CaO	SiO_2	Al_2O_3	Fe_2O_3	MgO	SO_3	K_2O	Na_2O	L.O.I	Specific Gravity	Blaine Fineness (m^2/kg)
FA-F (%)	1.57	62.35	21.14	7.85	1.76	0.10	0.73	2.45	2.07	2.30	387
FA-C (%)	15.54	46.95	11.68	7.98	6.51	3.47	3.13	2.33	2.45	2.27	306
OPC (%)	62.58	20.25	5.31	3.04	2.28	2.71	0.62	0.22	3.02	3.15	326

3.1.3 Superplasticizer (SP)

Sulphonated naphthalene formaldehyde (SNF) based high range water reducing SP with a specific gravity of 1.19 was used in the study as shown in Figure 3.2. The super-plasticizer was added at the time of mixing to enhance the workability of the mixture. SP was bought from a local supplier and all details are presented in Table 3.2.

Table 3.2 Properties of Super Plasticizer

Properties	Superplasticizer
Name	Viscocrete 30
Color tone	Dark brown
State	Liquid
Specific gravity (kg/l)	1.09
Chemical description	Modified polycarboxylic type polymer
Recommended dosage (%)	%1-2 (% binder content)

Figure 3.2 Super-plasticizer used in ECC mixes

3.1.4 Fine Aggregate

Micro-silica sand with an average grain size and a maximum grain size of 110 µm and 200 µm, respectively used in the study since the ductility performance of ECC was affected by an increase in the aggregate size (Sahmaran *et al.*, 2009).

3.1.5 PVA fiber

The polyvinyl alcohol (PVA) with a fraction of 2% was utilized in the study, with a length and diameter of 8 mm and 39 µm, respectively as can be seen in Figure 3.3. The elastic modulus, tensile strength and maximum elongation of PVA fibers were 42.8 GPa, 1620 MPa and 6.0%, respectively (Li *et al.*, 2002). Research showed that the peak load of unoiled fibers was greater than the oiled PVA fibers due to chemical bond and higher friction. However, the crack opening was found much smaller, which resulted in decreased energy absorption capacity for the unoiled fibers (Pan *et al.*, 2015). It was attributed to the rupture of the unoiled PVA fiber from the matrix instead of pullout of fibers from matrix. During the peak load, unoiled PVA fibers had higher frictional and chemical bond and it reached the maximum load at small pullout lengths. The unoiled fibers did not completely pull out of the matrix and rupture occurred (Fischer and Li, 2002). Therefore, the surfaces of the PVA fibers were oiled with a proprietary hydrophobic oiling agent of 1.2% by weight in order to reduce the frictional and chemical bond and to improve strain hardening performance of ECC (Sahmaran and Li, 2007).

Figure 3.3 PVA fibers used in ECC mixes

3.1.6 Fiber Reinforced Polymer (FRP)

In this study, ECC specimens were confined by using uni-directional carbon fiber reinforced polymer (CFRP) and basalt fiber reinforced polymer (BFRP) fabrics to observe the durability and mechanical performance of these materials under chemical attack. Table 3.3 presents the mechanical and physical properties of the FRP materials. An epoxy-based adhesive, Teknobond 300 Tix, was used and its general properties were given in Table 3.4. The application of the epoxy-based adhesive to the ECC specimens was realized according to the user guide of the technical document.

Table 3.3 The properties of fabric sheets

FRP types	Tensile Strength (MPa)	Modulus of Elasticity (GPa)	Elongation (%)	Thickness (mm)	Area Weight (g/m^2)
BFRP	2100	105	2.6	0.3	300
CFRP	4900	240	2	0.3	300

Table 3.4 General properties of epoxy based adhesive material

Epoxy Type	Pot life at 20°C (Min)	Flexural Strength 7 days (N/mm^2)	Compressive Strength 7 days (N/mm^2)	Bond Strength 7 days (N/mm^2)	Mixing ratio	Modulus of Elasticity 7 days (GPa)	Fluid density (kg/lt)
Teknobond 300 Tix	30	≥ 25	≥62.5	≥3	4:1	>20	1,02 ± 0,02

3.2 Mixture Proportioning and Concrete Casting

Table 3.5 presents the mix design of the ECC specimens. The ratio of FA to OPC and the ratio of micro silica sand to the binder were selected as 1.2 and 0.36 by weight, respectively. Research indicated that water to binder ratio of 0.3 was the balance point for both strain hardening performance (improved toughness) of ECC and good fiber dispersion due to the high rheological behavior. Therefore, the water to binder ratio was selected as 0.27, which was under the balance value and it was expected to perform enhanced post peak behavior. High range water reducing admixture was also used in the ECC mixes until the desired fresh properties of ECC mixes were obtained as specified in the earlier investigation (Yang *et al.*, 2009). As a result, two mixes were obtained as the LCFA-ECC mix (produced with low calcium F-type fly ash) and the HCFA-ECC mix (produced with high calcium C-type fly ash).

For the mixing period, the following procedure was used for all ECC mixtures produced for the present study: At the 4th minute of the first step, solid ingredients (OPC, FA and silica sand) were mix in a standard mortar mixer at a low speed. After 4 minutes of mix, the water was added into the mix and mixing was continued for 2 minute at low speed. Then, mixing continued at high speeds for an additional 5 minutes to obtain autogenous mix. Then, mixing was continued at high speed for additional 5 minute with addition of HRWRA. PVA fibers as a final stage were added into the fresh mixtures and all of the ingredients were mixed at high speed for 5 minutes. To get uniform mixture and avoid fiber interactions, mixing at high speed was continued for 3 more minutes with additional of chemical powder. As the completion of mixing process, all of the casting specimens were kept inside their molds at 50±5% RH, 23±2 ^{o}C for 24 hours. After 24 hours later, cylinder specimens were removed from their molds and kept in water at 23±2 ^{o}C until the predetermined testing ages.

Table 3.5 Typical mix design of ECC concrete (Yang *et al.*, 2009)

Cement	Water	Microsilica sand	Fly ash	HRWRA*	Fiber (%)
1.00	0.56	0.8	1.2	0.013	2.00

*HRWRA = High range water reducing admixture; all ingredients proportion by weight except for fiber.

3.3 Specimen preparation and curing condition

Cylinder specimens with dimensions of 100 mm in diameter and 200 mm in length were prepared to measure compressive strength of PVA-ECC specimens. After 24 hours, specimens were demolded and cured in a water tank for 28 days at 23±2 °C. Then specimens were left in an ambient condition for drying. After required strength, carbon and basalt FRP wrappings were realized on certain specimens according to the FRP application procedure as shown in Figure 3.4.

a) Preparation of concrete surface

b) Preparation of sheets

c) Application and impregnation of the FRP fabric

Figure 3.4 Main steps of applying FRP fabric

In the first step, concrete surfaces were cleaned by eliminating the residual powders with a wire brush and an air compressor. In the second step, FRP fabrics were prepared by cutting each of the sheets with a length of 115 cm (three-layer continuous wrapping length with an overlap of 15 cm between layers) and width of 19 cm (cylinder height minus 0.5 cm at both top and bottom sides to prevent axial load on FRP). In the final stage, implementation of FRP fabrics was realized by coating inner sides of the FRP fabrics with epoxy resin. Later, specimens were placed inside of the FRP fabrics, then three layers wrapping of the specimens were applied with epoxy resin. In the FRP application procedure, the surface of the specimens was also covered with epoxy resin to fill the pores on the surface and to obtain a perfect bond between concrete and FRP fabrics. In addition, the orientation of fibers of FRP fabrics was taken into consideration during the covering process to ensure alignment of fibers perpendicular to the axial direction of loading. For the outermost layers of FRP fabrics, 15 cm overlap length was provided to obtain a perfect bond between FRP layers and to prevent slippage of FRP layers. Separation of fibers from the edge of FRP sheets was prevented during wrapping process to prevent premature failure of the specimens. After FRP installation, specimens were left in the ambient environment for 7 days to obtain the required strength of the epoxy resins.

3.4 Specimens under Chemical Attack

There is no typical test method presented to measure the durability of concretes under chemical attack. However, ASTM C 267 test method (ASTM C267 - 01, 2012) proposes that specimens should be immersed in water for 24 hours prior to exposure to the chemical attacks to achieve water saturated specimens. Thus, specimens were soaked in water for 24 hours and left to drying at 23 ± 2 °C for 2 hours prior to record initial saturated weights of the specimens. Then specimens were soaked in 5% sulphuric acid (H_2SO_4), 5% magnesium sulfate ($MgSO_4$), and 3.5% seawater (NaCl) solutions for a period of two months. At the same time, ECC control specimens were left in ambient condition at a room temperature of 23±2ºC in the laboratory for each different concrete for two months for comparison purposes. After the end of each week, ECC specimens were taken from the chemical solution, chemical reaction products on the concrete surface were cleaned by water. Then the specimens were left to drying under laboratory conditions at temperatures of 23 ± 2 °C for 2 hours prior to weight measurements of the specimens.

3.5 Testing Procedure

Compressive strength tests were carried out on confined and unconfined cylinder specimens under static and cyclic loadings. Compressive strength tests were carried out according to ASTM C39 (ASTM C39, 2012). All compressive strength tests were performed under displacement controlled loading with a rate of 0.2 mm/min. Two linear variable displacement transducers (LVDT) were attached to measure axial deformations in the specimens as shown in Figure 3.5. Stress and strain data were obtained for each specimen. Before the test, sulfur capping process was implemented to level the surfaces of each specimen to achieve even stress distribution Figure 3.6.

a) Unconfined ECC specimen

b) Confined ECC specimen

Figure 3.5 ECC specimens under axial compression load

Figure 3.6 Sulfur capped specimens before the uniaxial compression test

CHAPTER 4
SULPHURIC ACID ATTACK

4.1 Visual inspection

Figure 4.1 illustrates the specimens exposed to 5 % sulphuric acid solutions for 15 days, one month and two months, respectively. The surface color of the high lime containing fly ash specimens (HCFA) changed from grey to white after 15 days of exposure, while the surface color of the low lime fly ash specimens (LCFA) remained grey even after two months of exposure. For HCFA specimens, white layer gypsum crystals were formed and the amount of the gypsum crystals increased with an increase in the exposure time, which resulted in higher deterioration on the concrete surfaces as shown in Figure 4.1. Moderate surface erosions and some small cracks were observed on LCFA specimen surface without color change. It was also visually observed that more lateral expansion occurred on HCFA specimens than LCFA specimens, which may be attributed to higher gypsum and ettringite formation due to high CaO content on HCFA specimens. When the outer surface colors of specimens confined with basalt and carbon FRP were compared, the colors of both specimens changed to white and most deterioration (most whiter one) was observed on basalt FRP specimens than carbon FRP specimens under sulphuric acid attack, as shown in Figure 4.1.

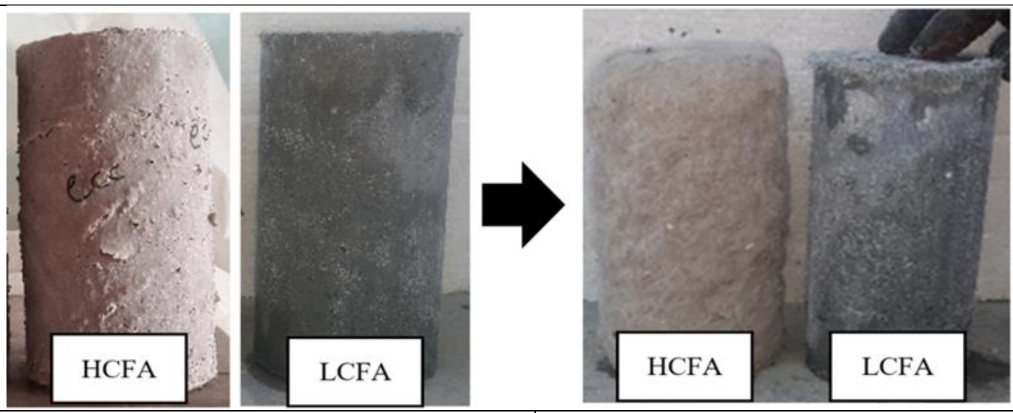

a) After 15 days of chemical exposure	b) After one month of chemical exposure

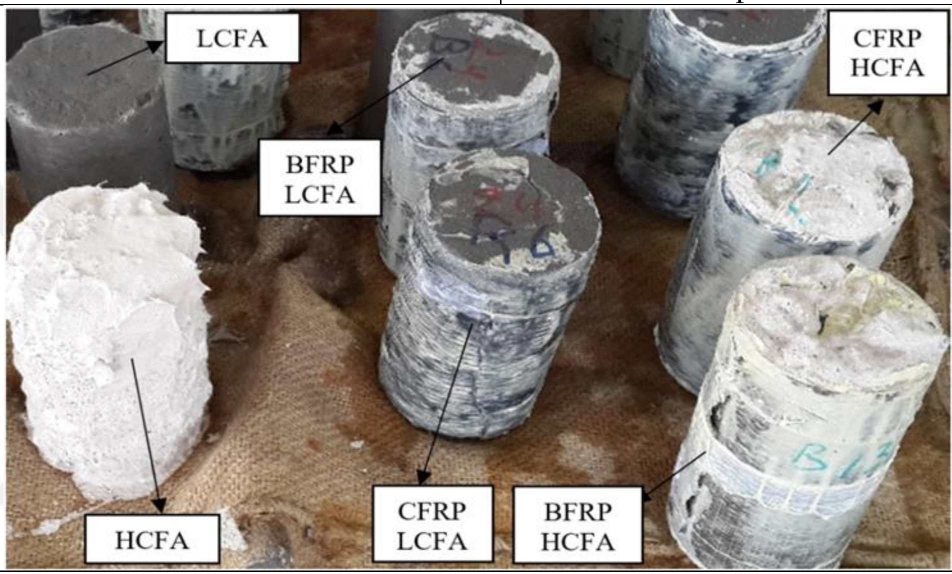

c) After two months of chemical exposure

Figure 4.1 Deterioration of specimens under sulphuric acid environment

PVA fibers were also deteriorated by spillage of fibers due to surface erosions exposed to sulphuric acid solutions. When specimens were investigated in details, PVA fibers of HCFA specimens deteriorated more severe than PVA fibers of LCFA specimens. PVA fiber deterioration was also observed on specimens wrapped with basalt and carbon FRP. However, in this case, PVA fiber deterioration was only observed at the bottom and top parts of the cylinder specimens (unwrapped part of the specimens). Due to the confinement in the lateral direction, PVA fiber deterioration was not observed.

Wallah and Rangan (Wallah and Rangan, 2006) studied the effect of 2% sulphuric acid attack on geopolymer concrete and found out that sulphuric acid damage was observed only in the 20 mm outer side of the cylinder concrete, which had a 100 mm diameter. In this study, slices of the cylinder concrete exposed to the sulphuric acid solution were also investigated and similar observations were obtained with the previous study (Wallah and Rangan, 2006). Acid penetration was observed at the 8 mm outer part of the cylinder specimens, and the remaining inner parts were found unexposed as shown in Figure 4.2. It was clearly observed that the acid damage in HCFA specimens was found more severe than LCFA specimens. This result was also supported by the earlier investigation, which stated that the acid attack is a surface phenomenon and the deterioration begins at the surface and progresses inside of the concrete (Attiogbe and Rizkalla, 1988). In addition, SEM observations were also realized at the acid affected and unaffected zones, as shown in Figure 4.2.

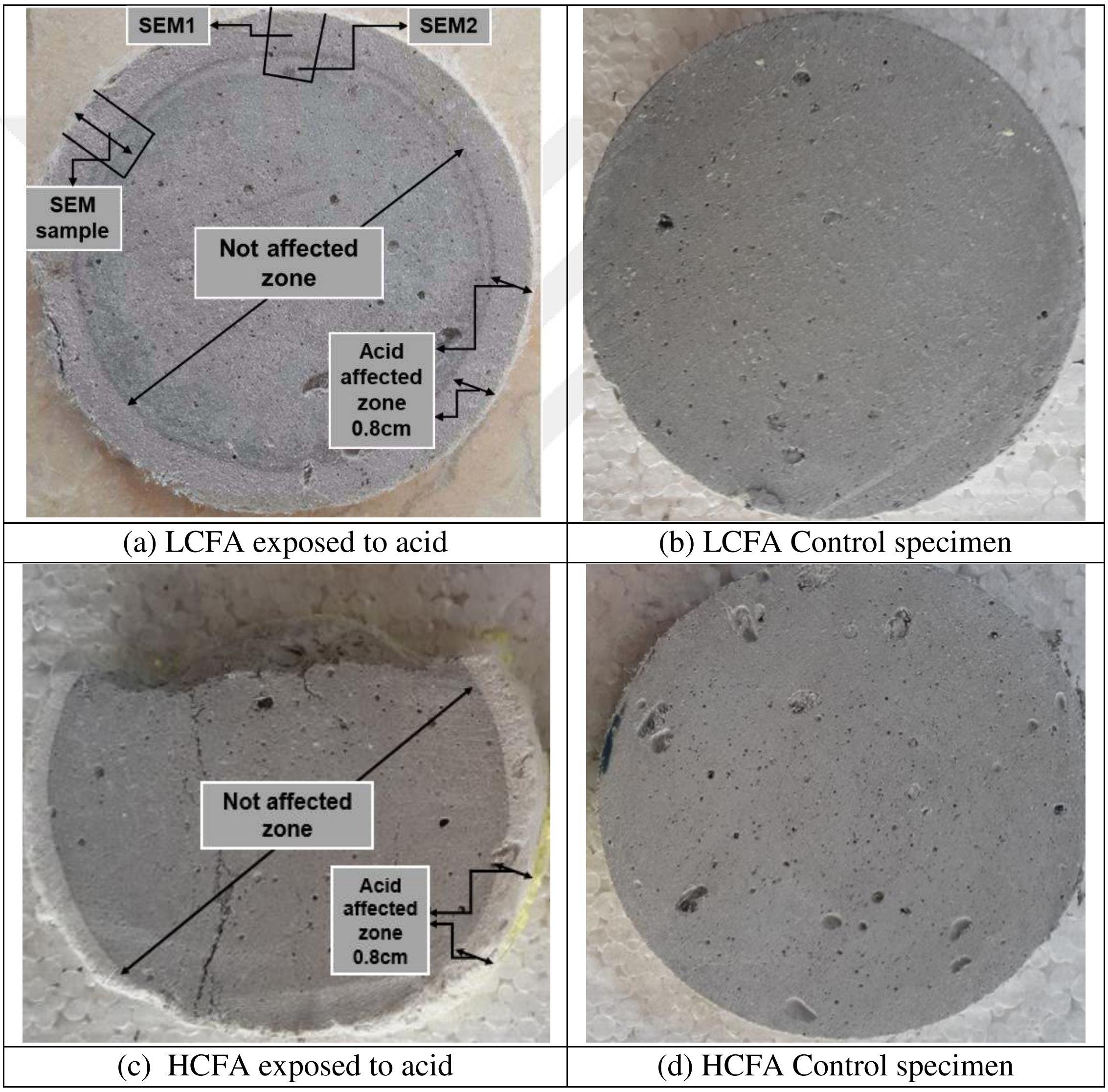

(a) LCFA exposed to acid | (b) LCFA Control specimen | (c) HCFA exposed to acid | (d) HCFA Control specimen

Figure 4.2 ECC Cylinder specimen slice showing acid affected zone

4.2 Weight change

Specimen weights were measured under two months of chemical exposure and weight change (%) of the specimens were given in Figure 4.3. Results showed that all specimens showed weight gain under sulphuric acid solution absorption, and highest weight increase was observed on specimens without wrapping. The gained weights were 6.4 % for HCFA specimens and 3% for LCFA specimens. For wrapped specimens, HCFA specimens also showed slightly higher weight gain than the LCFA specimens. In addition, LCFA specimens confined with carbon FRP showed the least weight gain and therefore, LCFA specimens with CFRP fabrics showed slightly better chemical resistance than BFRP fabrics under acid attack. Lower weight gains result of LCFA specimens with/out FRP wrapping may be attributed to the higher fineness ratio, which resulted in reduced porosity and decreased solution absorption. Weight gain due to acid exposure was also reported in the earlier research (Mohammed, 2007; Thokchom, 2014). In addition, HCFA specimens without wrapping showed weight loss (deterioration) after one month of exposure, which could be resulted from both alkali and some material dissolution from concretes into the acidic medium (Thokchom, 2014). The formation of gypsum and ettringite due to the reactions between chemical solution and cement caused increased volume by a factor of about two (Soroka, 1979) and reduced density of concrete. Therefore, initial weight gains of the specimens may result from the lower reduction amount in relative density than the increase in relative volume (Attiogbe and Rizkalla, 1988).

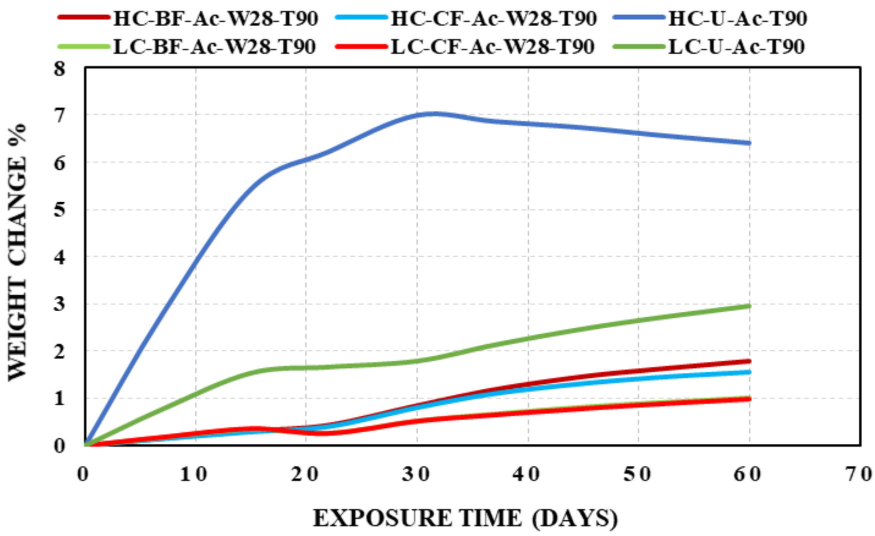

Figure 4.3 Weight change in ECC specimen exposed to acid attack for duration 60 days

4.3 Compressive strength of the specimens

In general, the performances of PVA - ECC specimens wrapped with FRP under axial load were found to be consistent with the behavior of FRP confined concrete in the literature. During early stages of compression loading, the noise associated with the micro-cracking of ECC concrete was obvious, which represented the initiation of the stress transfer from the expanded ECC concrete to the FRP fabrics. The intensity of the cracking noises could be heard prior to the failure that realized after the rupture of FRP fabrics slowly with a sudden and violent noise. Failure of the FRP fabrics started from an overlap area of the fabrics at the middle height and progressed to the top and bottom of the specimens. For the tested specimens, no de-bonding observed in wrapped specimens and all failures occurred due to the rupture of FRP fabrics followed by a ductile behavior of ECC. Figure 4.4 illustrates the average compressive strengths. Results indicated that FRP wrapped specimens showed superior performance than unwrapped specimens under both ambient and acid environments.

4.3.1 Specimen nomenclature

Three types of specimens were obtained in the scope of the research; CFRP-ECC hybrid specimens (specimens confined by carbon FRP fabrics), BFRP-ECC hybrid specimens (specimens confined by basalt FRP fabrics) and control specimens (unwrapped specimens). In addition, two mixes; high calcium fly ash mix (HCFA mix) and low calcium fly ash mix (LCFA) mix were prepared. Specimens were subjected to two different environments; 5% acid environment and control environment (unexposed specimens). Control specimens (unexposed specimens) were tested at the ages of 28 days and 90 days, while specimens subjected to acid environment were tested at the age of 90 days (28 days water curing and the remaining days under acid environment).

As shown in Table 4.1, eight test series were designed in this study as follows:

Table 4.1 Details of test series conducted in this chapter

Test series	Type of concrete	No. of samples	Unconfined	Confined: BFRP	Confined: CFRP	Control sample	Acid exposed	Wrapping age: 28-days	Wrapping age: 90-days	Testing age: 28-days	Testing age: 90-days	Specimen ID
A	LCFA	3	✓			✓				✓		LC-U-Co-T28
		3		✓		✓		✓		✓		LC-BF-Co-W28-T28
		3			✓	✓		✓		✓		LC-CF-Co-W28-T28
B		6_a	✓			✓		✓			✓	LC-U-Co-T90
		6_a		✓		✓		✓			✓	LC-BF-Co-W28-T90
		6_a			✓	✓		✓			✓	LC-CF-Co-W28-T90
C		6_a	✓				✓	✓			✓	LC-U-Ac-T90
		6_a		✓			✓	✓			✓	LC-BF-Ac-W28-T90
		6_a			✓		✓	✓			✓	LC-CF-Ac-W28-T90
D		3		✓			✓		✓		✓	LC-BF-Ac-W90-T90
		3			✓		✓		✓		✓	LC-CF-Ac-W90-T90
E	HCFA	3	✓			✓				✓		HC-U-Co-T28
		3		✓		✓		✓		✓		HC-BF-Co-W28-T28
		3			✓	✓		✓		✓		HC-CF-Co-W28-T28
F		6_a	✓			✓		✓			✓	HC-U-Co-T90
		6_a		✓		✓		✓			✓	HC-BF-Co-W28-T90
		6_a			✓	✓		✓			✓	HC-CF-Co-W28-T90
G		6_a	✓				✓	✓			✓	HC-U-Ac-T90
		6_a		✓			✓	✓			✓	HC-BF-Ac-W28-T90
		6_a			✓		✓	✓			✓	HC-CF-Ac-W28-T90
H		3		✓			✓		✓		✓	HC-BF-Ac-W90-T90
		3			✓		✓		✓		✓	HC-CF-Ac-W90-T90

Note: a Three specimens under static loading and three specimens under cyclic loading.

In the Table 4.1, HC and LC indicates the high calcium FA and low calcium FA, U, CF and BF points out unconfined, confined by carbon FRP and basalt FRP fabrics, Co and Ac represents the control and acid environments, W28 and W90 shows the wrapping ages of 28 days and 90 days, T28 and T90 demonstrates the age of compressive strength at 28 days and 90 days, respectively.

Series A: 9 LCFA-ECC control cylindrical samples (3 unconfined and 6 confined) were tested at 28 days. The FRP wrappings were also applied at 28 days.

Series B: 18 LCFA-ECC control cylindrical samples (6 unconfined and 12 confined) were tested at 90 days. The FRP wrappings were applied at 28 days.

Series C: 18 LCFA-ECC (6 unconfined and 12 confined) specimens were cured in a water tank until 28 days and FRP wrappings were applied. Then, these confined specimens immersed into 5% acid solution at the age of 90 days.

Series D: 6 LCFA-ECC unconfined specimens were cured in a water tank until 28 days and these unconfined specimens subjected to 5% acid solution at the age of 90 days. Then, acid exposed specimens were confined at the age of 90 days to evaluate the influence of FRP confinement as a rehabilitation method.

Series E: 9 HCFA-ECC control cylindrical samples (3 unconfined and 6 confined) were tested at 28 days. The FRP wrappings were also applied at 28 days.

Series F: 18 HCFA-ECC control cylindrical samples (6 unconfined and 12 confined) were tested at 90 days. The FRP wrappings were applied at 28 days.

Series G: 18 HCFA-ECC (6 unconfined and 12 confined) specimens were cured in a water tank until 28 days and FRP wrappings were applied. Then, these confined specimens immersed into 5% acid solution at the age of 90 days.

Series H: 6 HCFA-ECC unconfined specimens were cured in a water tank until 28 days and these unconfined specimens subjected to 5% acid solution at the age of 90 days. Then, acid exposed specimens were confined at the age of 90 days to evaluate the influence of FRP confinement as a rehabilitation method.

In total, 102 cylindrical specimens were cast and tested in the scope of study the effect of sulphuric acid attack.

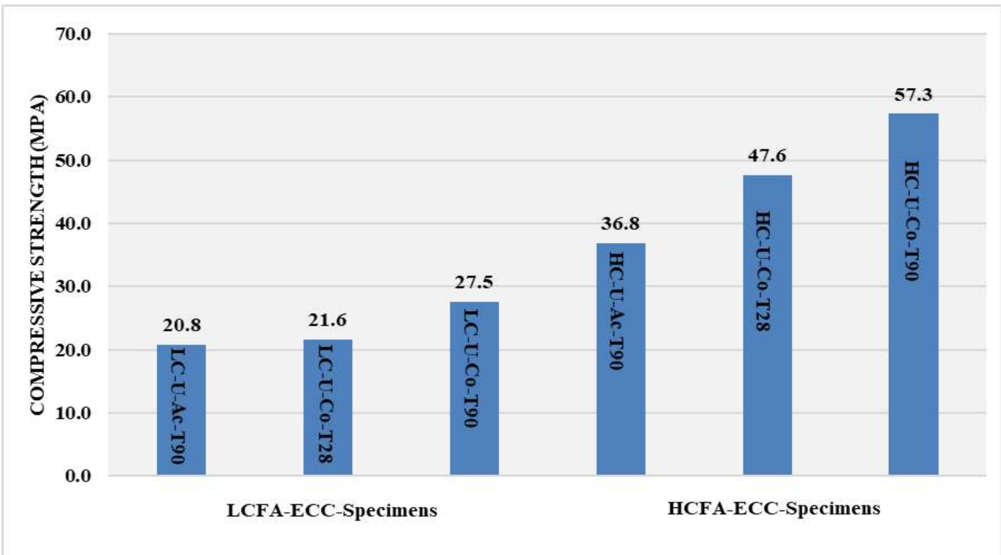

a) Unconfined ECC specimens

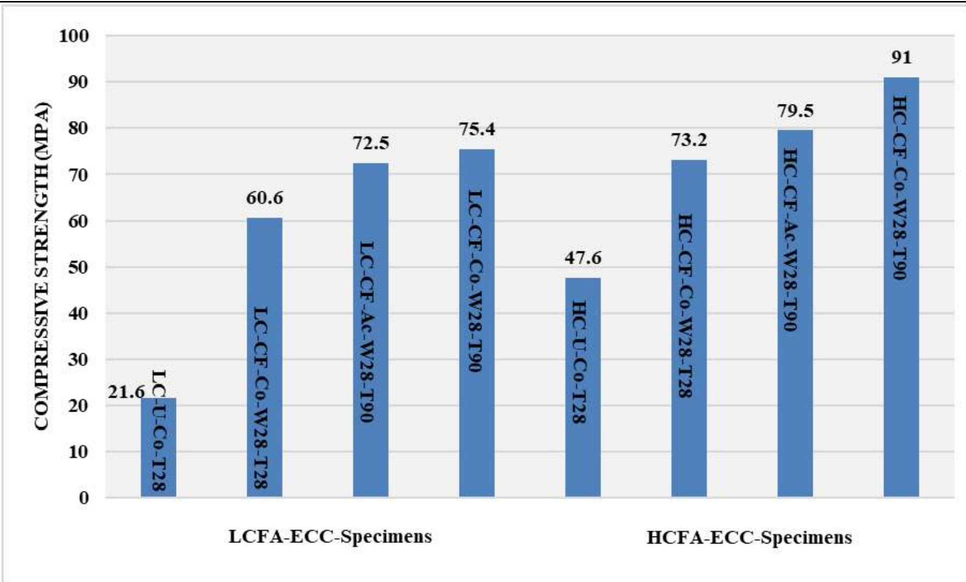

b) Unconfined ECC specimens and ECC specimens wrapped by CFRP

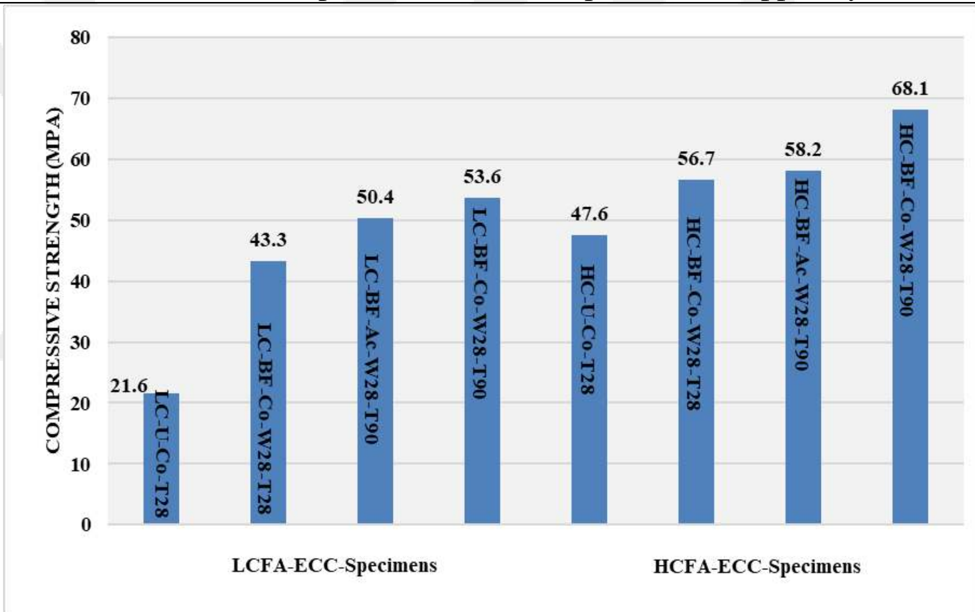

c) Unconfined ECC specimens and ECC specimens wrapped by BFRP

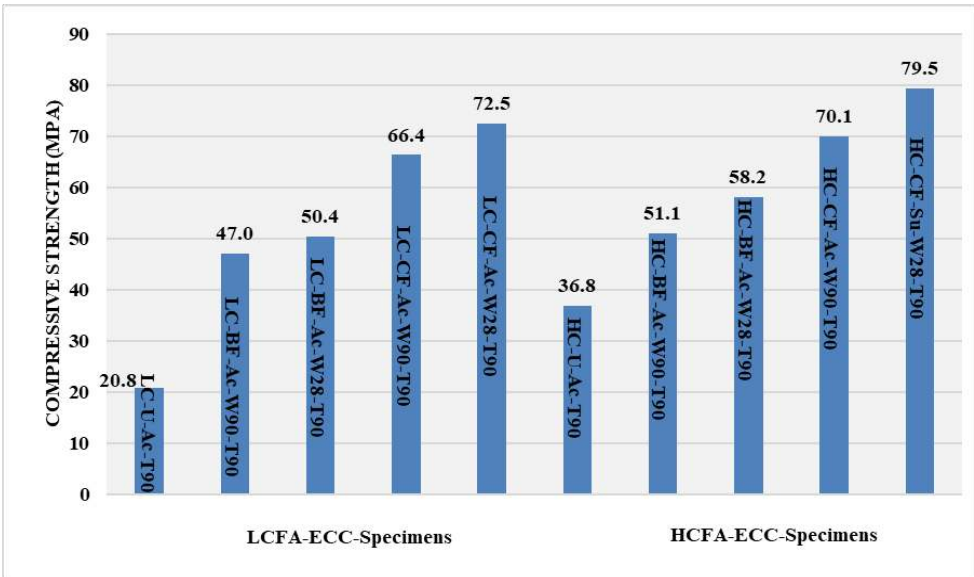

d) Unconfined ECC specimens and ECC specimens wrapped by both FRP exposed to acid and exposure specimens wrapped by both FRP

Figure 4.4 Compressive strength of confined and unconfined ECC specimens

4.3.2 Compressive behavior of unwrapped specimens

Figure 4.5 shows the typical compressive stress-strain curves of unwrapped PVA - ECC specimens. Results indicated that compressive strength of unwrapped specimens increased up to 90 days. The increase in the compressive strength can be attributed to the continuous hydration reactions and the slow pozzolanic reaction of fly ash. Similar investigations were also reported in the previous studies (Liu *et al.*, 2017; Zhang and Zhang, 2017).

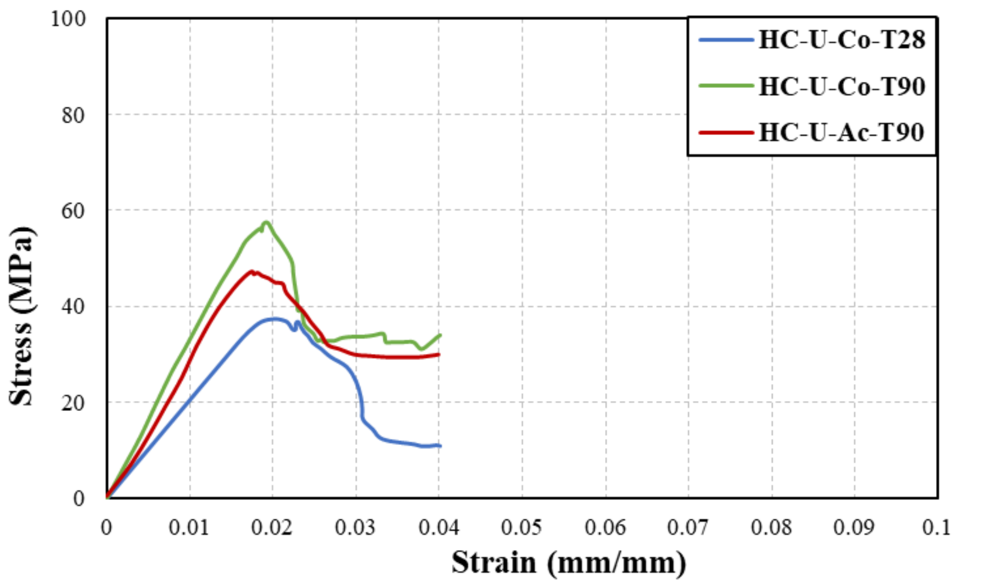

a) Unwrapped HCFA-ECC specimens

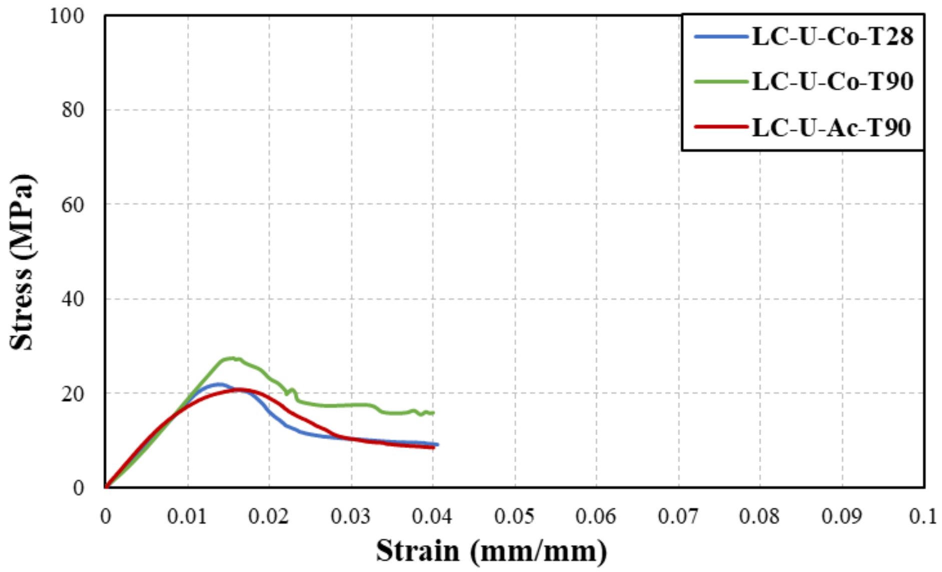

b) Unwrapped LCFA-ECC specimens

Figure 4.5 Stress-strain curves of unwrapped ECC specimens

The compressive strength values of 90-day curing specimens were 20.3% and 27.2% higher than the 28-day curing compressive strength values for HCFA and LCFA specimens, respectively. The higher increase in the compressive strengths of LCFA specimens at later ages was expected due to lower CaO content in the low lime fly ash particles as the rate of hydration reactions was slow, in which strength development (C_3S and C_2S production) became time dependent. Reductions in strength due to sulphuric acid attack were 22.7% and 4% for 28-days, 35.7% and 24.4% for 90-days strengths of HCFA and LCFA specimens, respectively. Higher strength reduction for HCFA specimens may be also attributed to high CaO amount in the HCFA specimens.

4.3.3 Compressive behavior of wrapped specimens

Figure 4.6 represents the compressive behavior of wrapped PVA-ECC specimens. The results showed significant compressive strength increase (more than 2-3 times) when compared to unwrapped specimens. In general, when the outermost FRP fiber ruptured, the compressive load reduced suddenly and then the load began to increase or remain constant due to stress transfer from FRP fabrics to PVA-ECC concrete until the failure of inner FRP fibers and PVA fibers inside the ECC matrix (Li *et al.*, 2002).

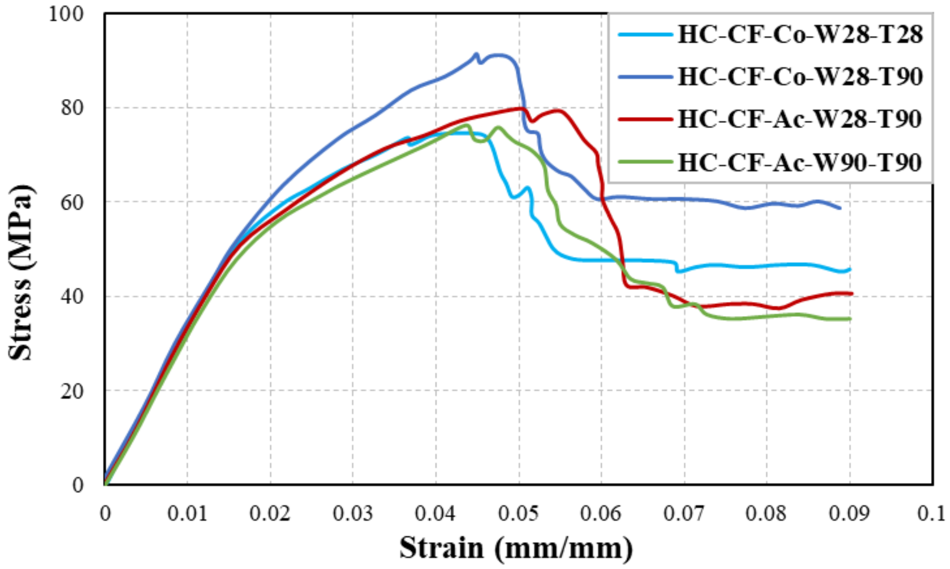

a) HCFA-ECC specimen wrapped by CFRP

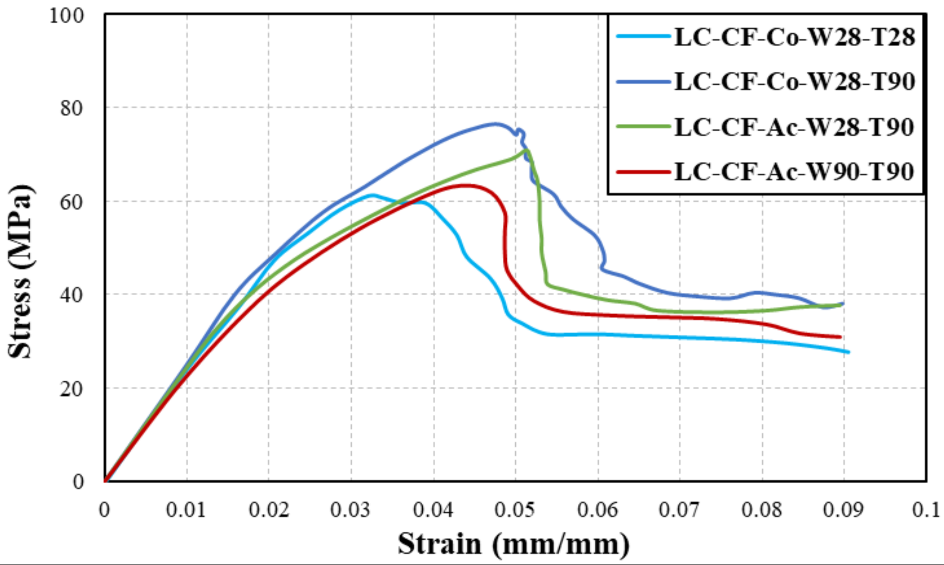

b) LCFA-ECC specimen wrapped by CFRP

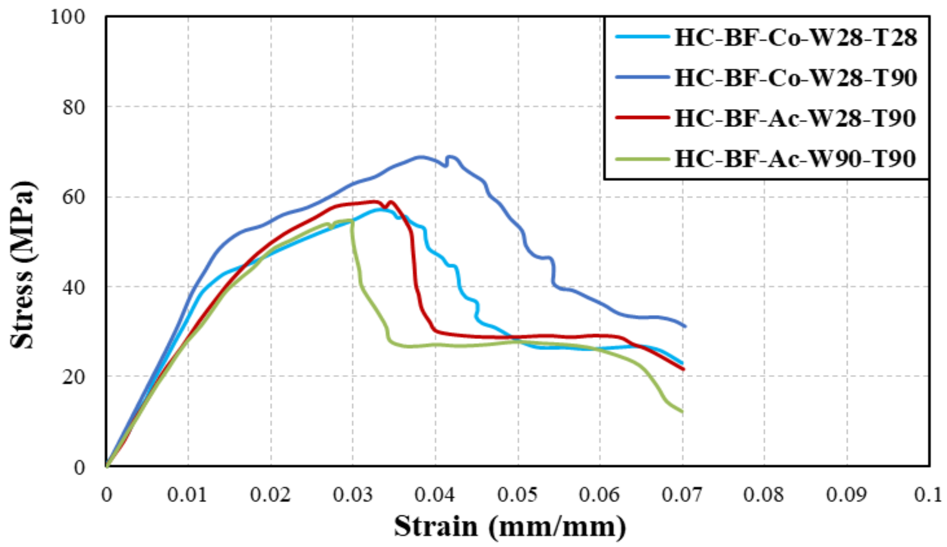

c) HCFA-ECC specimen wrapped by BFRP

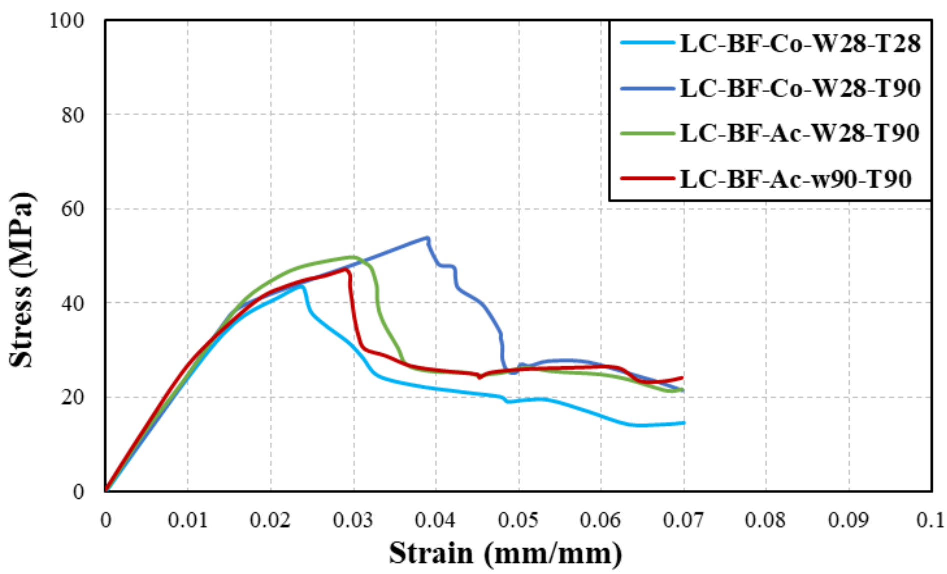

d) LCFA-ECC specimens wrapped by BFRP

Figure 4.6 Stress-strain curves of CFRP and BFRP wrapped ECC specimen

Similar to unwrapped specimens, compressive strengths of the wrapped specimens also enhanced from 28-days to 90-days. The amounts of enhancement were 24.3% and 20.3% for HCFA specimens and 24.4% and 23.7% for LCFA specimens wrapped with CFRP and BFRP fabrics, respectively. It can be concluded that the effect of concrete matrix on compressive strength was also significant when FRP fibers were also available.

Compressive strengths of the wrapped specimens exposed to the acid solution at the age of 90-days were found higher than the 28-day compressive strengths of the wrapped ones. The amount of increase was found to be 19.6% and 16.4% for the LCFA-ECC specimens and 8.6% and 2.8% for the HCFA-ECC specimens wrapped with CFRP and BFRP fabrics, respectively. This lower increase in the HCFA specimens can be attributed to the deterioration effect of CaO content especially for the high lime fly ash including specimens. In addition, the strengths of the wrapped specimens under acid attack were lower than the unexposed specimens at the age of 90-days, as expected. The reduction amounts due to acid attacks were 12.6% and 14.5% for HCFA specimens and 5.94% and 7.36% for LCFA specimens wrapped with CFRP and BFRP fabrics, respectively.

In the study, unwrapped specimens were exposed to acid attack and then the installations of FRP fabrics were realized on the same specimens in order to find out the effect of FRP materials as rehabilitation/retrofit materials. Results showed that compressive strength of the after wrapped specimens (The acid deteriorated specimens wrapped by both FRP fabric after exposure duration (Age of 90 days)) were lower than the before wrapped specimens under acid attack, as expected. The reduction amounts only were 12% and 12.3% for LCFA specimens and 23% and 25% for HCFA specimens wrapped with CFRP and BFRP, respectively. Results indicated that both FRP installation can be also a solution to acid affected concrete and FRP fabrics can be used as a retrofit or rehabilitation material under acid attack.

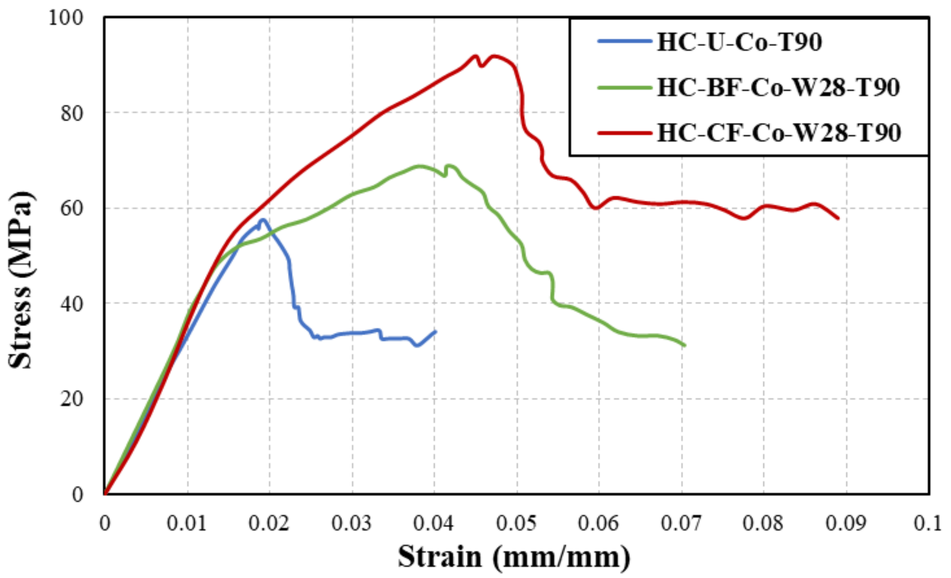

a) HCFA-ECC specimens

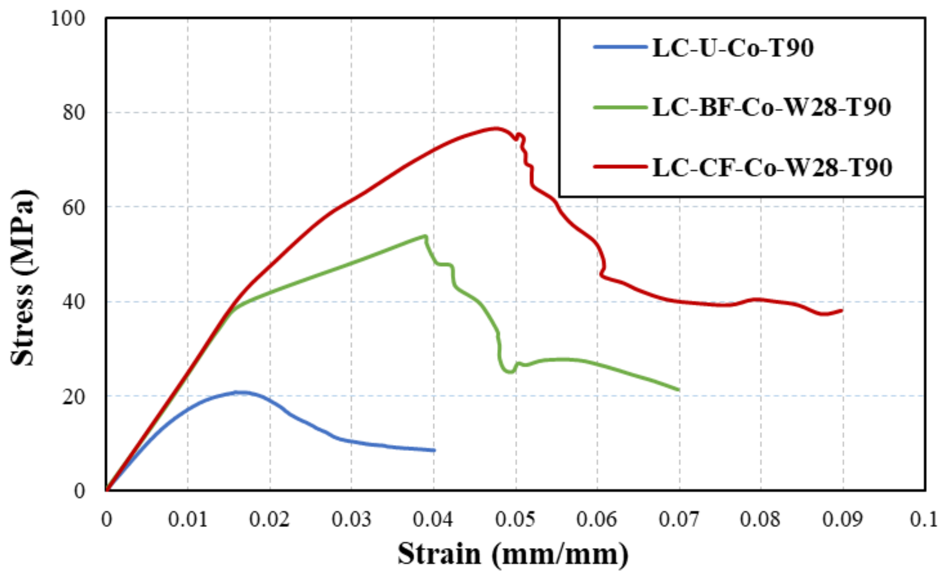

b) LCFA-ECC specimens

Figure 4.7 Stress-Strain Curves of wrapped and unwrapped PVA- ECC specimens

In addition to compressive strength, ductility was also increased as a result of the FRP wrappings of the specimens. The increase in ductility was reported in the literature for ordinary concrete wrapped with FRP (Photiou *et al.*, 2004; Mesbah and Benzaid, 2017). ECC specimens generally show strain hardening response, which resulted in an increased ductility and toughness. In addition, FRP wrappings also enhance the ductile behavior. The FRP wrapped ECC specimens showed very high lateral displacement capacities and toughness, especially for the post-peak curve of the stress-strain curve, which makes FRP-ECC specimens essential in structural elements requires high strength and ductility. In the study, basalt and carbon FRP fabrics increased the strain from 0.04 to 0.07 and 0.04 to 0.09, respectively as shown in Figures 4.5 and 4.6. The obtained higher strength and strain resulted from the confinement effect of FRP fibers, which create a triaxial state of the stress along the concrete specimen height. After FRP rupture, ECC concrete continued to carry the load until the failure of PVA fibers. Specimens wrapped with carbon FRP fabrics showed superior performance than the specimens wrapped with basalt FRP fabrics, and the poor performance was obtained in the unwrapped specimens as shown in Figure 4.7.

4.3.4 Failure modes of specimens under compression load

During compression load, expansion of concrete expected on cylinder specimens and both PVA fibers and FRP fabrics resisted the expansion and created a confinement in the circumferential direction of the cylinder specimens. When tensile stresses due to axial load exceed the FRP-ECC matrix composite tensile strength resistance, FRP rupture occurred and ECC matrix continued to carry the axial load until the failure of the PVA fibers. In the study, all failure mechanism realized first FRP rupture and then the failure of PVA-ECC matrix. However, the failure due to poor vertical lap joints had rarely been reported by some studies (Nanni and Bradford, 1995; Demers and Neale, 1999).

Figure 4.8 shows the fracture or failure shapes of the specimens. The crack formation started around the top or bottom region of the specimen and crack openings progressed until the failure at these locations due to high-stress concentrations caused by the friction between the machine plates and the specimen. Since FRP fabrics oriented uni-directional, sudden rupture of the FRP fabrics was realized due to FRP fabrics rupture and hence stress transfer cannot be possible between FRP fibers. During various stages of tests, small popping noises were heard as stated previous studies (Lau and Zhou, 2001; Chaallal *et al.*, 2003; Taghia and Bakar, 2013; Chakrabortty and Khennane, 2014). It was clearly observed that the failure of the most of the specimens occurred at the top or bottom region of the specimen when the FRP fabrics were taken off upon specimen failure.

Failure of the unwrapped ECC specimens occurred more violent than the specimens wrapped with FRP fabrics. Due to the high bond strength of PVA fibers, the formed cracks cannot propagate into the mid-lengths of the specimens in general (Li *et al.* 2002). The failure of the unwrapped specimens occurred near the top and bottom of the specimens as similar to the wrapped ones. However, failure of the specimens subjected to acid became under axial or shear failure as shown in Figure 4.8. This may result from gypsum and ettringite formation at the outer surface (~ 1 cm) under sulphuric acid environment. The sulphuric acid created additional tensile stresses and caused defects in the concretes. When the acid effect combined with the external axial load, the cracking may occur at the weakest defects and further elongate along the specimen heights.

(a) U-LCFA (b) U-HCFA (c) BF-LCFA (d) CF-LCFA

(e) U-LCFA (f) U-HCFA (g) BF-LCFA (h) CF-LCFA

Figure 4.8 Failure mode of PVA-ECC specimens under acid (a,b,c,d) and under ambient (e,f,g,h) environments

4.4 Cyclic Loading

Figures 4.9 and 4.10 illustrate the axial stress-strain curves of the tested specimens under both static and cyclic loading. The pre-peak behavior of unwrapped specimens under static and cyclic loading was found almost linear until the peak loads even for the specimens exposed to acid attack, Figure 4.9. However, for the post-peak behavior of unwrapped specimens under acid attack, the static and cyclic curve separated from each other, which may be resulted from the further decrease in elastic modulus due to the softening and decreased rigidity of specimens with increasing loading/unloading cycles. This result can be observed especially for HCFA specimens due to high CaO content.

For wrapped specimens, the pre-peak behavior of wrapped specimens assumed as linear until the points that correspond to the failure of unwrapped ones, Figure 4.10. After that (at higher stresses), the elastic modulus of PVA-ECC composite decreased due to the cracks occurred in the concrete matrix. However, higher stresses were attained due to the existence of the FRP fabrics. In the post-peak curve, similar stress relaxation was also observed for both static and cyclic loading. It may be attributed to the elastic behavior of the FRP, which improved the resistance of the specimens under cyclic loadings. The favorable effect of carbon and basalt FRP material on the post-peak curve can be easily observed under acid attack.

The envelopes of all stress-strain curves of ECC-specimens under cyclic loading can be attained by connecting the peaks of the unloading cycles (envelope curve) on the stress-strain curves and the obtained curve matches well with the stress-strain curve of the specimens under static loading. Similar observations were also reported by previous studies (Lam *et al.*, 2006) and (Shah *et al.*, 1983) and they also stated that this is also valid for concretes that confined by FRP. In this study, the cyclic and static curves of specimens confined by basalt FRP and carbon FRP complied with each other as shown in Figure 4.10. The similar findings were also observed in previous studies (Shah, *et al.*, 1983; Theodoros, 2001; Lam *et al.*, 2006).

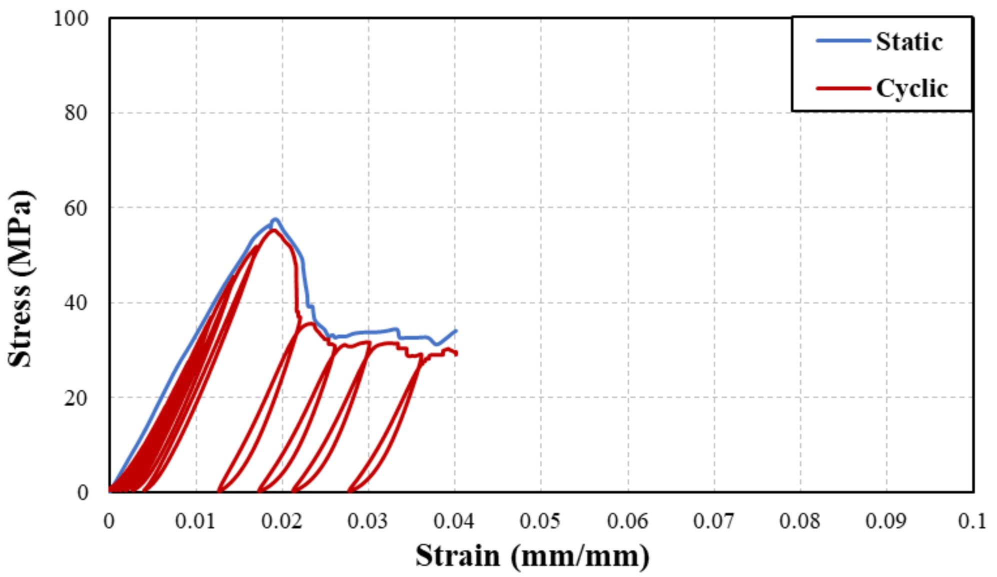

a) HCFA-ECC specimen exposed to ambient environment

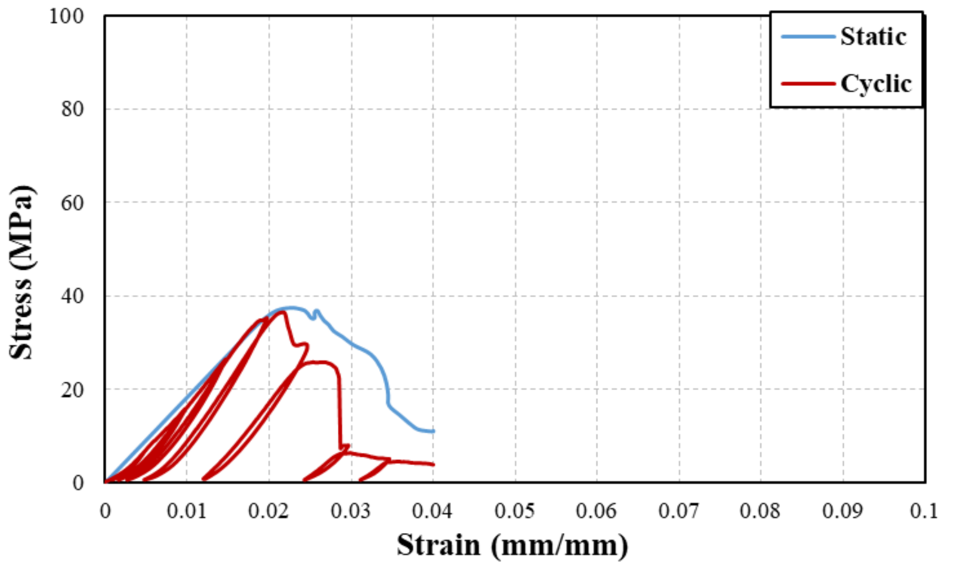

b) HCFA-ECC specimen exposed to acid environment

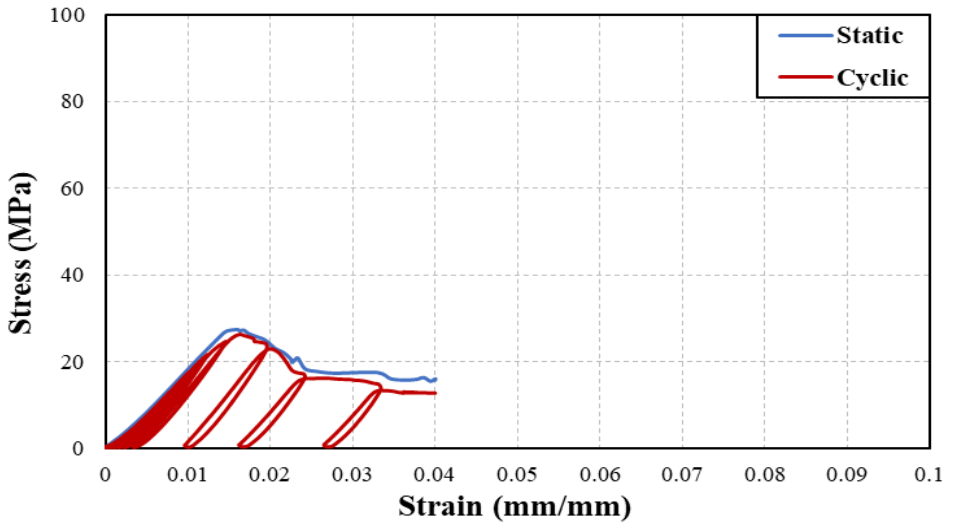

c) LCFA-ECC specimen exposed to ambient environment

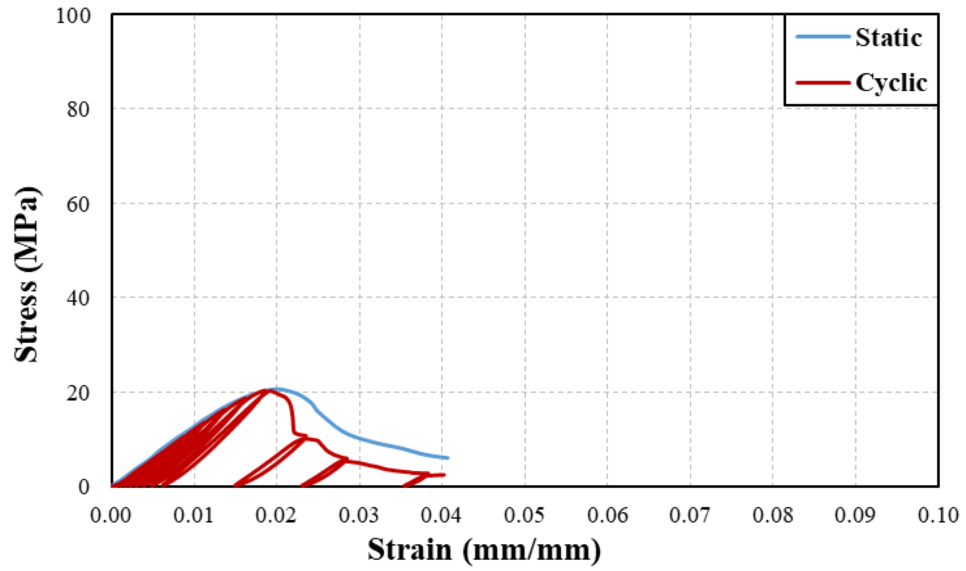

d) LCFA-ECC specimens exposed to acid environment

Figure 4-9 Static and cyclic loading diagrams of unwrapped ECC specimens

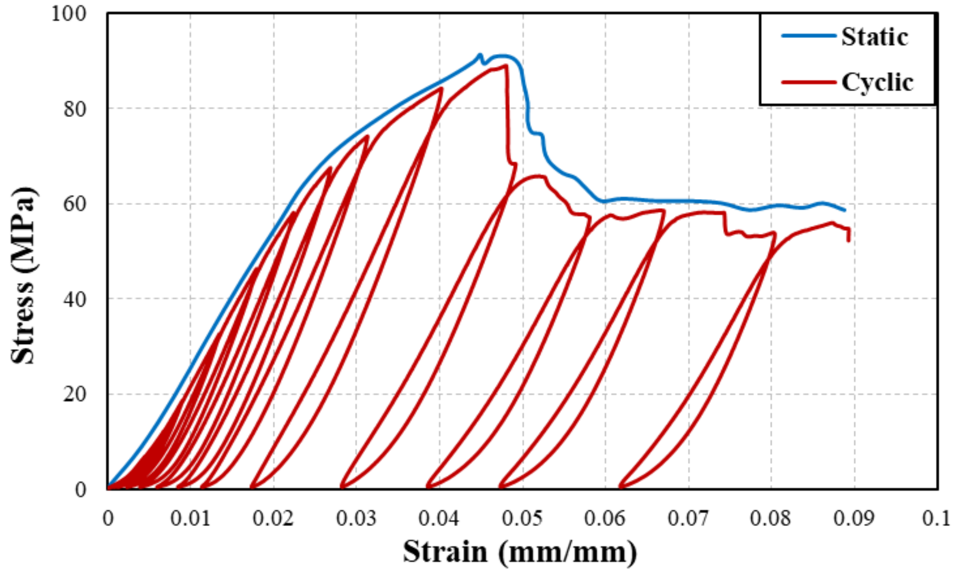

a) HCFA-ECC specimen wrapped by CFRP exposed to ambient environment

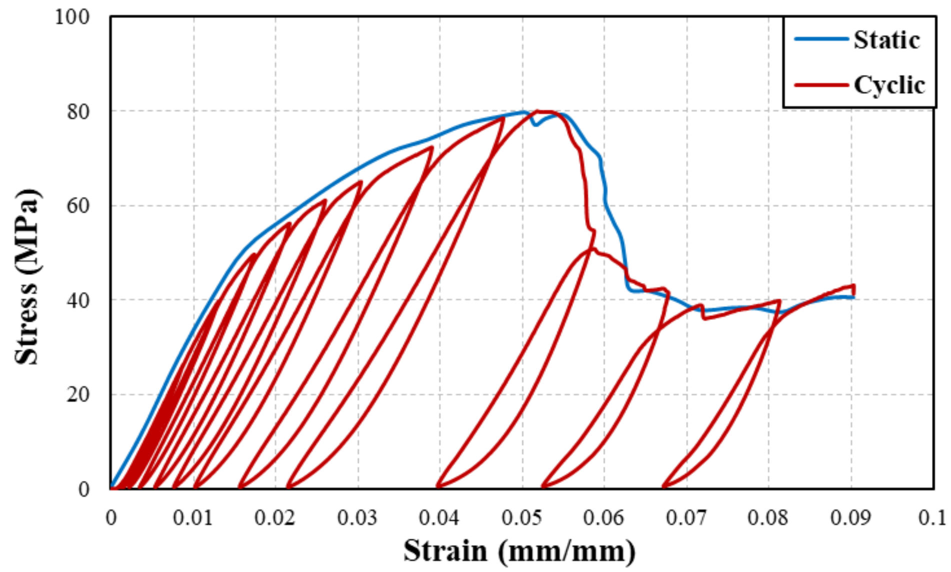

b) HCFA-ECC specimen wrapped by CFRP exposed to acid environment

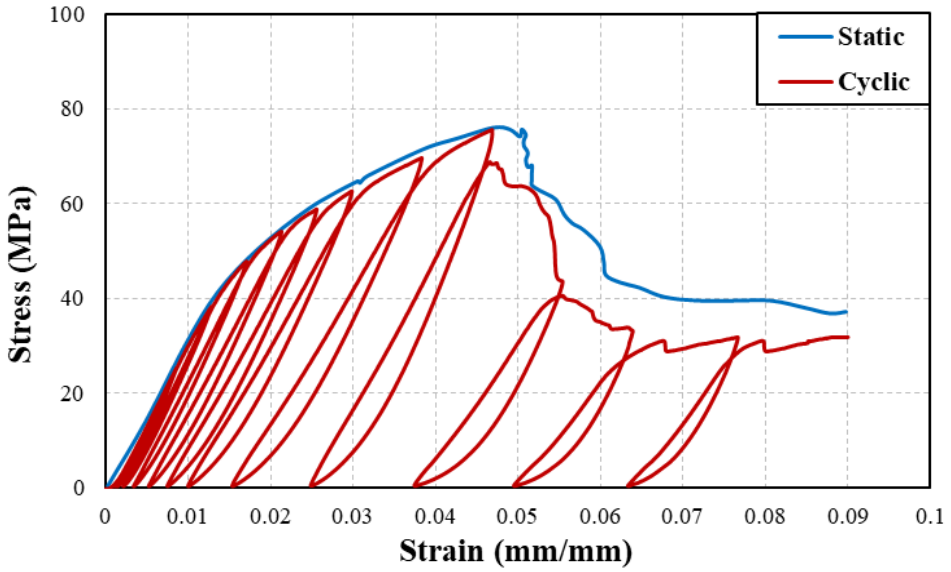

c) LCFA-ECC specimen wrapped by CFRP exposed to ambient environment

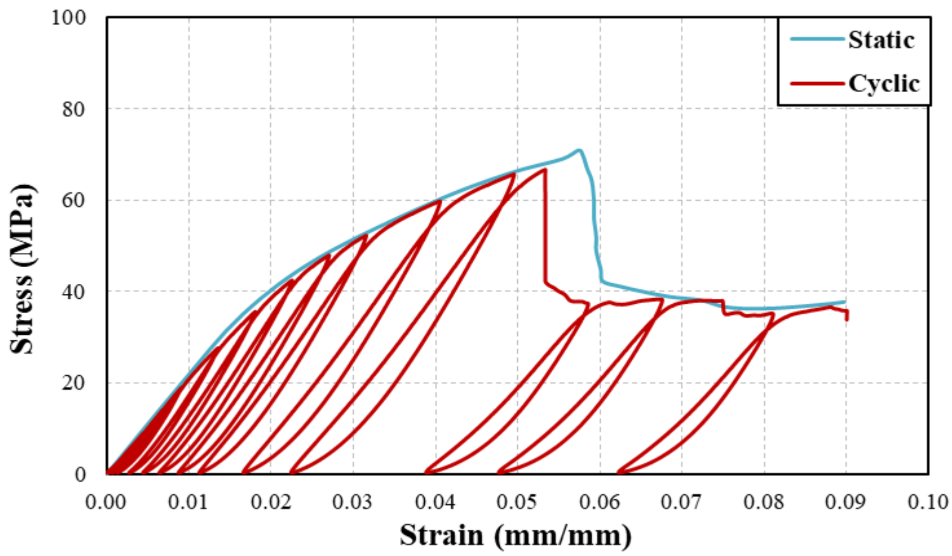

d) LCFA-ECC specimens wrapped by CFRP exposed to acid environment

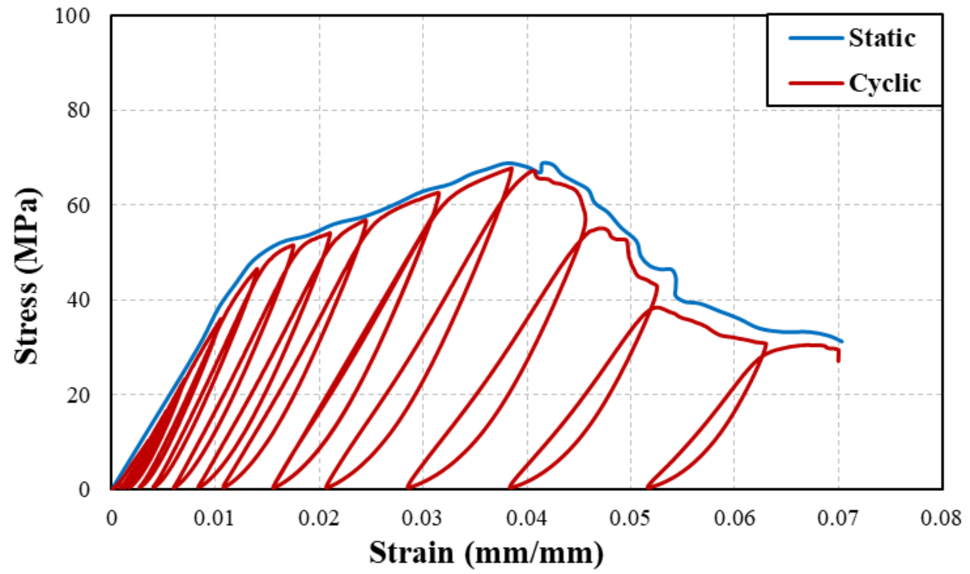

e) HCFA-ECC specimen wrapped by BFRP exposed to ambient environment

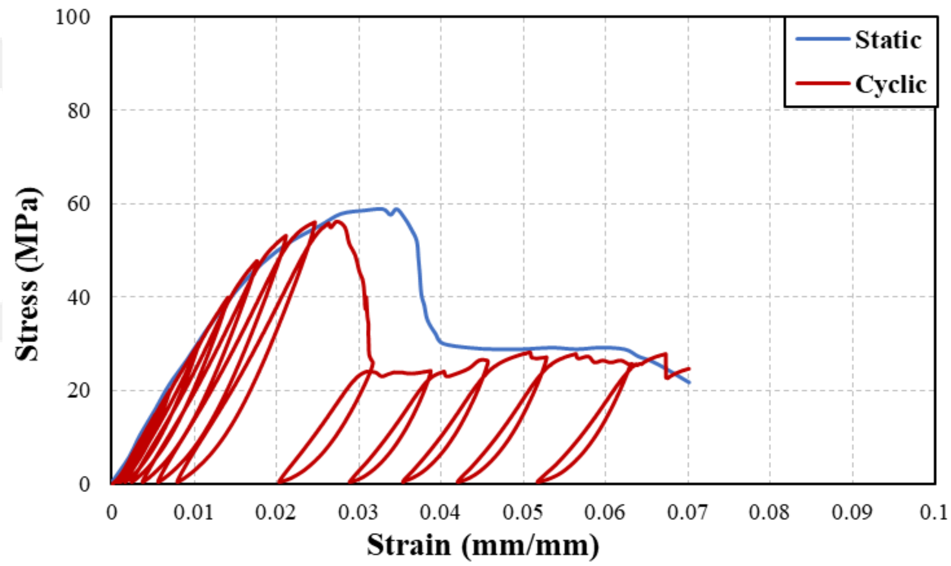

f) HCFA-ECC specimen wrapped by BFRP exposed to acid environment

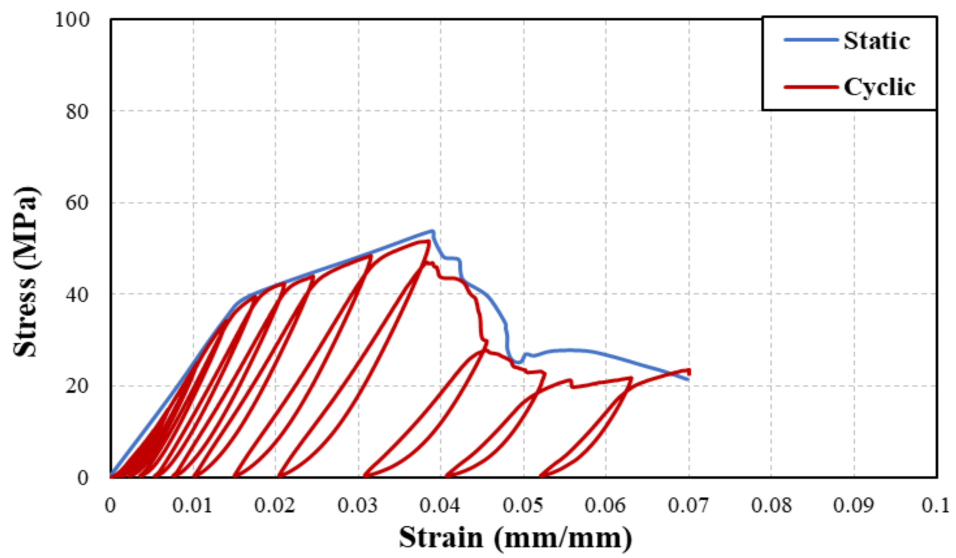

g) LCFA-ECC specimen wrapped by BFRP exposed to ambient environment

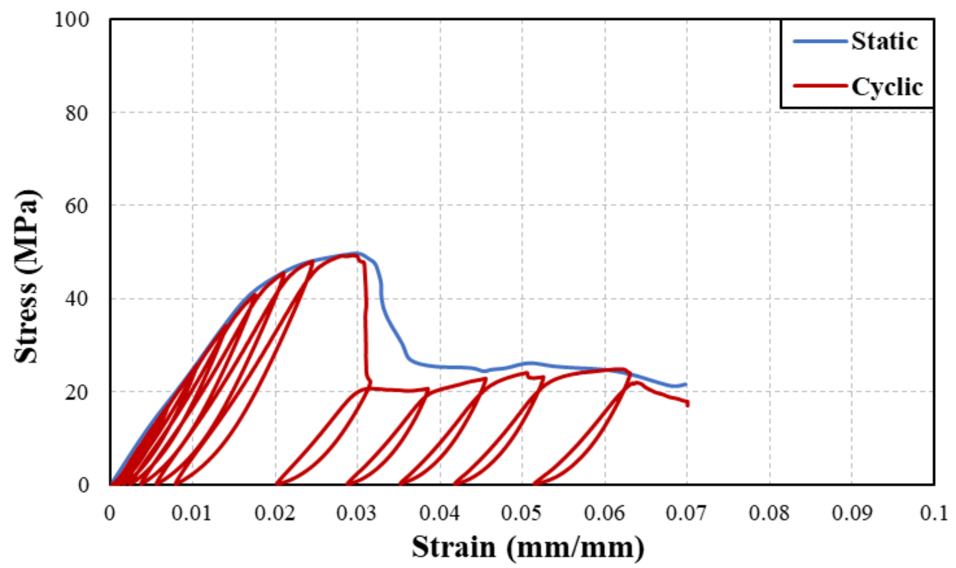

h) LCFA-ECC specimens wrapped by BFRP exposed to acid environment

Figure 4.10 Static and cyclic loading diagrams for wrapped ECC specimens

4.5 Scanning Electron Microscopy (SEM)

Wrapped and unwrapped ECC samples were analyzed in details by scanning electron microscopy (SEM) to observe changes in the surface of PVA fibers and the interfacial transition zone between the fiber and the matrix. In addition, the changes on the surfaces of basalt and carbon FRP fabrics were investigated in microscale. One inch (2.54 cm) slices of the specimens were cut and discarded from both top and bottom regions and 1 cm thick circular slice from the middle sections of the specimens was used for SEM analysis. The width of the acid affected zone was about 8 mm from the outer layer of the cylinder specimen as shown in Figure 4.2. Therefore, two SEM photos were taken for each specimen, one of them was taken at the acid affected zone (0-1 cm from the surface) and the other one was taken from the unaffected zone (close to the affected zone but out of the 1 cm outer layer).

Figure 4.11 illustrates the SEM images of the ECC specimens without wrapping under different environments. The white deposits composed on the surface of the PVA fibers and the number of white deposits was higher especially for HCFA specimens than LCFA specimens. Due to the high calcium content, Ca/Si ratio becomes higher and the free calcium results in deterioration of the cement paste. In addition, the formation of gypsum and ettringite can cause expansion, dimensional instability, cracking, spalling and loss of mechanical performance (Bassuoni and Nehdi, 2007; Ariffin *et al.*, 2013). As indicated previously, SEM pictures were also taken out of the acid affected zone (the region after 1cm from the outer surface) and less vitreous phases were concentrated on the PVA fibers. SEM results indicated that sulphuric acid attacks started from the outer layer and progressed into the inner side of the specimens. The white deposits also observed in the interfacial transition zone, which deteriorated the bond between PVA fibers and cement matrix. The adverse effect of sulphuric acid on LCFA specimens was lower than the HCFA specimens in both acids affected and unaffected zones.

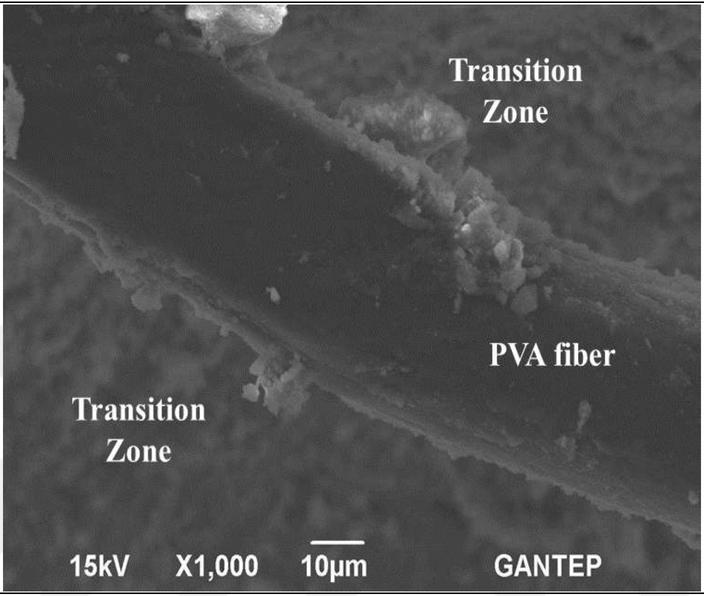

a) HCFA-ECC specimen exposed to ambient environment

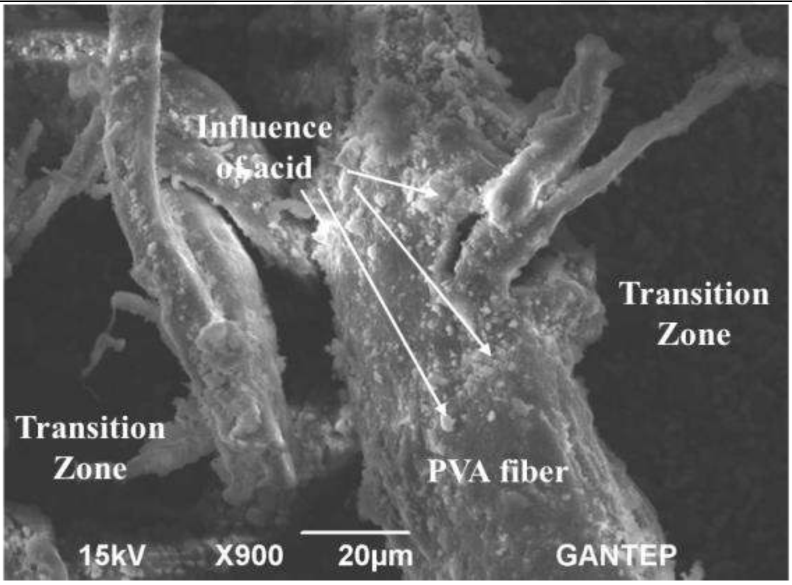

b) HCFA-ECC specimen exposed to acid environment (at the outer part 0.8cm)

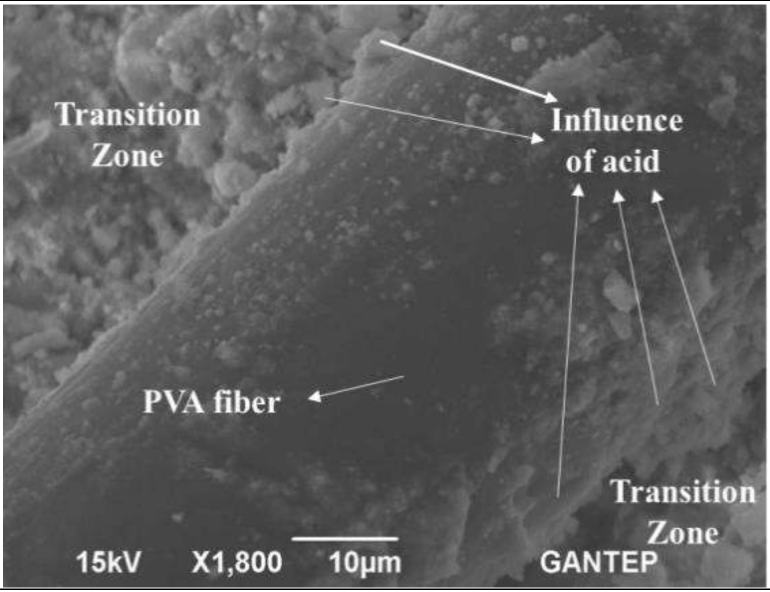

c) HCFA-ECC specimen exposed to acid environment (after 1cm from the outer surface)

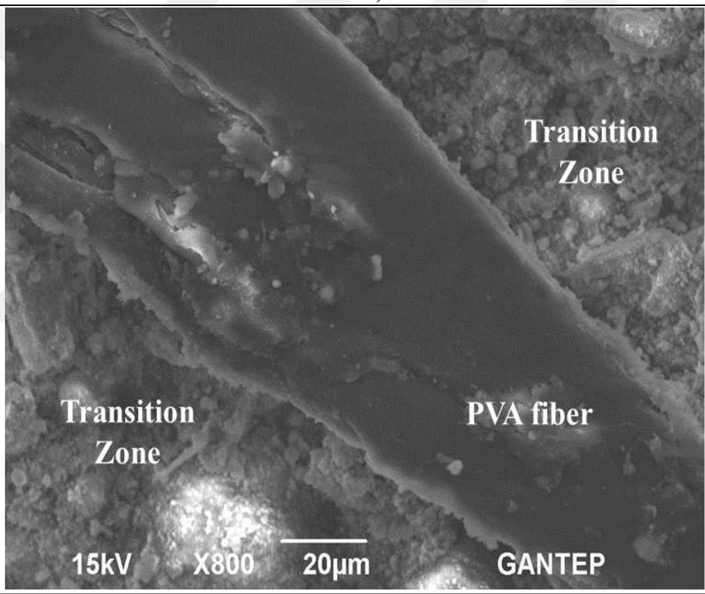

d) LCFA-ECC specimens exposed to ambient environment

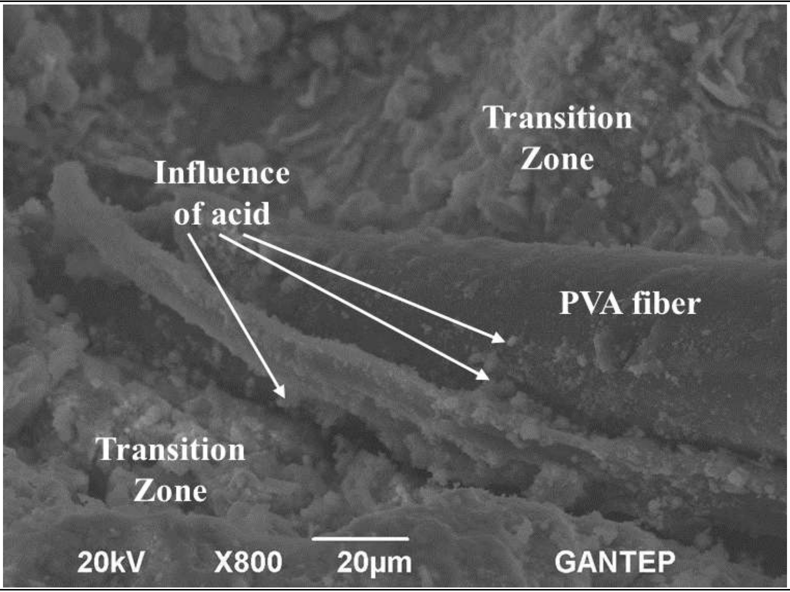

e) LCFA-ECC specimen exposed to acid environment at the outer part (0-1 cm)

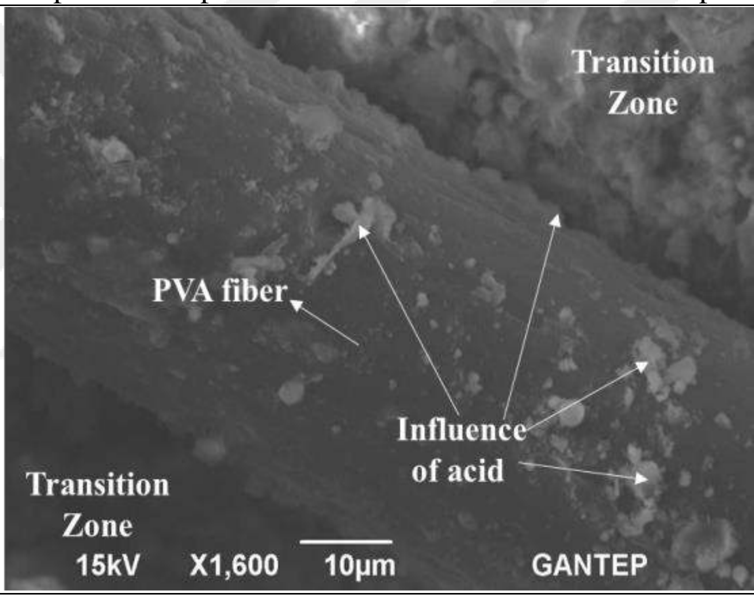

f) LCFA-ECC specimens exposed to acid environment at the part after 1cm

Figure 4.11 SEM photos of unwrapped ECC specimens exposed to ambient and acid environment

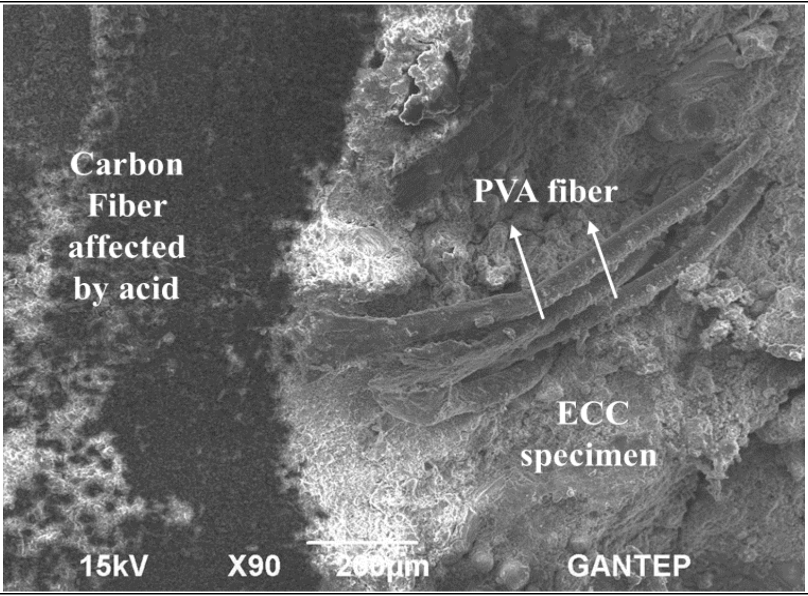

a) 200µm scale of LCFA-ECC specimen wrapped by CFRP exposed to acid environment at the outer part (0-1cm)

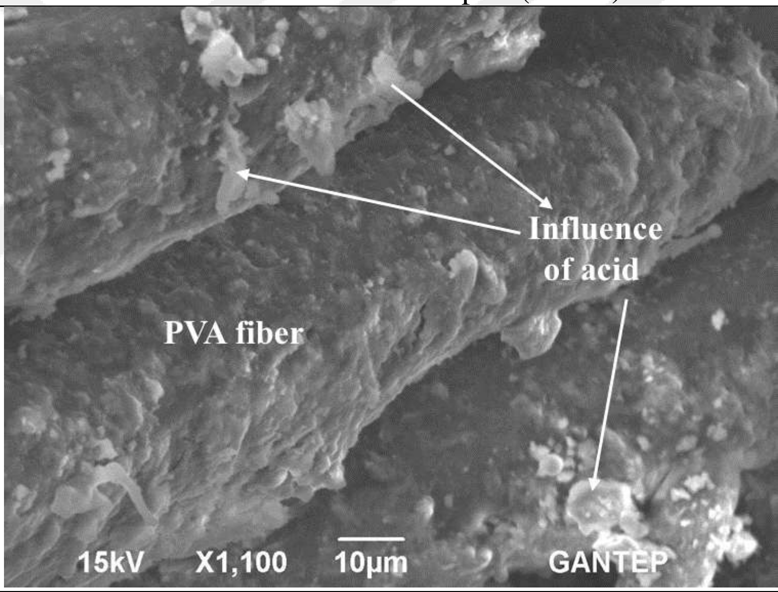

b) 10µm scale of LCFA-ECC specimen wrapped by CFRP exposed to acid environment at the outer part (0-1cm)

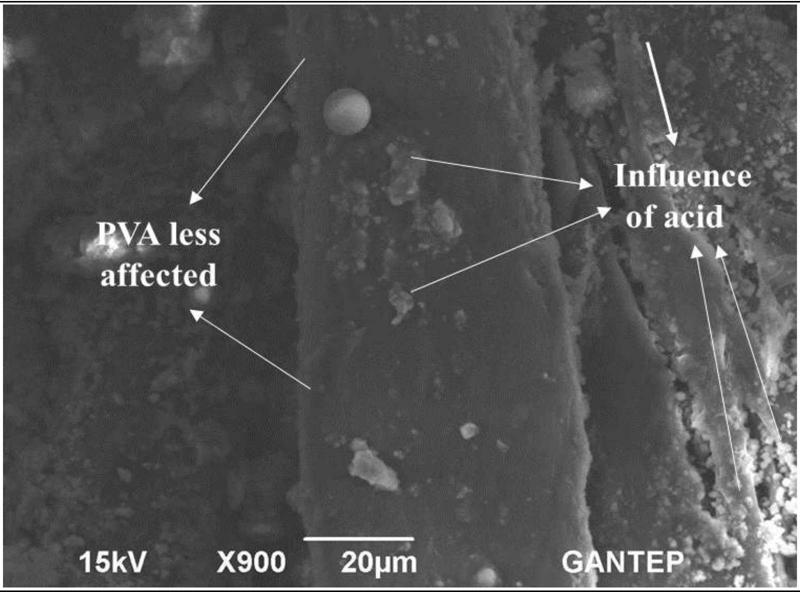

c) 20µm scale of LCFA-ECC specimen wrapped by CFRP exposed to acid environment at the part after 1cm

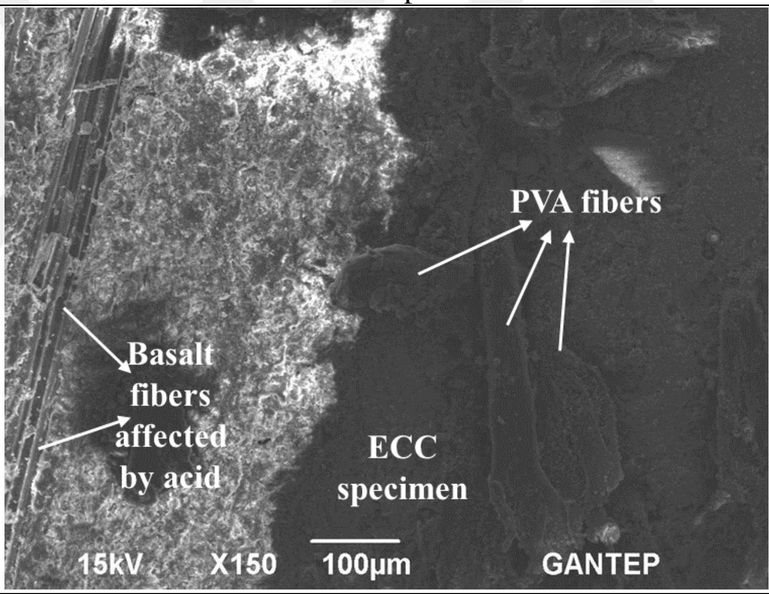

d) 100µm scale of LCFA-ECC specimen wrapped by BFRP exposed to acid environment at the outer part (0-1cm)

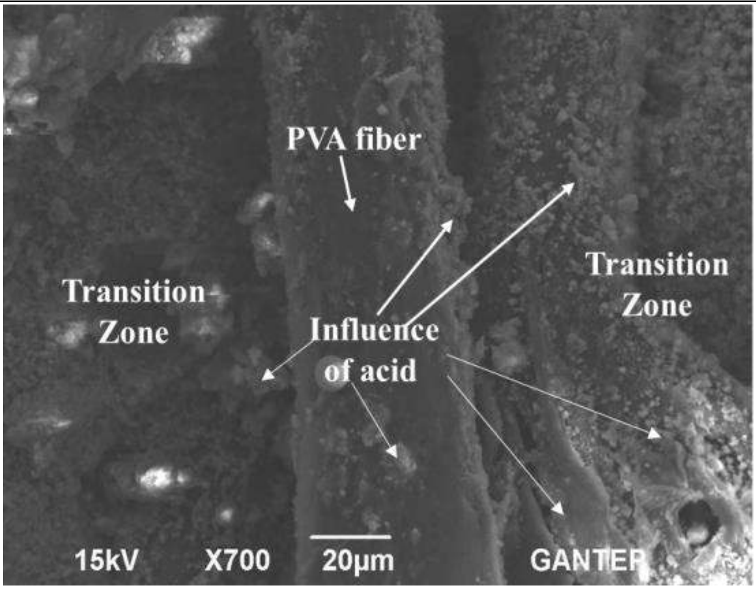

e) 20μm scale of LCFA-ECC specimen wrapped by BFRP exposed to acid environment at the outer part (0-1cm)

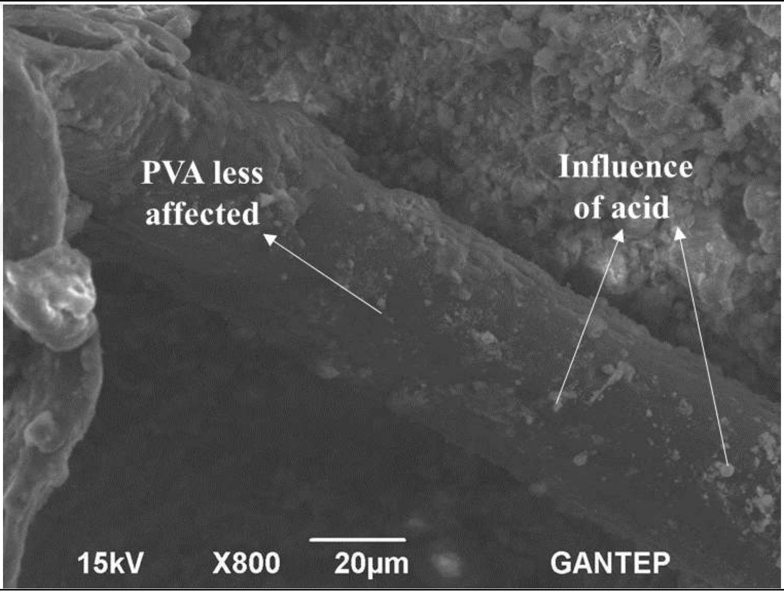

f) 20μm scale of LCFA-ECC specimen wrapped by BFRP exposed to acid environment at the part after 1cm

Figure 4.12 SEM photos of FRP wrapped ECC specimens exposed to ambient and acid environment

Figure 4.12 presents the SEM pictures of carbon and basalt FRP wrapped LCFA specimens. Results indicated that PVA fibers wrapped with carbon and basalt FRP deteriorated less than unwrapped PVA fibers in the acidic environment. Due to the sensitivity of the epoxy to the acidic environment, CFRP and BFRP fabrics were also significantly affected by the acid attack. In addition, CFRP wrapped specimens were less influenced compared to BFRP wrapped specimens due to the higher bond between CFRP fabrics and the epoxy as shown in Figure 4.13.

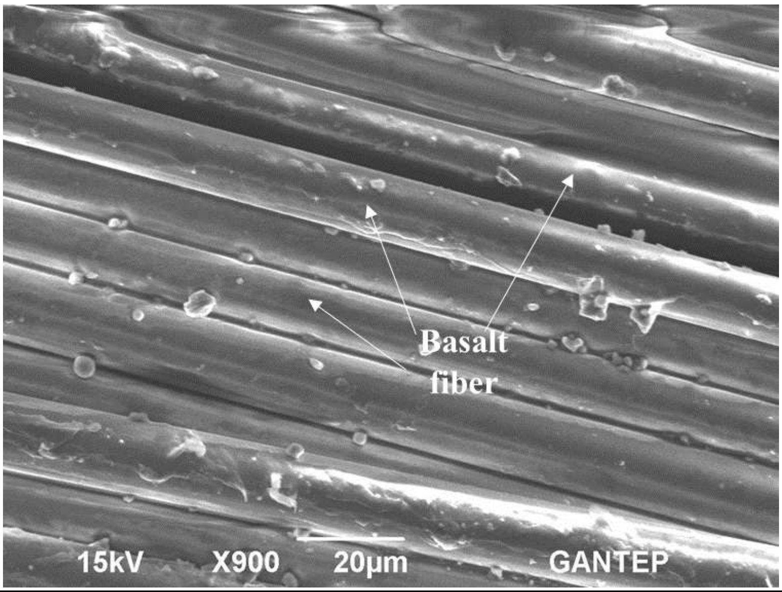

a) BFRP sheet without epoxy exposed to ambient environment

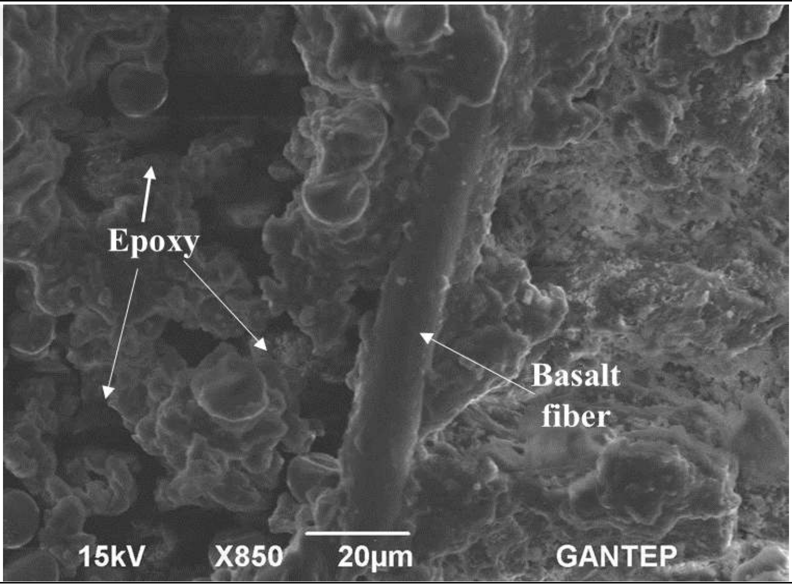

b) BFRP sheet with epoxy exposed to ambient environment

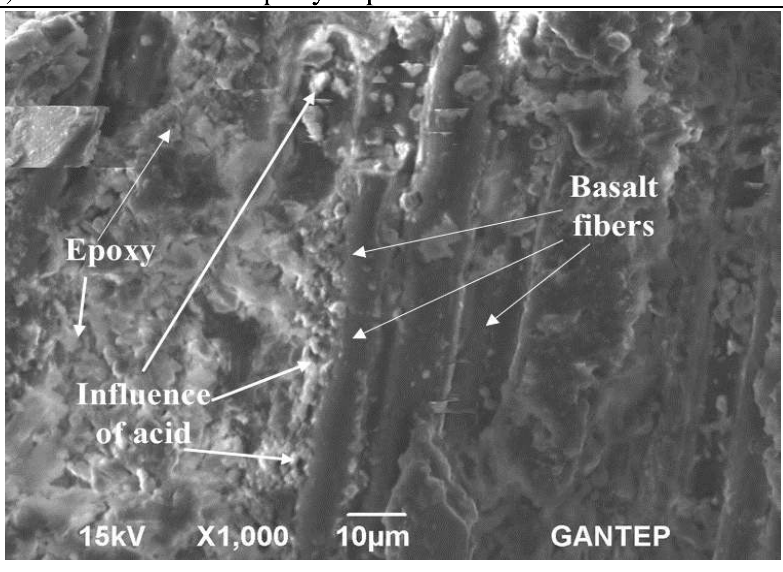

c) BFRP sheet with epoxy exposed to acid environment

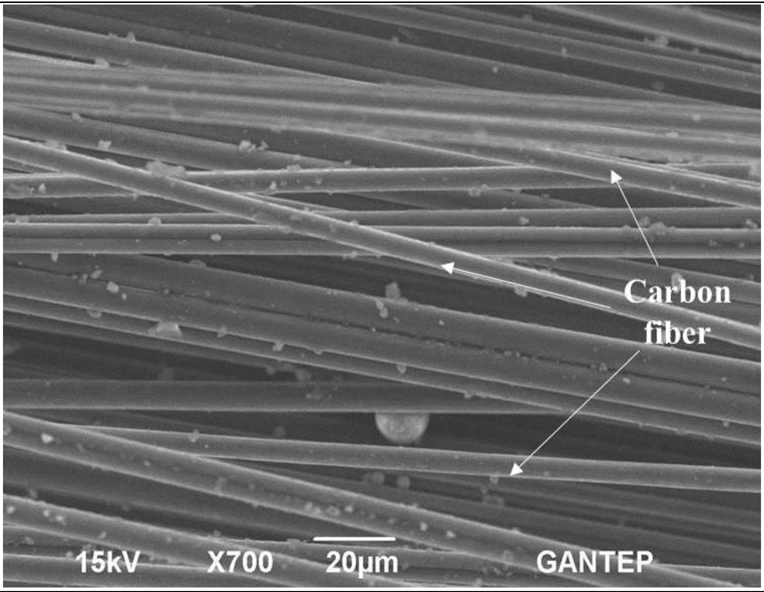

d) CFRP sheet without epoxy exposed to ambient environment

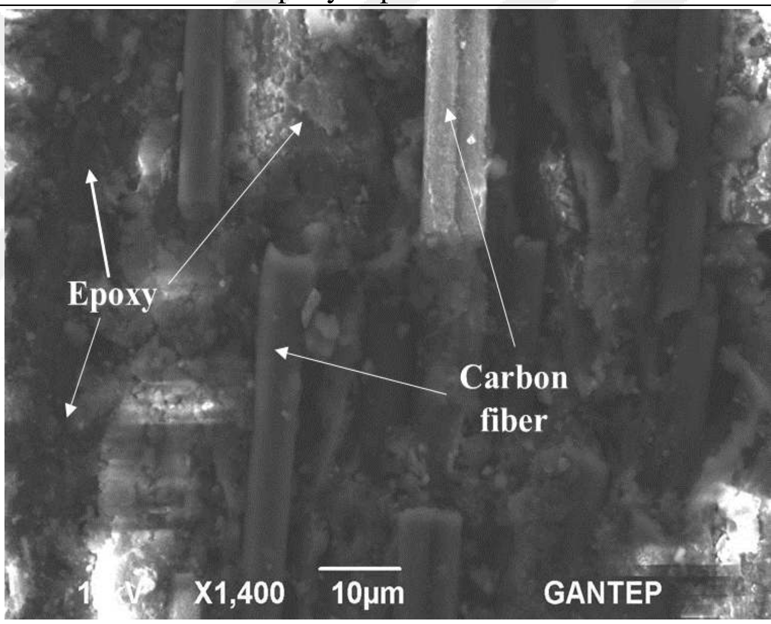

e) CFRP sheet with epoxy exposed to ambient environment

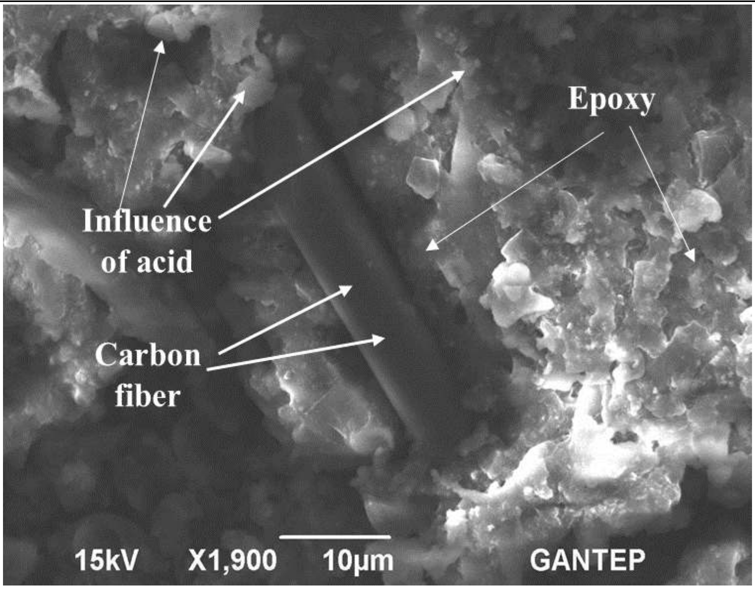

f) CFRP sheet with epoxy exposed to acid environment

Figure 4.13 SEM photos of BFRP and CFRP fabric sheets exposed to ambient and acid environment

CHAPTER 5
MAGNESIUM SULFATE ATTACK

5.1 Visual inspection

Visual inspection of specimens indicated after 8-weeks of exposure to sulfate attack. It was observed that there is no change in visual appearance, cracking or spalling on the specimens, sign of surface erosion except seen a very thin layer of efflorescence on the outer surface of exposed specimens as compared to the state before they were exposed. When specimens were inspected in details, unconfined ECC specimens deteriorated and PVA fibers were also deteriorated by sulfate solutions. ECC specimen confined by both FRP fabrics also deteriorated by sulfate solution. However, in this case, the deterioration was only noticed at the unwrapped part of the specimens (the top and bottom parts of the cylinder specimens). Due to the confinement in the lateral direction, the deterioration was not noticed as seen in Figure 5.1. In previous study on the resistance of conventional concretes and geopolymer to sodium sulfate, there was no obvious change in visual examination on the outer surface of exposure specimens (Visitanupong, 2009).

Wallah and Rangan (Wallah and Rangan, 2006) investigated the influence of 2% sulphuric acid attack on geopolymer concrete and stated that the 20 mm outer side of the cylinder concrete only were affected by sulphuric acid damage, which had a 100 mm diameter. In this study, also 100 mm cylinder concrete exposed to magnesium sulfate attack was studied and similar observations with the previous study were found (Wallah and Rangan, 2006). Sulfate penetration was found at the 8 mm outer part of the cylinder specimens, and the remaining inner parts were noticed unaffected as shown in Figure 5.1. It was clearly noticed that the sulfate damage in unconfined specimens was found more severe than specimens confined by carbon and basalt FRP fabrics. This result was also supported by the previous study, which found out that the chemical solution is a surface phenomenon and the damage starts at the surface and progresses within the concrete (Attiogbe and Rizkalla, 1988). In addition, SEM inspections were also achieved at the sulfate influenced and uninfluenced zones, as shown in Figure 5.1.

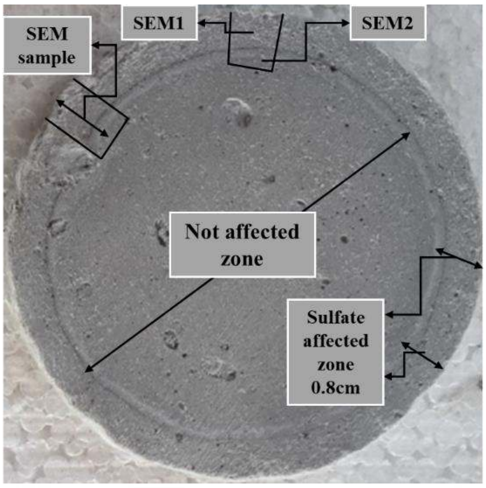

(a) LCFA specimen exposed to sulfate

(b) LCFA Control specimen

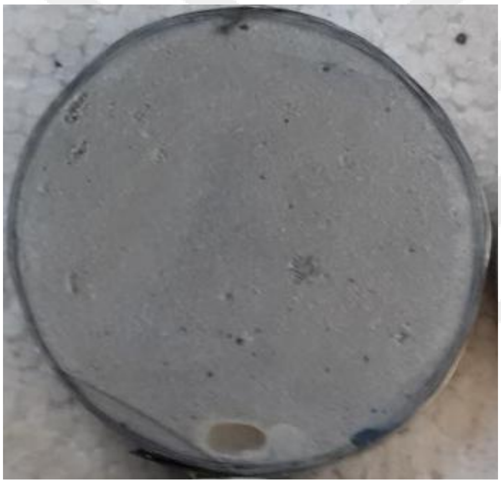

(c) CFRP-ECC exposed to sulfate

(d) BFRP-ECC exposed to sulfate

Figure 5.1 Detail of ECC cylinder specimen showing sulfate affected zone and SEM samples places

5.2 Weight change

Figure 5.2 indicates weight change (%) of the specimens under two months of chemical exposure. Results presented that all specimens had weight gain under sulfate solution absorption, and unconfined specimens showed highest weight gain. The gained weights were 0.98 % for LCFA specimens and 1.22% for HCFA specimens. Confined HCFA also showed slightly higher weight gain than the confined LCFA specimens. Moreover, the lower weight gain showed in LCFA specimens confined by carbon FRP and therefore, the specimens confined by CFRP fabrics showed slightly better chemical resistance than BFRP fabrics under sulfate attack. Lower weight gains showed in confined and unconfined LCFA specimens may be due to the higher fineness ratio, which caused a reduction in porosity and reduced chemical solution absorption. The earlier research was also reported the weight gain due to chemical exposure (Mohammed, 2007; Thokchom, 2014). The penetration of harmful actions from chemical solution reacted with cement and caused the formation of gypsum and ettringite. As a result, increased volume by a factor of about two and reduced density of concrete (Soroka, 1979). Therefore, initial weight gains of the specimens exposed to the chemical solution may be due to the increase in relative volume was more than the reduction amount in relative density (Attiogbe and Rizkalla, 1988).

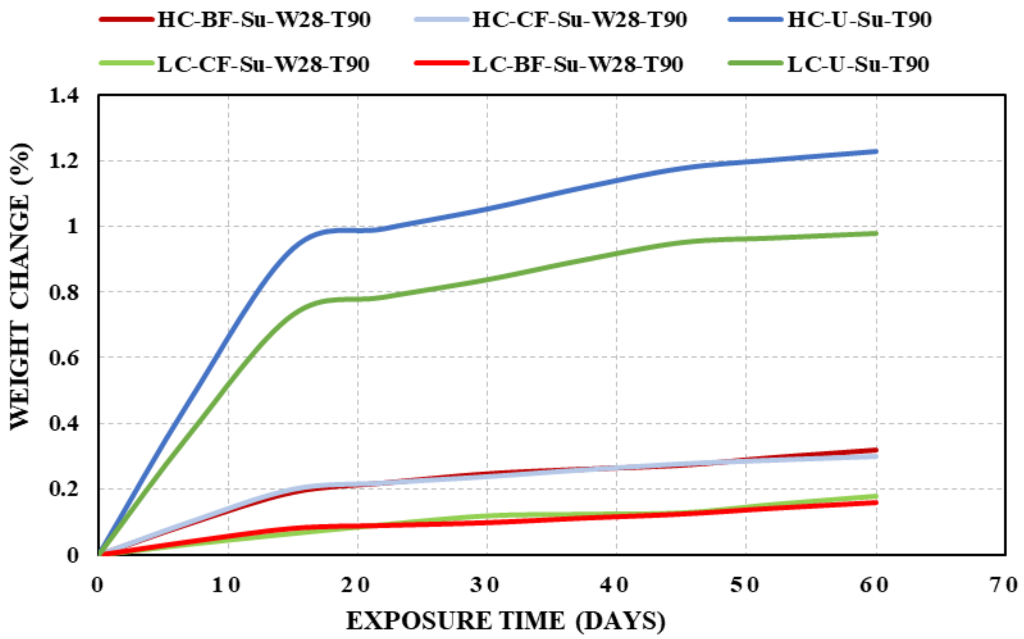

Figure 5.2 Weight change in ECC specimen exposed to sulfate attack for duration 60 days

5.3 Compressive strength of the specimens

In general, the behaviors of ECC specimens confined by FRP fabrics under axial load were found to be consistent with the performance of conventional concrete confined by FRP in the literature. During early stages of the axial loading process, the noise related to the micro-cracking of ECC-concrete was clear, which indicate the beginning of the stress transfer from the expanded ECC specimen to the FRP fabrics. The cracking noises intensity could be heard pre-failure that achieved after the slow rupture of FRP fabrics with a violent and sudden noise. Failure initiated from an overlap place of the FRP fabrics at the middle height of specimen and moved to the bottom and top of the specimens. For the tested specimens, all failures happened as a result of the rupture of FRP fabrics followed by a ductile performance of ECC and failure due to de-bonding was not observed in confined specimens. Figure 5.3 represents the compressive strengths of specimens. Results showed that specimen confined by FRP indicated superior performance than unconfined specimens under both sulfate and ambient environments.

5.3.1 Specimen nomenclature

Three types of specimens were obtained in the scope of the research; CFRP-ECC hybrid specimens (specimens confined by carbon FRP fabrics), BFRP-ECC hybrid specimens (specimens confined by basalt FRP fabrics) and control specimens (unwrapped specimens). In addition, two mixes; high calcium fly ash mix (HCFA mix) and low calcium fly ash mix (LCFA) mix were prepared. Specimens were subjected to two different environments; 5% magnesium sulfate environment and control environment (unexposed specimens). Control specimens (unexposed specimens) were tested at the ages of 28 days and 90 days, while specimens subjected to sulfate environment were tested at the age of 90 days (28 days water curing and the remaining days under sulfate environment).

As shown in Table 5.1, eight test series were designed in this study as follows:

Table 5.1 Details of test series conducted in this chapter

Test series	Type of concrete	No. of samples	Unconfined	Confined		Control sample	Sulfate exposed	Wrapping age		Testing age		Specimen ID
				BFRP	CFRP			28-days	90-days	28-days	90-days	
A	LCFA	3	✓			✓				✓		LC-U-Co-T28
		3		✓		✓		✓		✓		LC-BF-Co-W28-T28
		3			✓	✓		✓		✓		LC-CF-Co-W28-T28
B		6_a	✓			✓		✓			✓	LC-U-Co-T90
		6_a		✓		✓		✓			✓	LC-BF-Co-W28-T90
		6_a			✓	✓		✓			✓	LC-CF-Co-W28-T90
C		6_a	✓				✓	✓			✓	LC-U-Su-T90
		6_a		✓			✓	✓			✓	LC-BF-Su-W28-T90
		6_a			✓		✓	✓			✓	LC-CF-Su-W28-T90
D		3		✓			✓		✓		✓	LC-BF-Su-W90-T90
		3			✓		✓		✓		✓	LC-CF-Su-W90-T90
E	HCFA	3	✓			✓				✓		HC-U-Co-T28
		3		✓		✓		✓		✓		HC-BF-Co-W28-T28
		3			✓	✓		✓		✓		HC-CF-Co-W28-T28
F		6_a	✓			✓		✓			✓	HC-U-Co-T90
		6_a		✓		✓		✓			✓	HC-BF-Co-W28-T90
		6_a			✓	✓		✓			✓	HC-CF-Co-W28-T90
G		6_a	✓				✓	✓			✓	HC-U-Su-T90
		6_a		✓			✓	✓			✓	HC-BF-Su-W28-T90
		6_a			✓		✓	✓			✓	HC-CF-Su-W28-T90
H		3		✓			✓		✓		✓	HC-BF-Su-W90-T90
		3			✓		✓		✓		✓	HC-CF-Su-W90-T90

Note: a Three specimens under static loading and three specimens under cyclic loading.

In the Table 5.1, HC and LC indicates the high calcium FA and low calcium FA, U, CF and BF points out unconfined, confined by carbon FRP and basalt FRP fabrics, Co and Su represents the control and sulfate environments, W28 and W90 shows the wrapping ages of 28 days and 90 days, T28 and T90 demonstrates the age of compressive strength at 28 days and 90 days, respectively.

Series A: 9 LCFA-ECC control cylindrical samples (3 unconfined and 6 confined) were tested at 28 days. The FRP wrappings were also applied at 28 days.

Series B: 18 LCFA-ECC control cylindrical samples (6 unconfined and 12 confined) were tested at 90 days. The FRP wrappings were applied at 28 days.

Series C: 18 LCFA-ECC (6 unconfined and 12 confined) specimens were cured in a water tank until 28 days and FRP wrappings were applied. Then, these confined specimens immersed into 5% sulfate solution at the age of 90 days.

Series D: 6 LCFA-ECC unconfined specimens were cured in a water tank until 28 days and these unconfined specimens subjected to 5% sulfate solution at the age of 90 days. Then, sulfate exposed specimens were confined at the age of 90 days to evaluate the influence of FRP confinement as a rehabilitation method.

Series E: 9 HCFA-ECC control cylindrical samples (3 unconfined and 6 confined) were tested at 28 days. The FRP wrappings were also applied at 28 days.

Series F: 18 HCFA-ECC control cylindrical samples (6 unconfined and 12 confined) were tested at 90 days. The FRP wrappings were applied at 28 days.

Series G: 18 HCFA-ECC (6 unconfined and 12 confined) specimens were cured in a water tank until 28 days and FRP wrappings were applied. Then, these confined specimens immersed into 5% sulfate solution at the age of 90 days.

Series H: 6 HCFA-ECC unconfined specimens were cured in a water tank until 28 days and these unconfined specimens subjected to 5% sulfate solution at the age of 90 days. Then, sulfate exposed specimens were confined at the age of 90 days to evaluate the influence of FRP confinement as a rehabilitation method.

In total, 102 cylindrical specimens were cast and tested in the scope of study the effect of sulfate attack.

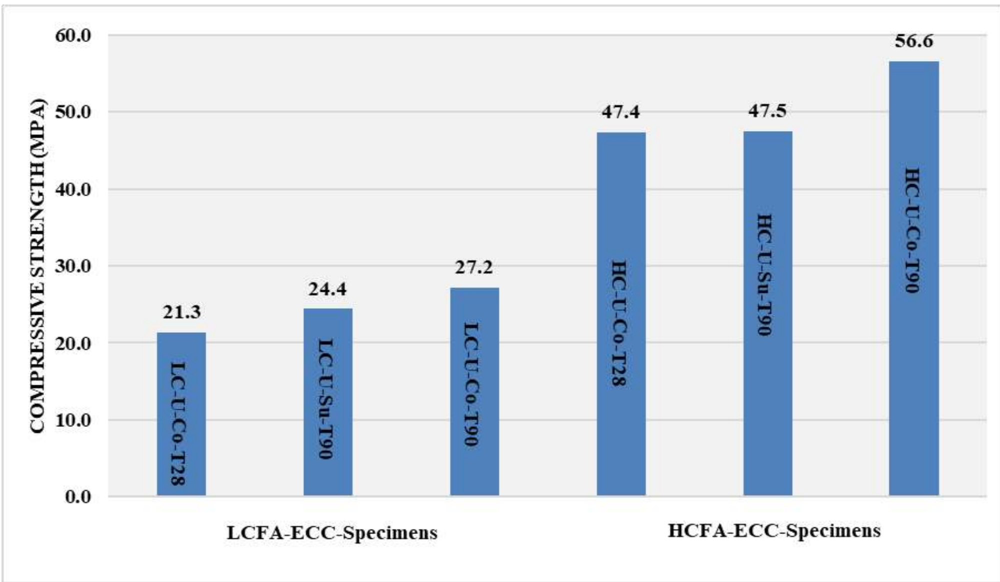

a) Unconfined ECC specimens

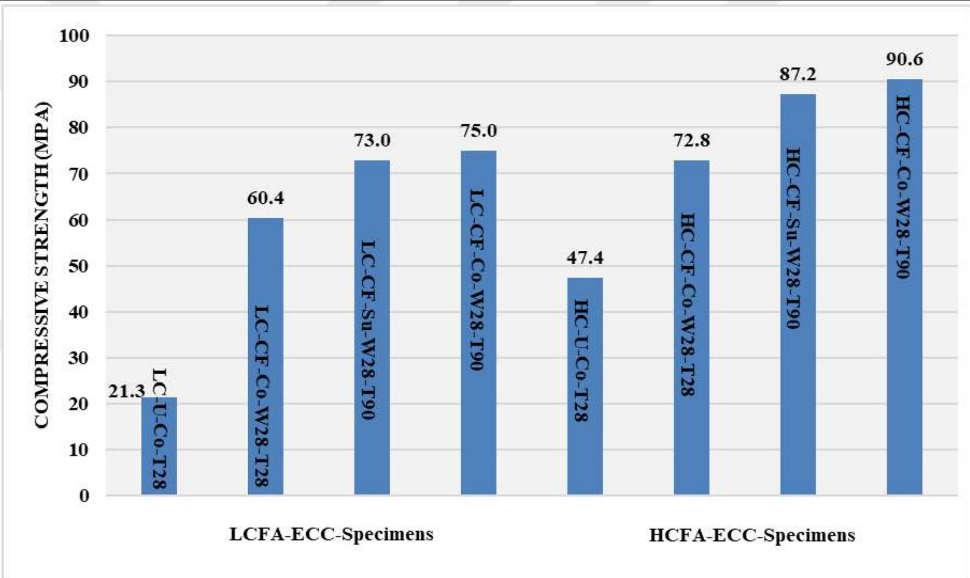

b) Unconfined ECC specimens and ECC specimens wrapped by CFRP

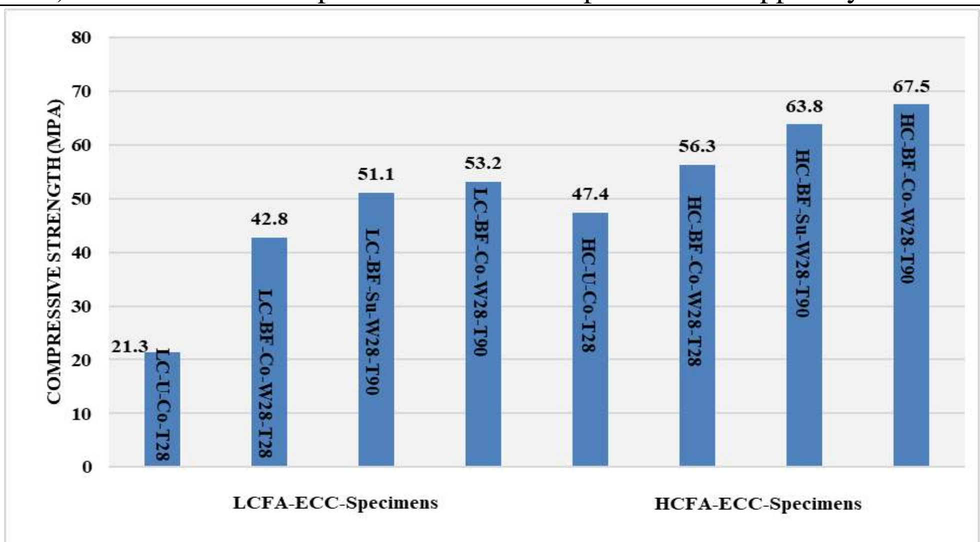

c) Unconfined ECC specimens and ECC specimens wrapped by BFRP

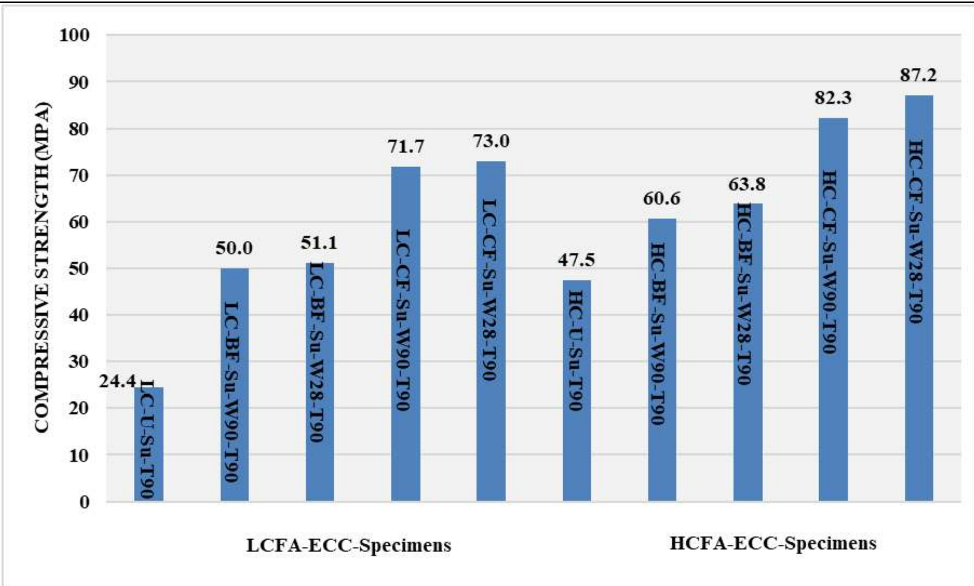

d) Unconfined ECC specimens and ECC specimens wrapped by both FRP exposed to sulfate and exposure specimens wrapped by both FRP

Figure 5.3 Compressive strength of confined and unconfined ECC specimens

5.3.2 Compressive behavior of unwrapped specimens

Figure 5.4 indicates typical compressive stress-strain curves of unconfined ECC specimens. Results showed that compressive strength of unconfined specimens increased up to 90 days. The continuity of hydration reactions and the slow pozzolanic reaction of fly ash may be the reason for the increase in the compressive strength. Similar outcomes were also stated in the previous investigations (Liu *et al.*, 2017; Zhang and Zhang, 2017).

The compressive strength values of 90-day curing specimens were 27.72% and 19.94% higher than the compressive strength values of 28-day curing for LCFA and HCFA specimens, respectively. Higher improve in the compressive strengths of LCFA specimens at 90-days ages compared to HCFA specimens was expected because of lower CaO amount in the low lime-fly ash particles (LCFA specimens) since the rate of hydration reactions was slow, where strength improvement (C_3S and C_2S creation) became time dependent. Reductions in compressive strength for the specimens exposed to sulfate attack were 10% and 16.48% for 90 days strengths of LCFA and HCFA specimens, respectively. Higher reduction in compressive strength for HCFA specimens may be also attributed to high CaO content in the in the high lime-fly ash particles (HCFA specimens).

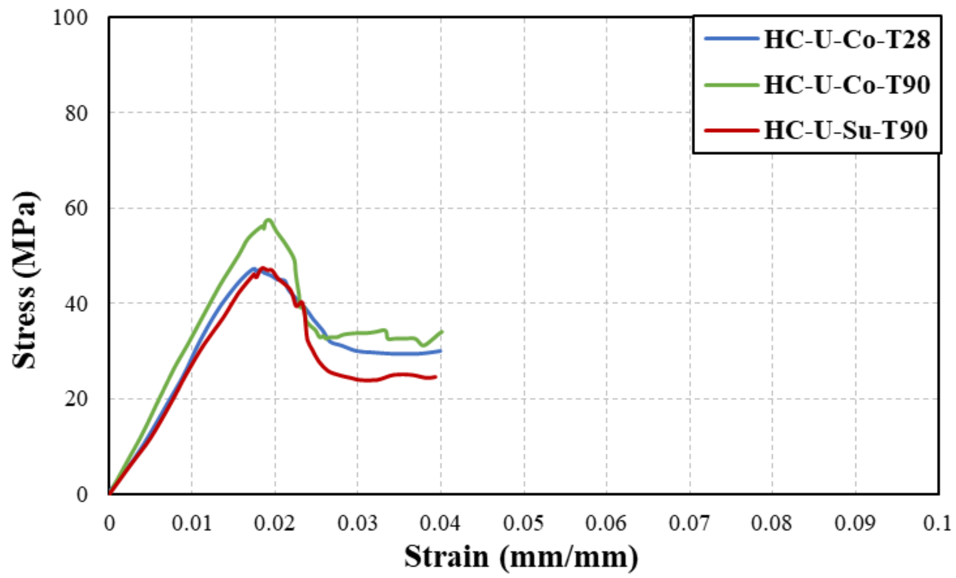

a) Unwrapped HCFA-ECC specimens

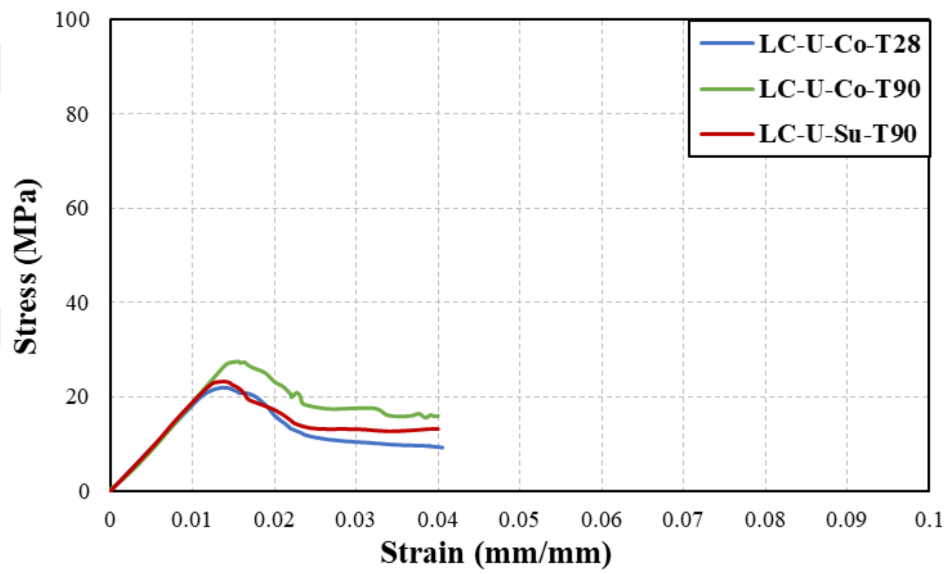

b) Unwrapped LCFA-ECC specimens

Figure 5.4 Stress-strain curves of unwrapped ECC specimens

5.3.3 Compressive behavior of wrapped specimens

Figure 5.5 represents the compressive performance of confined ECC specimens. Results showed a significant increase in compressive strength for ECC confined by FRP fabrics (more than 2-3 times) when compared to unconfined specimens. In general, the compressive load decreased suddenly as the outermost layer of FRP fabrics ruptured and then the load started to increase or continue at a constant value due to stress move from FRP fabrics to ECC concrete until the failure of the inner layer of FRP fibers and PVA fibers inside the ECC specimens (Li *et al.*, 2002).

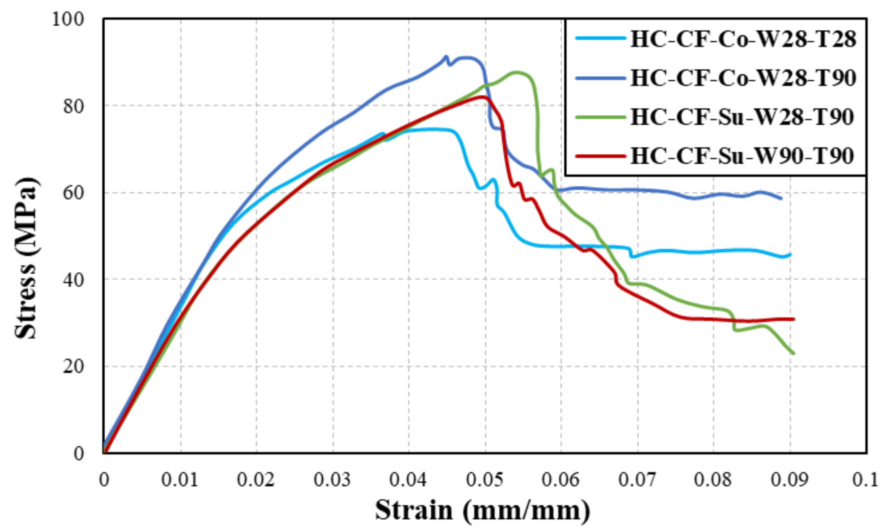

a) HCFA-ECC specimen wrapped by CFRP

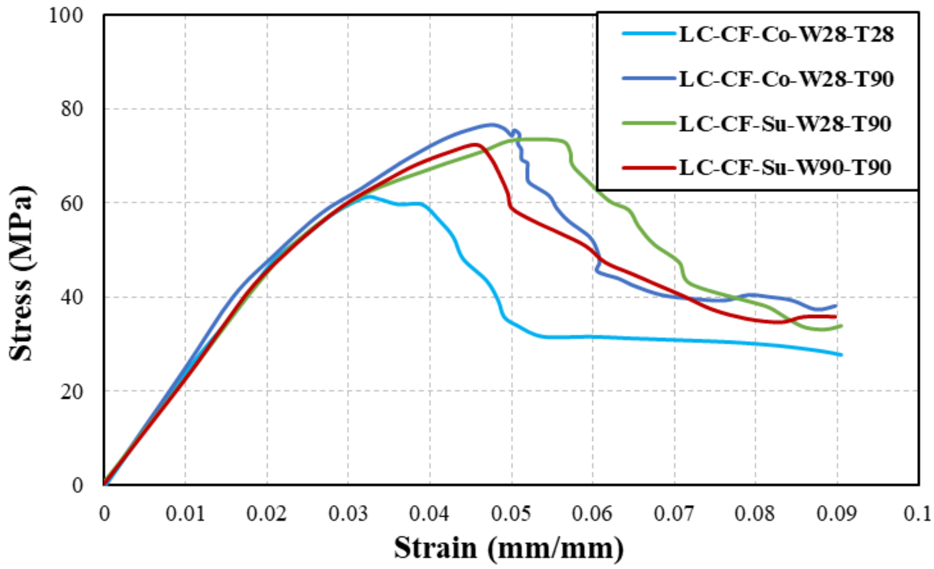

b) LCFA-ECC specimen wrapped by CFRP

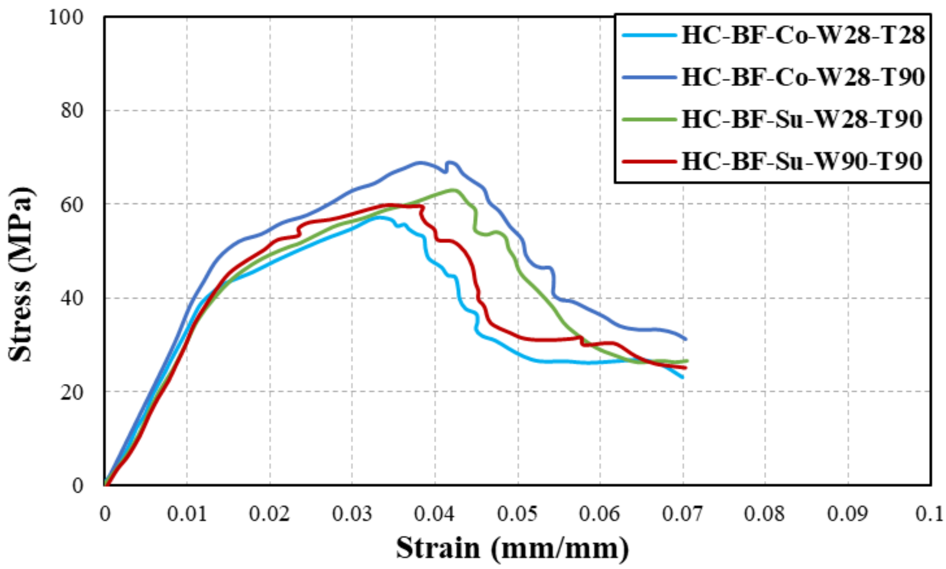

c) HCFA-ECC specimen wrapped by BFRP

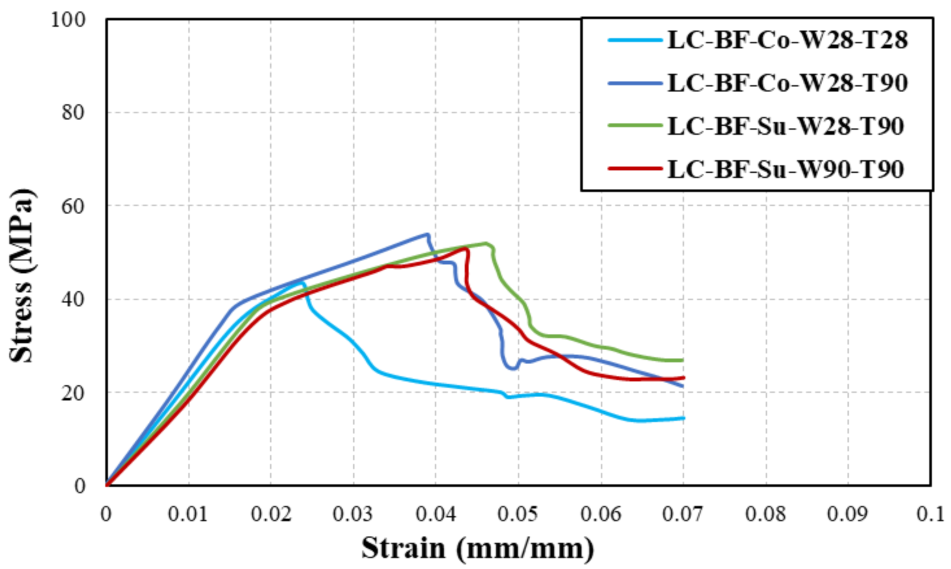

d) LCFA-ECC specimens wrapped by BFRP

Figure 5.5 Stress-strain curves of FRP confined ECC specimens

Similar to unconfined specimens, compressive strengths values of the confined specimens also increased up to the age of 90-days. The improvement amounts were 24.17% and 24.25% for LCFA specimens and 24.46% and 20.46% for HCFA specimens confined with CFRP and BFRP fabrics, respectively. Results showed that influence of concrete matrix on strength values was also important when specimens confined by FRP fibers.

Compressive strengths values of the confined specimens exposed to sulfate attack at the age of 90-days were found to be greater than the compressive strengths of the confined specimens at age of 28-day. The increasing amounts were 19.71% and 13.4% for the HCFA-ECC specimens and 20.84% and 19.37% for the LCFA-ECC specimens confined with CFRP and BFRP fabrics, respectively. Lower increase in compressive strength for the HCFA specimens may be due to the deterioration result of CaO amount especially for the specimens includes high lime fly ash. Furthermore, the compressive strengths of the confined specimens exposed to sulfate solution at the age of 90-days were found lower than the strength of unexposed confined specimens at the age of 90-days, as predictable. The reduction amounts as a result of sulfate solution were 2.68% and 3.93% for LCFA specimens and 3.82% and 5.45% for HCFA specimens confined with CFRP and BFRP fabrics, respectively.

In this study, unconfined specimens were exposed to sulfate solution and then FRP fabrics were placed on the same specimens in order to investigate the influence of FRP fabrics as retrofit/rehabilitation materials. Results indicated that the strength of the specimens wrapped after exposed to sulfate attack (The sulfate deteriorated specimens wrapped by both FRP fabric after exposure duration (Age of 90 days)) were lower than the strength of before wrapped specimens exposed to sulfate attack, as predictable. The reduction amounts were only 9.15% and 10.63% for HCFA specimens and 4.41% and 5.96% for LCFA specimens confined with CFRP and BFRP, respectively. Outcomes showed that both FRP fabrics can be also a resolution of sulfate deteriorated concrete and can be utilized as a rehabilitation or retrofit material under sulfate attack.

In addition to compressive strength, confined the specimens by FRP fabrics also increased the ductility behavior of specimens. The ductility improvement was stated in literature for conventional concrete confined by FRP materials (Photiou *et al.*, 2004; Sadeghian *et al.*, 2018). In general, ECC specimens exhibit strain hardening behavior, which resulted in an enhanced toughness and ductility. In addition, confined ECC specimens by FRP fabrics resulted in very high lateral displacement amounts and toughness, especially post-peak curve of the axial stress-strain curve. This outcome makes the composite FRP-ECC important in structural fundamentals demands high strength and high ductility. In the study, carbon FRP fabrics enhanced the strain from 0.04 to 0.09 and basalt FRP fabrics improved up to 0.07 as indicated in Figures 5.5 and 5.6 due to the effect of FRP fabric confinement, which forms a triaxial condition of the stress along the ECC specimen height which leads to higher strength and strain amounts. After the rupture failure of FRP fabrics, ECC concrete including PVA fibers continued to resist the axial load until failure of PVA fibers. Carbon FRP fabrics confined specimens exhibits superior strength and ductility amount than the basalt FRP fabrics confined specimens and the poor behavior was achieved in the unconfined specimens as indicated in Figure 5.6.

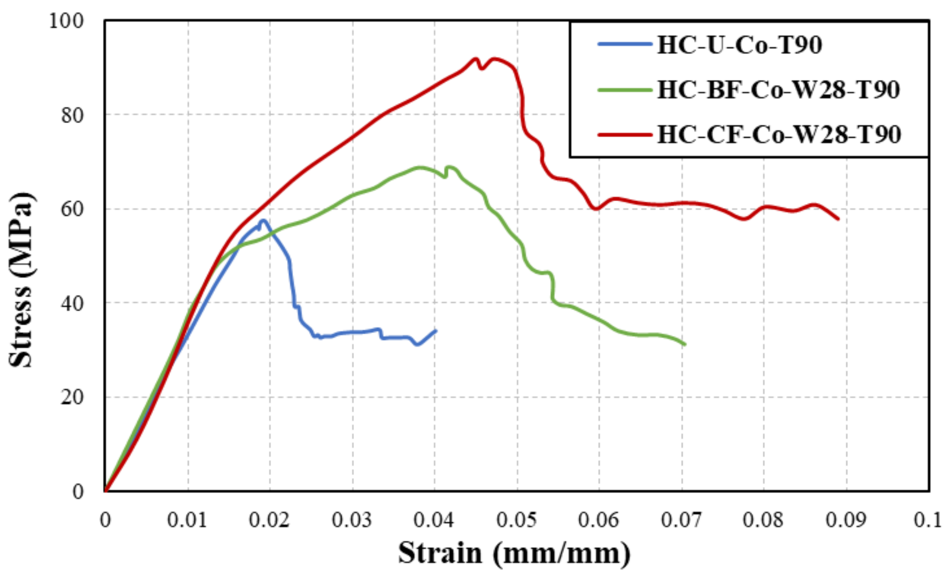

a) HCFA-ECC specimens

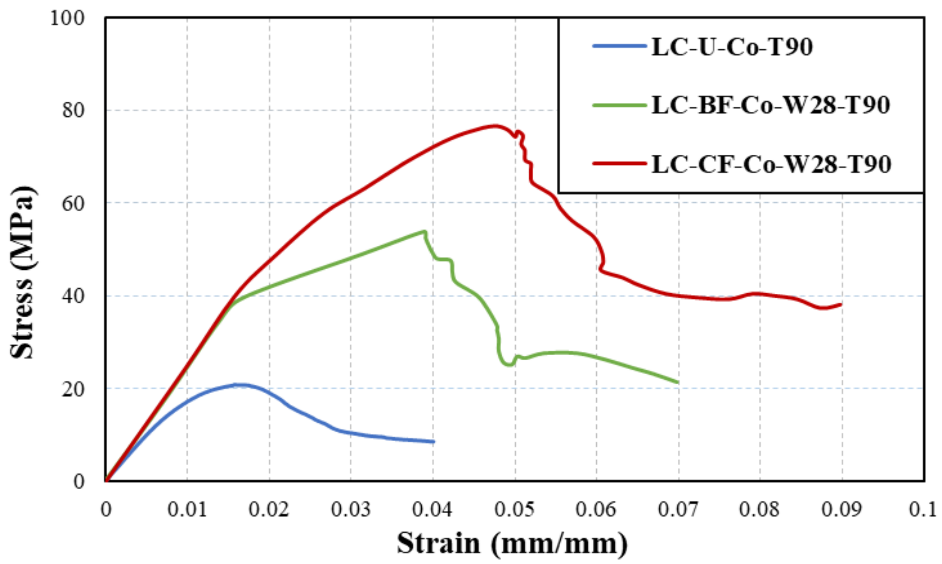

b) LCFA-ECC specimens

Figure 5.6 Stress-Strain Curves of wrapped and unwrapped ECC specimens

5.3.4 Failure modes of specimens under compression load

During axial compression load process, the concrete expansion expected on ECC cylinder specimens and both PVA fibers-matrix and FRP fabrics prevented the expansion and formed a confinement in the circumferential direction along the cylinder specimen's height. As tensile stresses resulted by axial load exceed the tensile strength resistance of FRP-ECC matrix composite, FRP rupture happened and the resistance of axial load continued by ECC matrix until the failure occurs due to the PVA fibers-matrix. In this study, all failure mechanism obtained due to FRP rupture followed by failure of ECC matrix. However, the failure related to de-bonding had rarely been stated by some researchers (Nanni and Bradford, 1995; Demers and Neale, 1999).

Figure 5.7 summarizes the Fracture or failure modes of the specimens. For these specimens, crack creation initiated at the top or bottom part of the cylinder specimen and crack openings developed until the failure occurs at these places as a result of high-stress concentrations created due to the friction between the specimen and the machine plates. As FRP fabrics were placed uni-directional, sudden failure was realized of the FRP fabrics caused by shearing off FRP fabrics and later the load transfer between FRP fibers cannot be possible. As reported in previous studies on FRP confinement concrete, low popping noises were heard during various stages of loading process (Lau and Zhou, 2001; Yao *et al.*, 2005; Taghia and Bakar, 2013). As the FRP fabric was taken off regarding the failure modes, it was noted obviously that the failure occurred at the bottom or top part of the specimens of most of the specimens.

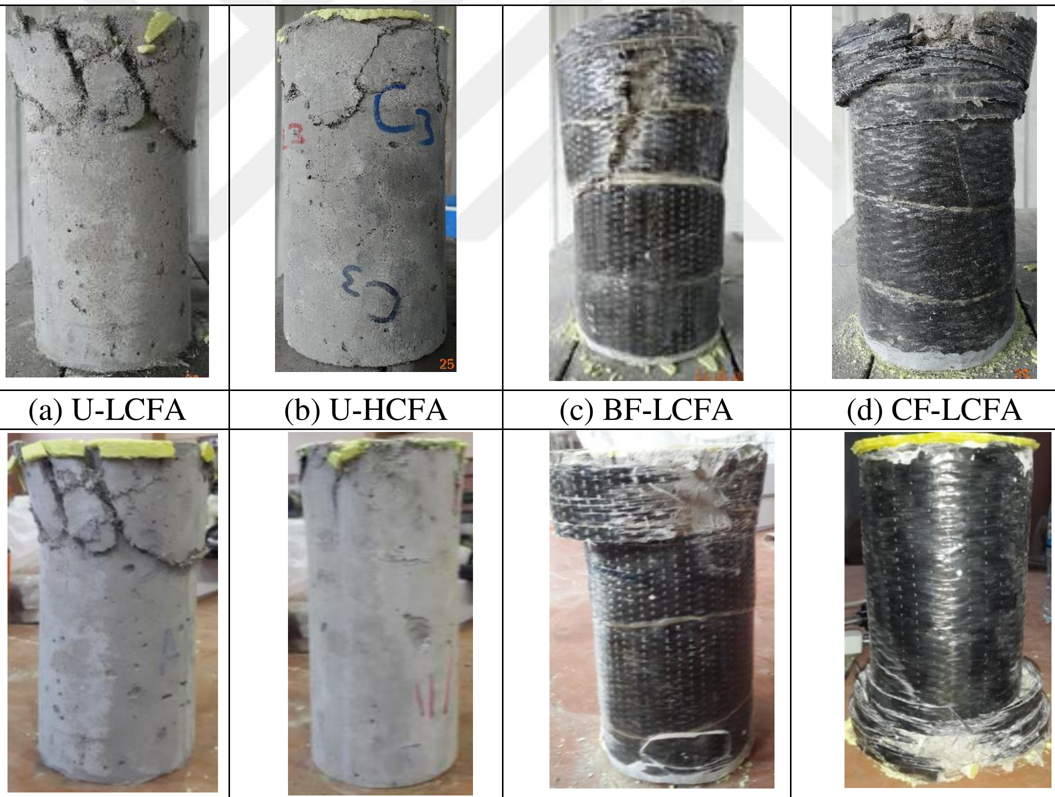

(a) U-LCFA | (b) U-HCFA | (c) BF-LCFA | (d) CF-LCFA

(e) U-LCFA | (f) U-HCFA | (g) BF-LCFA | (h) CF-LCFA

Figure 5.7 Failure mode of ECC specimens under sulfate (a,b,c,d) and under ambient (e,f,g,h) environments

Failure of the unconfined ECC specimens occurred more violent than the specimens wrapped with FRP fabrics. Due to the high bond strength of PVA fibers, the formed cracks cannot propagate into the mid-lengths of the specimens in general (Li and

Fischer, 2002). The failure of the unwrapped specimens occurred near the top and bottom of the specimens as similar to the wrapped ones. However, failure of the specimens subjected to sulfate was more violent than unexposed specimens as shown in Figure 5.7. This may result from gypsum and ettringite formation at the outer surface (~ 1 cm) under magnesium sulfate environment. The sulfate produced additional tensile stresses and caused weaknesses in the concretes. When the sulfate influence combined with the external axial load, the cracking may form at the weakest defects and further elongate along the specimen heights.

5.4 Cyclic Loading Behavior

Figures 5.8 and 5.9 illustrate the axial stress-strain curves resulted from both static and cyclic loadings of the tested specimens. Results showed that the pre-peak performance of unconfined specimens resulted from static and cyclic loading was obtained almost linear up to the peak loads even for the specimens exposed to sulfate attack as shown in Figure 5.8. However, regarding the post-peak performance of unconfined specimens exposed to sulfate solution, the static and cyclic curve moved away from each other, which may be due to the extra reduction in elastic modulus resulted from softening and decreased the rigidity of specimens with an increase in loading/unloading cycles. This behavior can be detected clearly for HCFA specimens due to high amount of CaO.

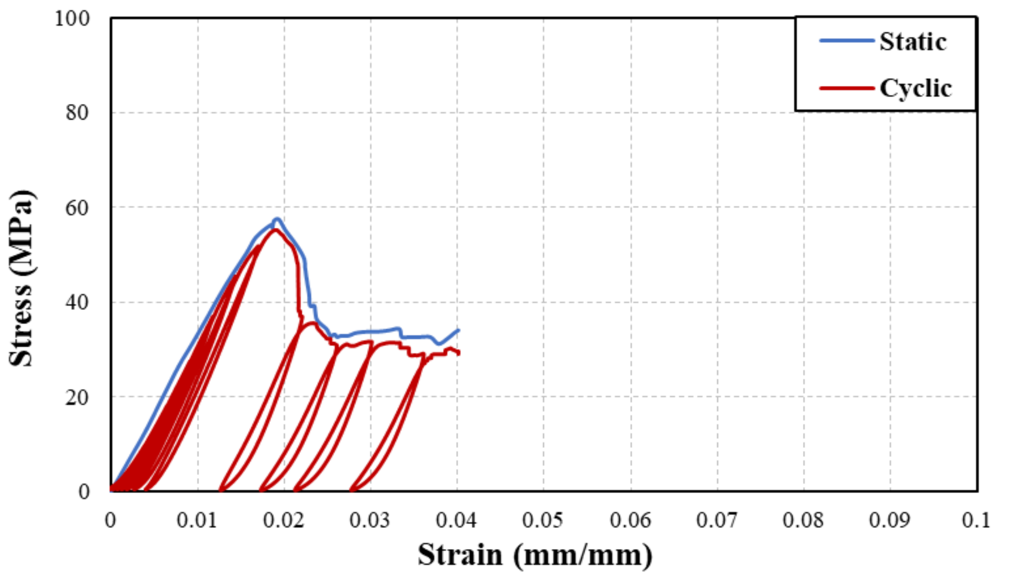

a) HCFA-ECC specimen exposed to ambient environment

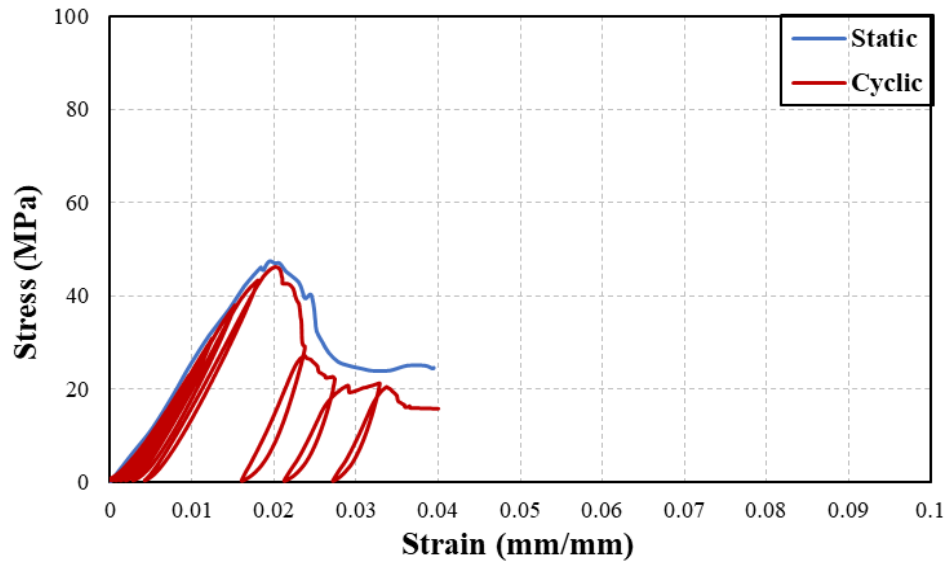

b) HCFA-ECC specimen exposed to sulfate environment

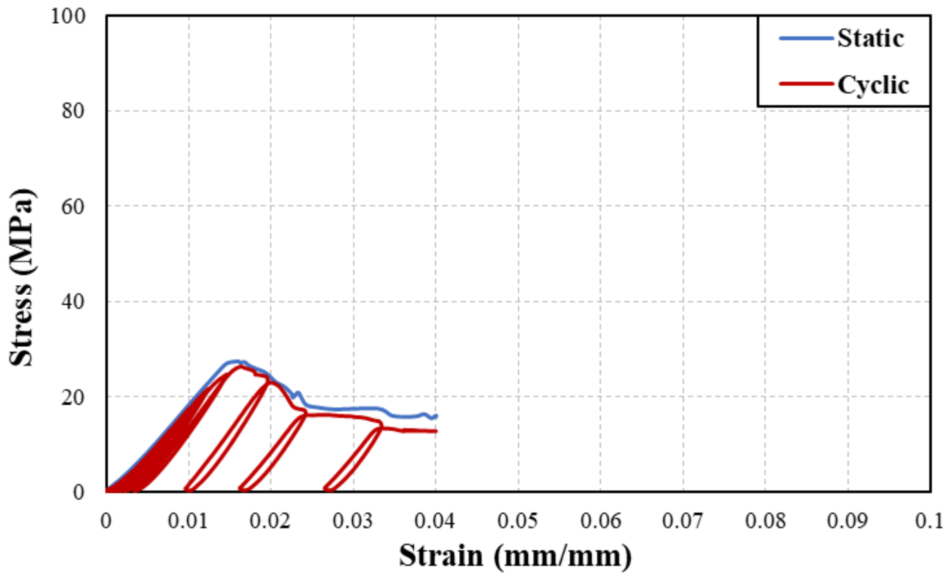

c) LCFA-ECC specimen exposed to ambient environment

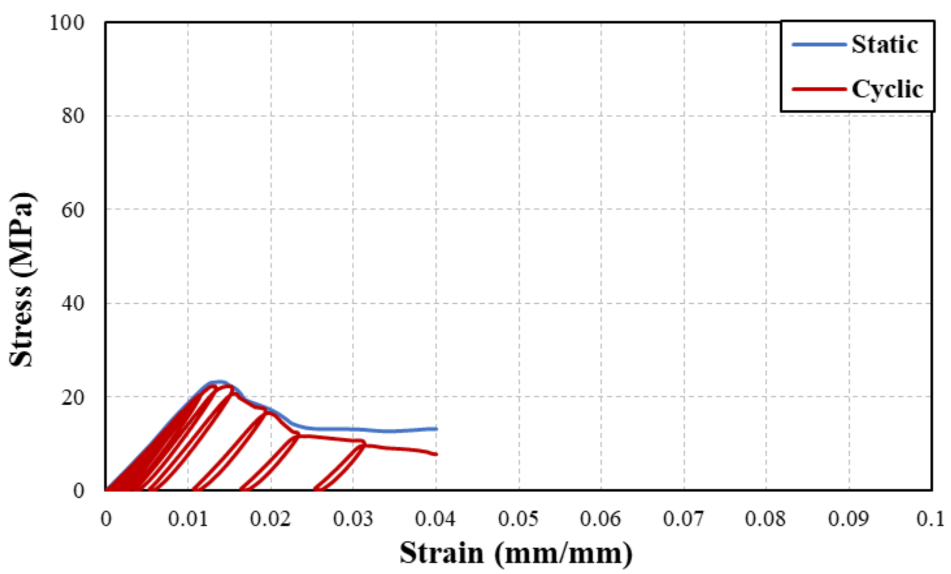

d) LCFA-ECC specimens exposed to sulfate environment

Figure 5.8 Static and cyclic loading diagrams of unwrapped ECC specimens exposed to sulfate and ambient environment

For confined specimens, the pre-peak performance of confined specimens expected as linear up to the points that match to the failure of unconfined specimens as presented in Figure 5.9. After that due to the cracks formed in the ECC matrix at higher stresses, elastic modulus of ECC composite were decreased. However, higher stresses were achieved due to the presence of the FRP fabrics. However, similar stress relaxation was also indicated in the post-peak part for both static and cyclic loadings, which may be due to the elastic performance of the FRP, which enhanced the resistance of the specimens to cyclic loadings. The favorable effect of carbon and basalt FRP material on the post-peak curve can be easily observed under sulfate attack.

The envelopes of all stress-strain curves of ECC tested specimens under cyclic loading can be drowned by joining the peak points of the unloading cycles on the stress-strain curves and the resulted curve matches well with the resultant stress-strain curve of the specimens from static loading. Similar indications were also stated by previous studies Lam et al (Lam *et al.*, 2006) and Shah et al (Shah *et al.*, 1983) and they also reported that this behavior also suitable for concretes confined by FRP fabrics. In this study, the static and cyclic loading curves of tested specimens confined by carbon FRP and basalt FRP obeyed with each other as presented in Figure 5.9. The similar results were also indicated by previous researchers (Shah *et al.*, 1983; Lam *et al.*, 2006).

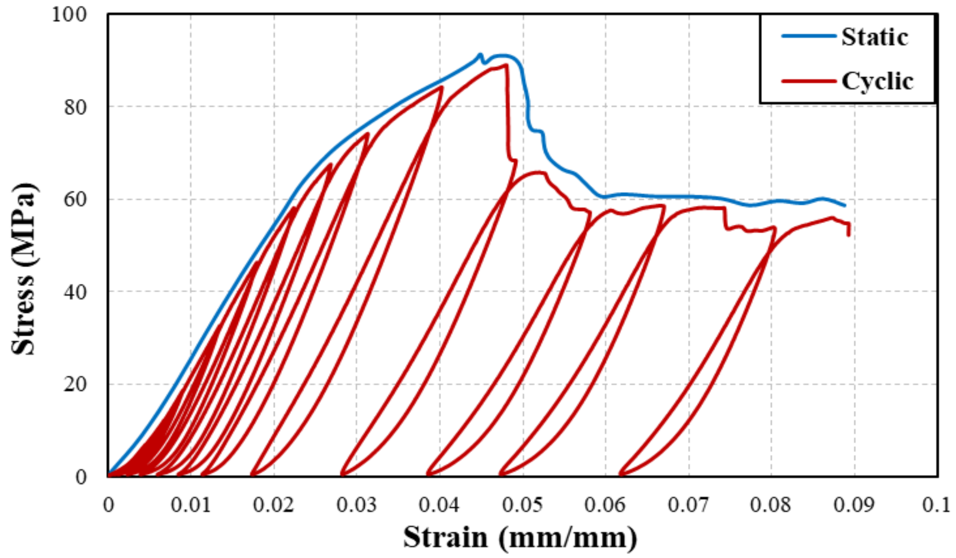

a) HCFA-ECC specimen wrapped by CFRP exposed to ambient environment

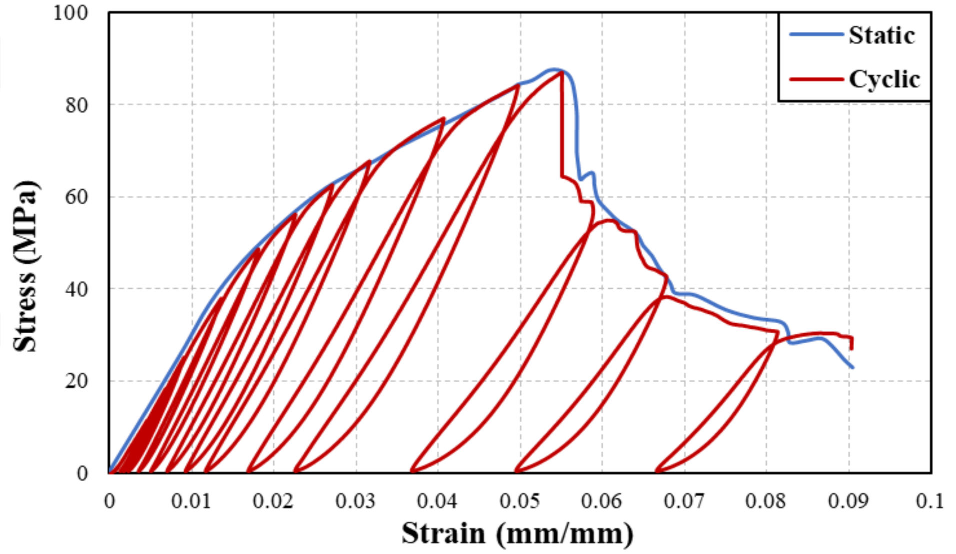

b) HCFA-ECC specimen wrapped by CFRP exposed to sulfate environment

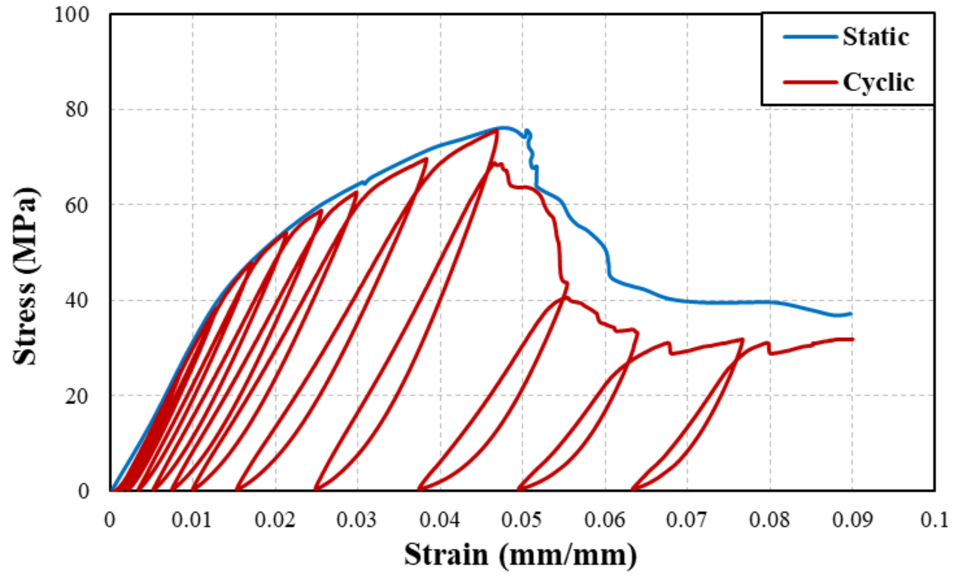

c) LCFA-ECC specimen wrapped by CFRP exposed to ambient environment

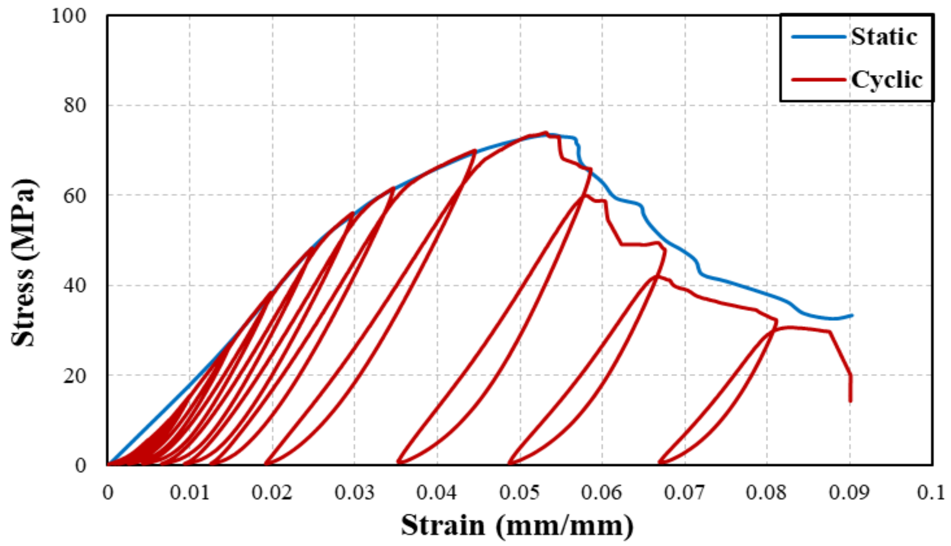

d) LCFA-ECC specimens wrapped by CFRP exposed to sulfate environment

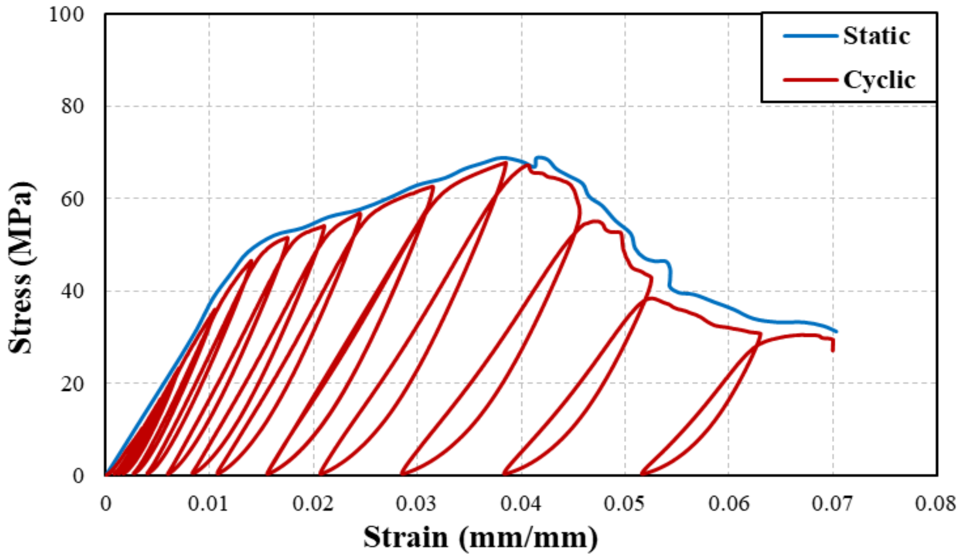

e) HCFA-ECC specimen wrapped by BFRP exposed to ambient environment

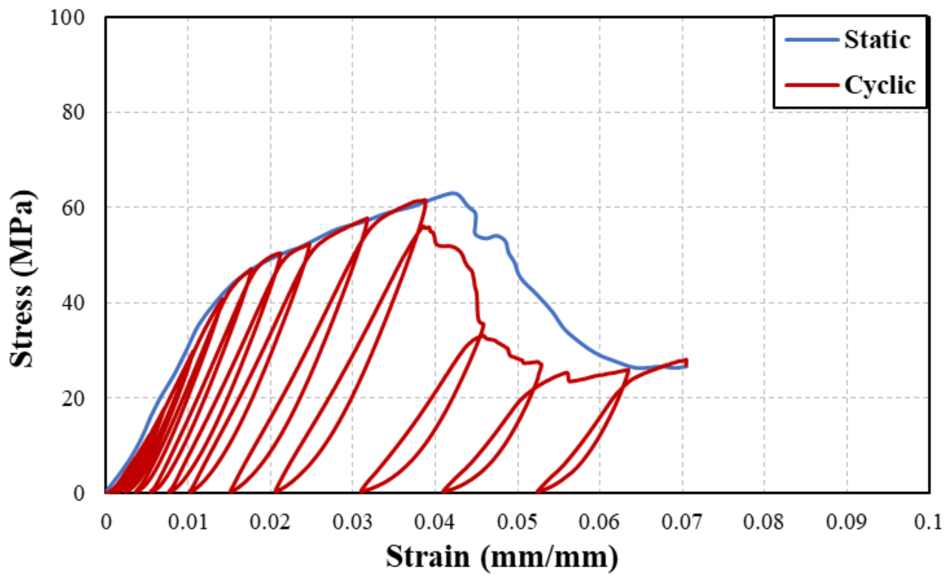

f) HCFA-ECC specimen wrapped by BFRP exposed to sulfate environment

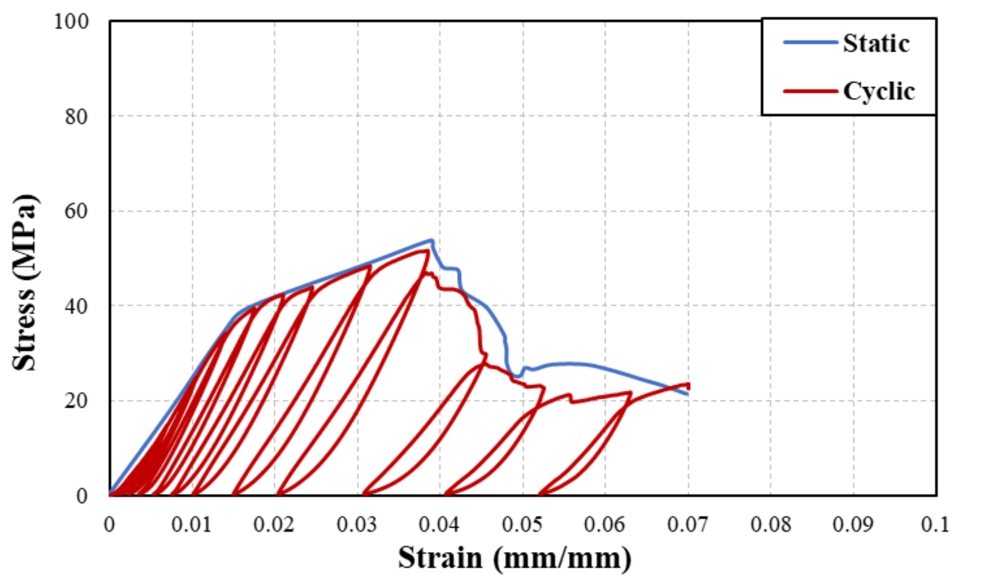

g) LCFA-ECC specimen wrapped by BFRP exposed to ambient environment

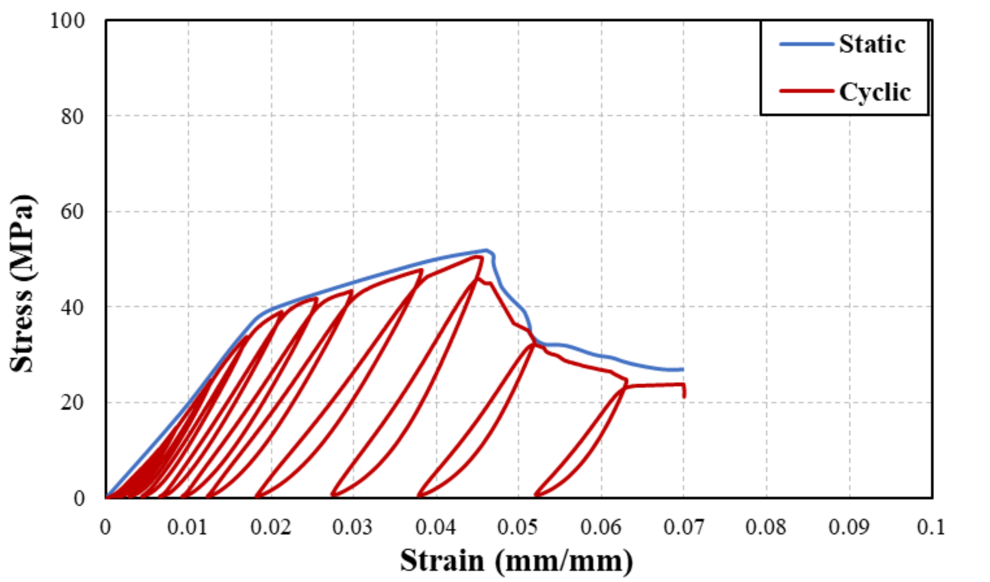

h) LCFA-ECC specimens wrapped by BFRP exposed to sulfate environment

Figure 5.9 Static and cyclic loading diagrams for wrapped ECC specimens exposed to ambient and sulfate environment

5.5 Scanning Electron Microscopy (SEM)

Confined and unconfined ECC specimens were analyzed by scanning electron microscopy (SEM) in details to detect the alters in the surface of PVA fibers and the transition zone between the fiber and the matrix as a result of chemical reaction of sulfate solution. In addition, the effects on the surfaces of carbon and basalt FRP fabrics were studied in microscale. In order to prepare SEM samples, one inch (2.54 cm) slices from both top and bottom sections of the specimens were cut and discarded, from the middle region of the specimens 1 cm thick circular slice was utilized for SEM analysis. The sulfate affected zone width was about 8 mm from the outer circumference of the cylinder specimen as indicated in Figure 5.1. Therefore, for each specimen two SEM images were taken, one of them was taken at the sulfate influenced region (0-1 cm from the surface) and the other one was taken from the uninfluenced region (close to the influenced region but out of the 1 cm outer layer).

SEM photos of the unconfined ECC specimens under various environments were organized in Figure 5.10. SEM images of sulfate influenced region shown that white sediments created on the surface of the PVA fibers and the number of white sediments for HCFA specimens was much higher than LCFA specimens. Due to the high amount of calcium, the higher ratio of Ca/Si and the free calcium lead to high deterioration of the cement paste and creation of gypsum and ettringite which can produce expansion, dimensional instability, cracking, spalling and reduction in mechanical properties (Bassuoni and Nehdi, 2007; Ariffin *et al.*, 2013). As specified previously, SEM photos were also taken out of the sulfate influenced region (specified after 1cm from outer surface) and low vitreous segments were concentrated on the surface of the PVA fibers. SEM photos specified that sulfate attacks begun from the outer layer and grew to the inside of the specimens. It was also investigated that the adverse influence of sulfate on HCFA specimens was higher than the LCFA specimens in both sulfates influenced and uninfluenced region. The white sediments also detected in the interfacial transition zone, which weakened the bond between cement matrix and PVA fibers.

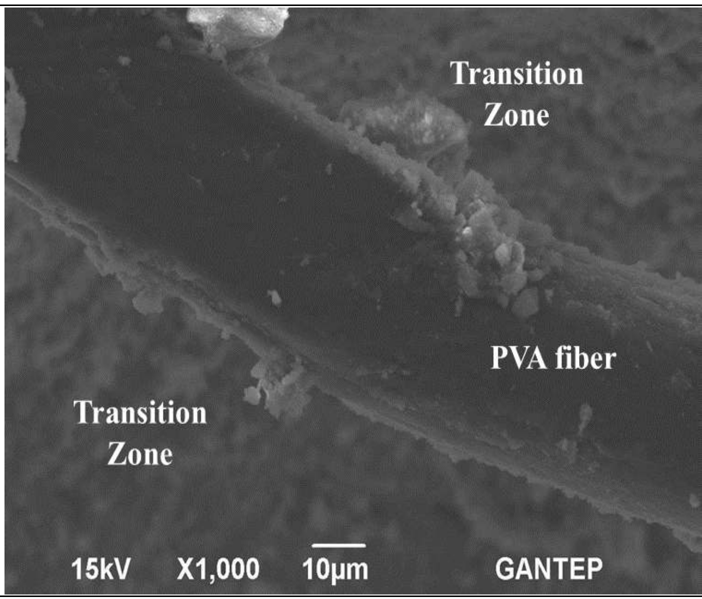

a) HCFA-ECC specimen exposed to ambient environment

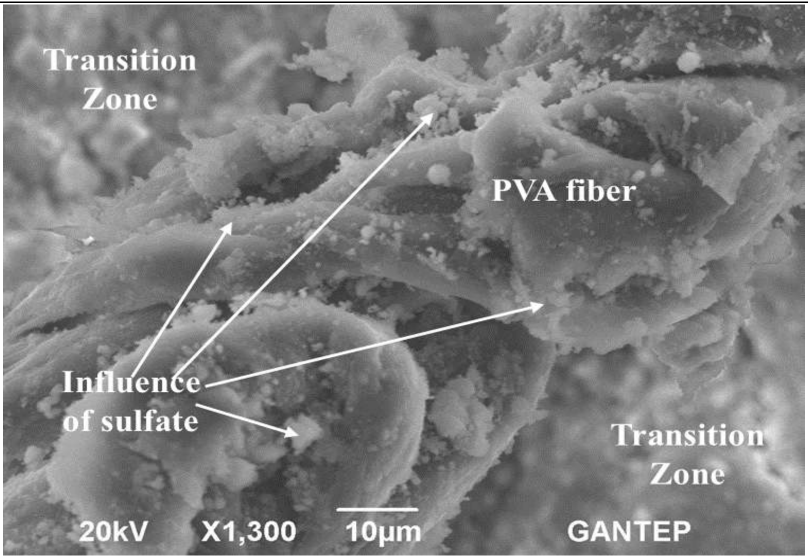

b) HCFA-ECC specimen exposed to sulfate environment (at the outer part 0.8cm)

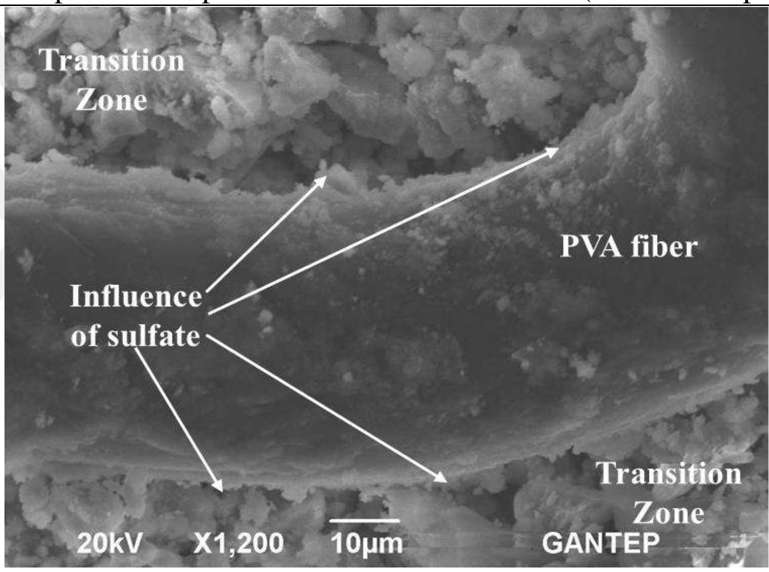

c) HCFA-ECC specimen exposed to sulfate environment (after 1cm from the outer surface)

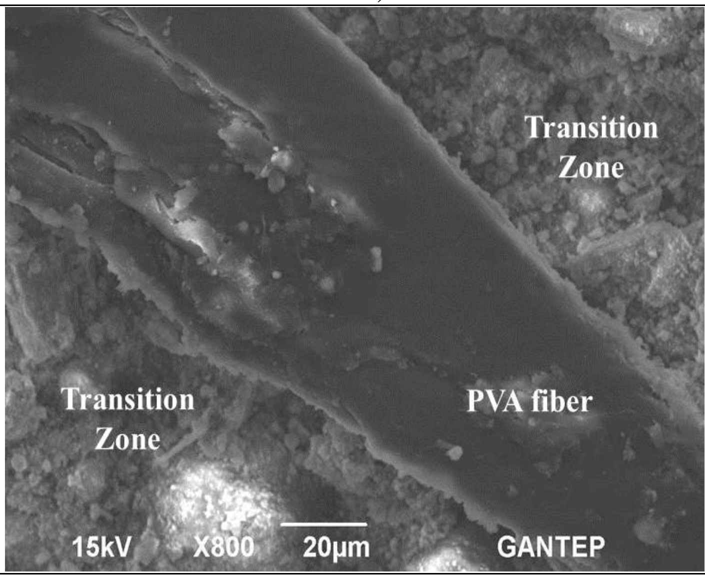

d) LCFA-ECC specimens exposed to ambient environment

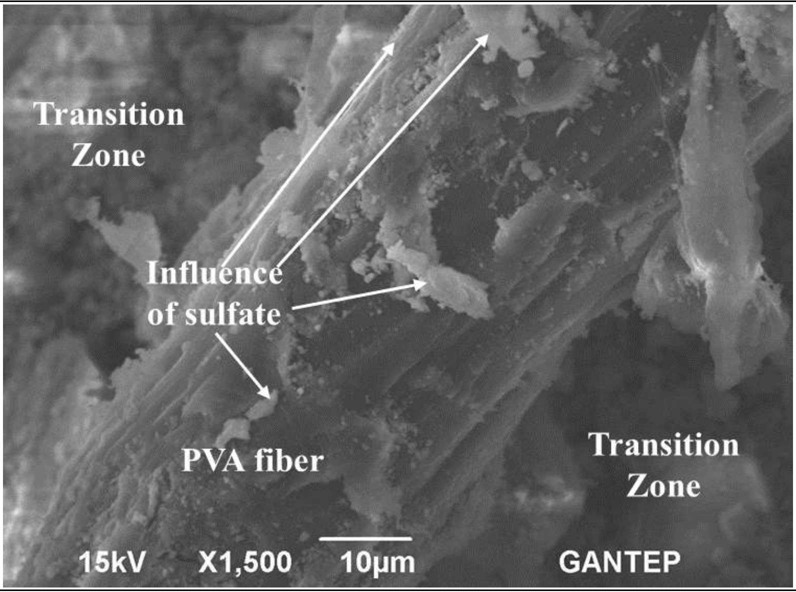

e) LCFA-ECC specimen exposed to sulfate environment at the outer part (0-1 cm)

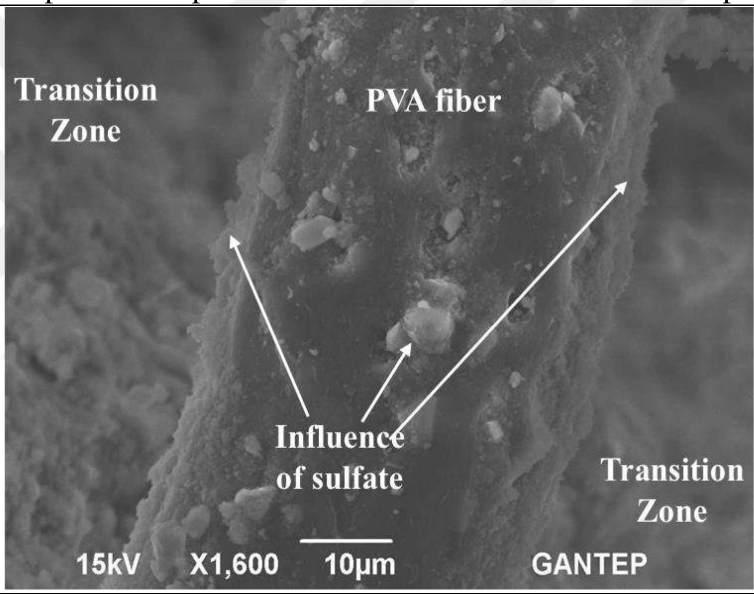

f) LCFA-ECC specimens exposed to sulfate environment at the part after 1cm

Figure 5.10 SEM photos of unwrapped ECC specimens exposed to ambient and sulfate environment

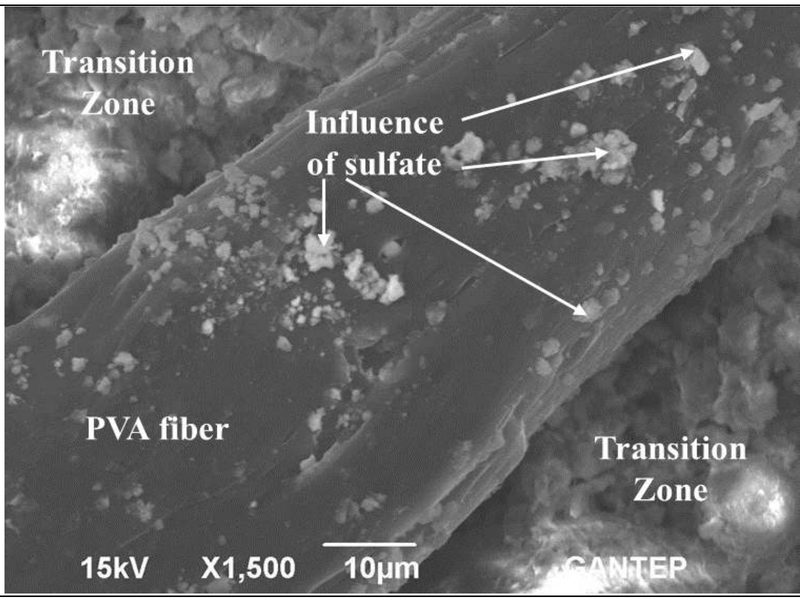

a) LCFA-ECC specimen wrapped by CFRP exposed to sulfate environment at the outer part (0-1cm)

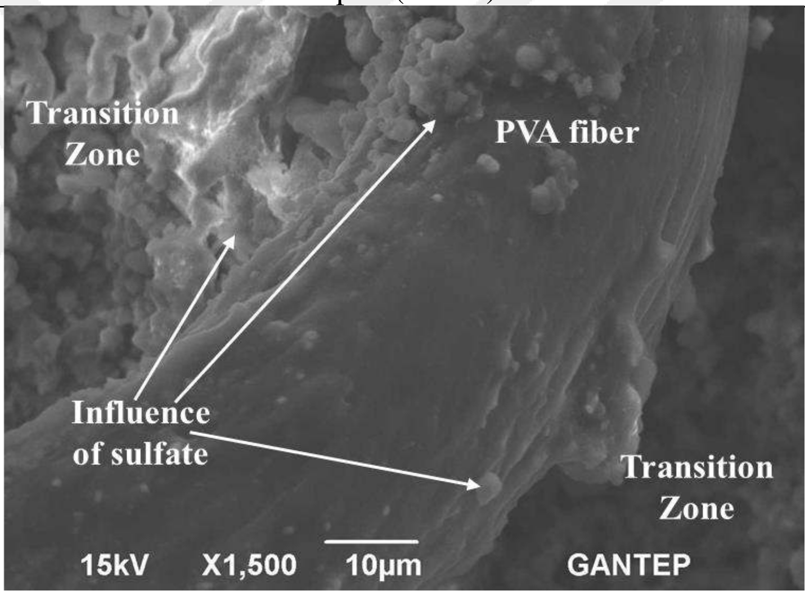

b) LCFA-ECC specimen wrapped by CFRP exposed to sulfate environment at the part after 1cm

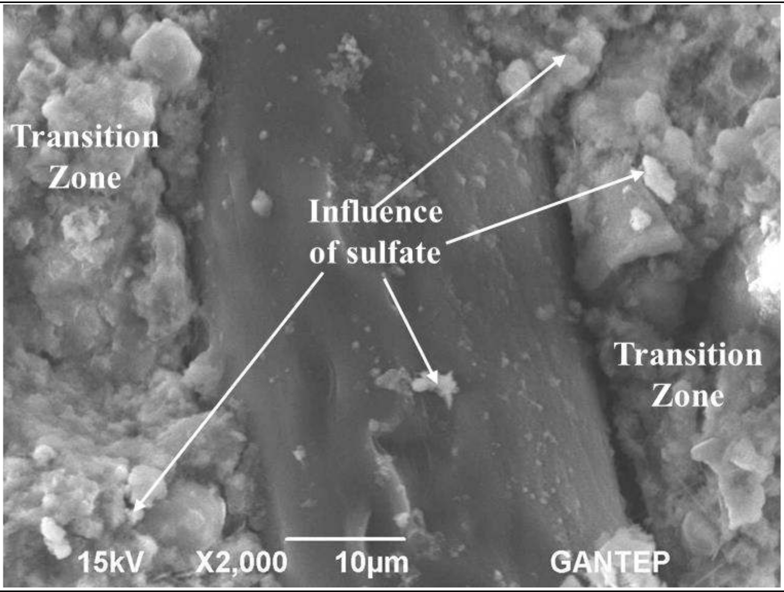

c) LCFA-ECC specimen wrapped by BFRP exposed to sulfate environment at the outer part (0-1cm)

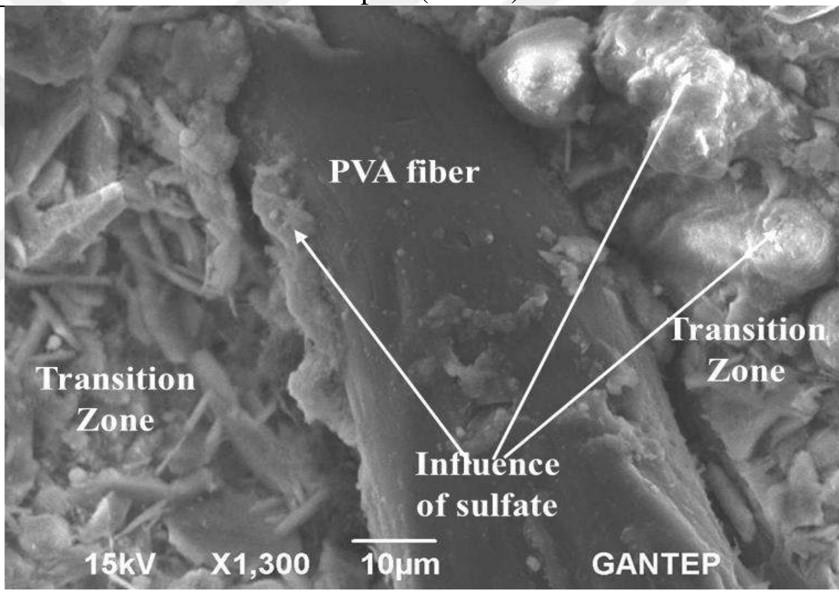

d) LCFA-ECC specimen wrapped by CFRP exposed to sulfate environment at the part after 1cm

Figure 5.11 SEM photos of FRP wrapped ECC specimens exposed to ambient and sulfate environment

SEM photos of basalt and carbon FRP confined HCFA specimens were presented in Figure 5.11. Outcomes specified that PVA fibers of ECC specimens confined by basalt and carbon FRP were deteriorated by sulfate attack less than PVA fibers of unconfined specimens. In addition, basalt and carbon FRP fibers also influenced by the sulfate attack. Due to the sensitivity of the epoxy resin to an alkaline environment, BFRP and CFRP fabrics were also substantially influenced by the sulfate solution. However, due to the higher bond between CFRP fabrics and the epoxy resin, specimens confined by

CFRP fabrics were less deteriorated compared to specimens confined by BFRP fabrics as indicated in Figure 5.12.

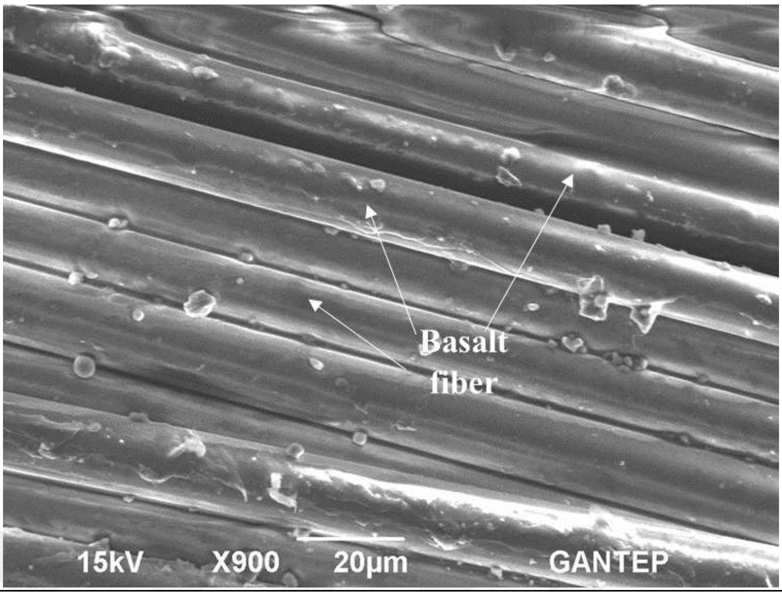

a) BFRP sheet without epoxy exposed to ambient environment

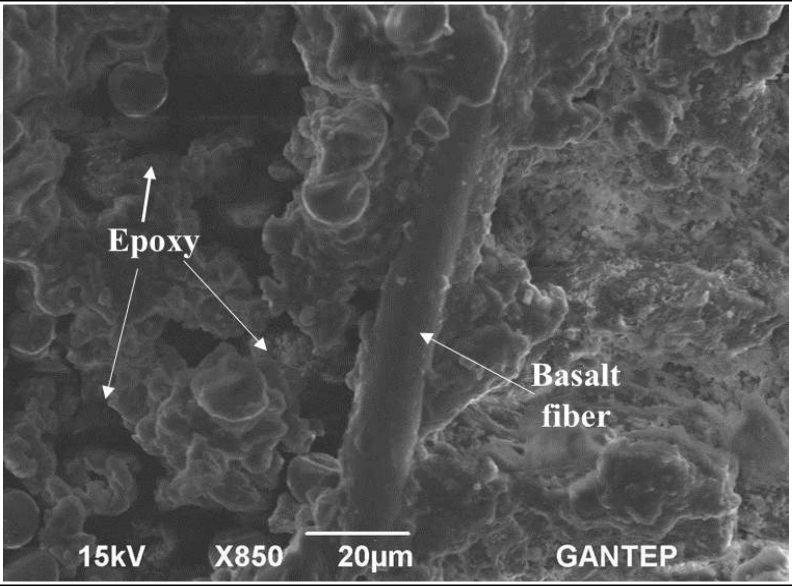

b) BFRP sheet with epoxy exposed to ambient environment

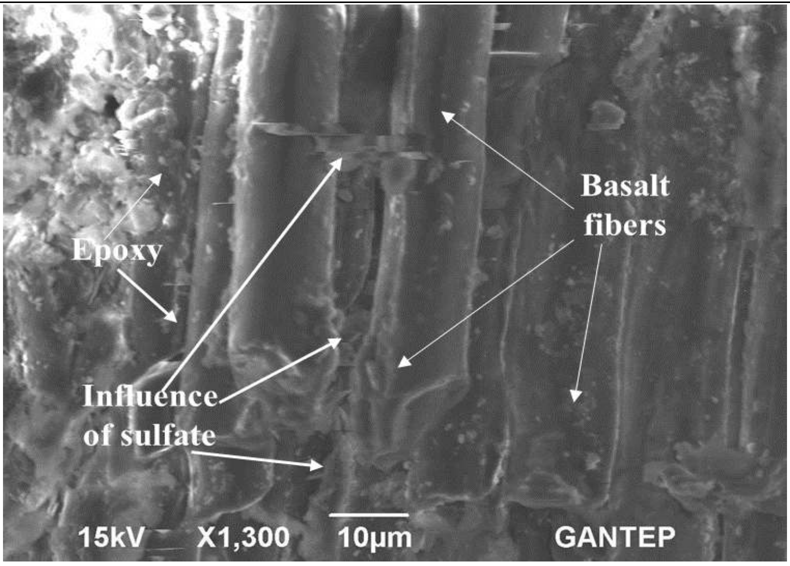

c) BFRP sheet with epoxy exposed to sulfate environment

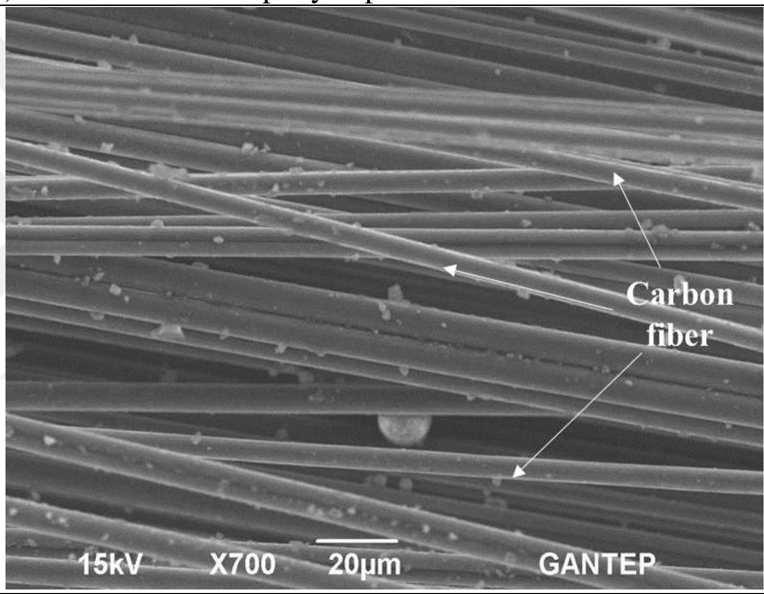

d) CFRP sheet without epoxy exposed to ambient environment

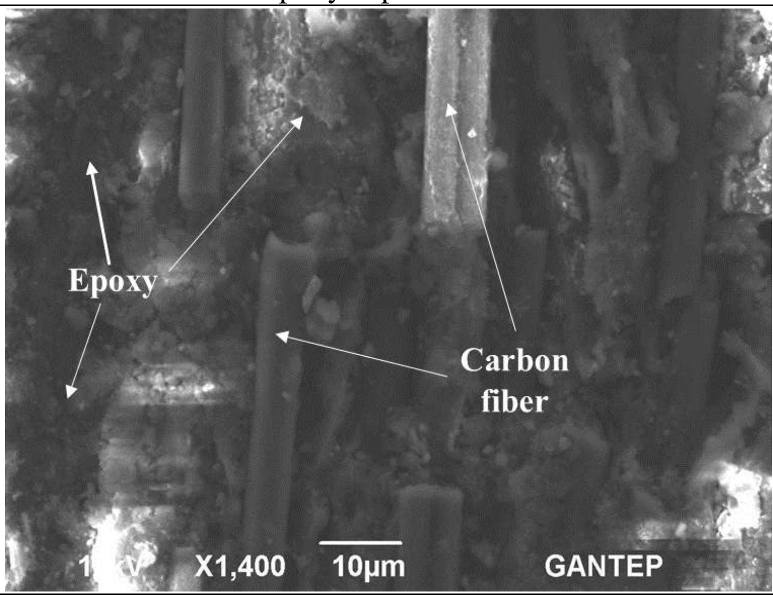

e) CFRP sheet with epoxy exposed to ambient environment

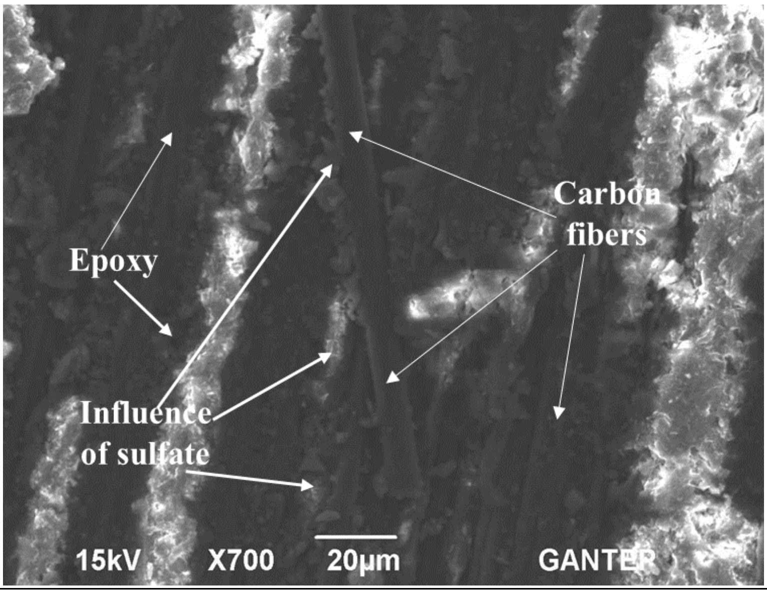

f) CFRP sheet with epoxy exposed to sulfate environment

Figure 5.12 SEM photos of BFRP and CFRP fabric sheets exposed to ambient and sulfate environment

CHAPTER 6
SEAWATER ATTACK

6.1 Visual inspection

Visual inspection of specimens after 8 weeks of exposure to 3.5% sea water solution were realized and the results revealed that specimens were kept their initial condition and there is no cracking and spalling observed. A small layer of efflorescence was observed on the specimen surfaces and the amount of surface erosion was further for the unwrapped ECC specimens at the end of the sea water exposure. In addition to this, the surface of the PVA fibers and FRP fabric sheets were also slightly eroded by sea water solution. However, the ECC concrete coated by the FRP fabrics remained their initial condition since FRP fabrics at the outermost layer influenced by sea water and the inner sides were observed to be unaffected as shown in Figure 6.1. All specimens were remained structurally intact after 8 weeks of exposure to sea water solution. As stated earlier, sea water is not hazardous for the plain concrete since numerous submerged concrete structures subjected to sea water for many years are still in a good condition. However, sea water can be very detrimental to reinforced concrete structural elements due to the corrosion of steel reinforcement (Visitanupong, 2009).

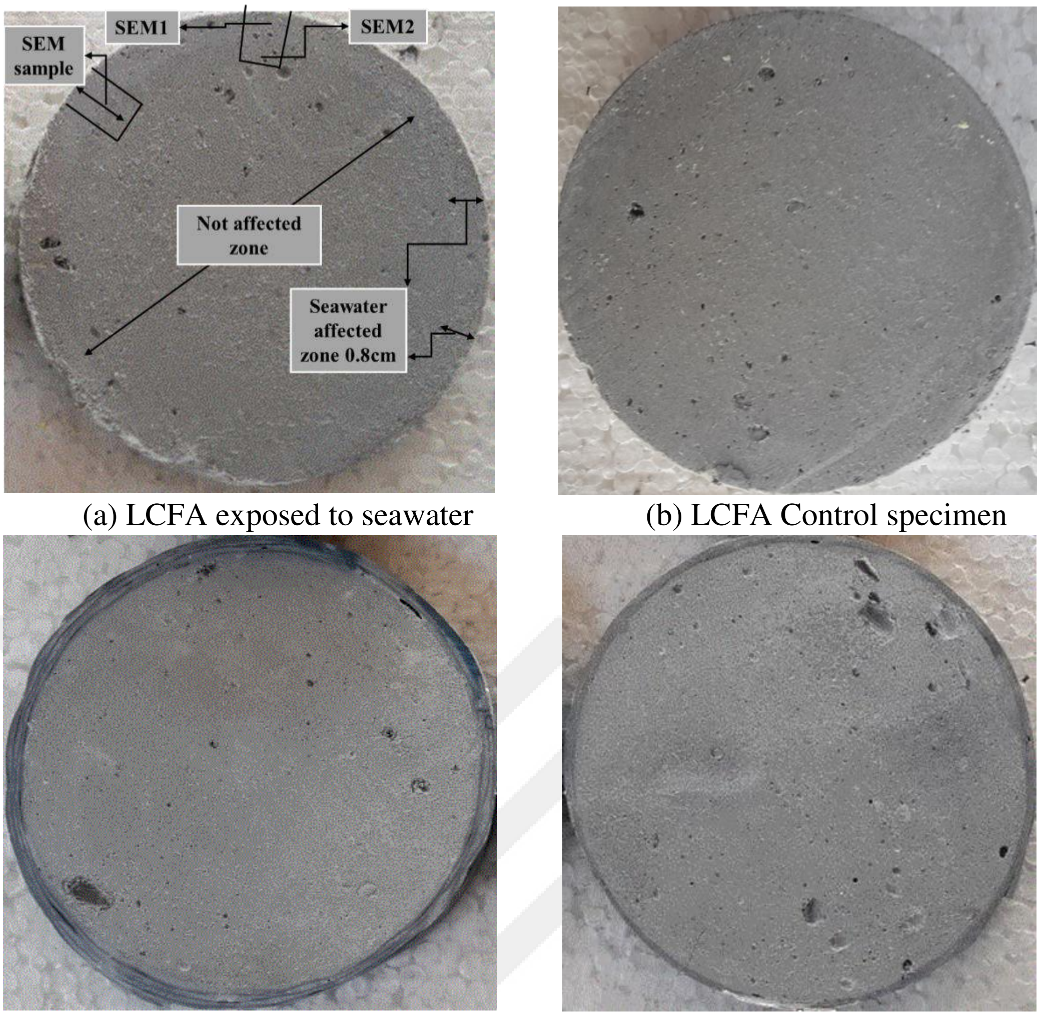

(a) LCFA exposed to seawater (b) LCFA Control specimen

(c) CFRP-ECC exposed to seawater (d) BFRP-ECC exposed to seawater

Figure 6.1 ECC Cylinder specimen slice showing seawater affected zone

In a previous study, researchers investigated 2 % sulphuric acid resistance of the geopolymer concrete and found that only 20 mm diameter of the 100 mm cylinder specimens were influenced by the acid attack. Therefore, they implemented SEM observations at the acid affected zone of 20 mm from the outermost surface (Wallah and Rangan, 2006). In this study, similar observations were made and the SEM images were investigated at the outermost layer of 20 mm for the sea water attack. Since chloride amount is different at the external surface and inner part of the concrete, diffusion of the chloride ions from the surface to the inner parts of the concrete is realized. Therefore, the sea water affected region is started from the external surfaces of the concrete. In the research, sea water diffusion was noticed at the 8 mm outer region of the specimens, and the remaining inner parts were observed to be unaffected as shown in Figure 6.1. SEM observations were realized at both sea water affected zone of 8 mm and unaffected zones. Similar observations that chemical attack is a surface phenomenon and deterioration initiates at the outermost surface and progresses to the inside regions were also realized in the previous study (Attiogbe and Rizkalla, 1988).

6.2 Weight change

Figure 6.2 illustrate the weight change (%) of the specimens exposed to 3.5 % seawater for a period of 60 days. All specimens under seawater environment had weight gain and the highest weight increase was observed unconfined specimens. Unconfined LCFA-ECC and HCFA-ECC specimens increased their weights up to 0.86 % and 1.16%, respectively. Besides, confined LCFA-CFRP hybrid specimens exhibited slightly lower weight gain than the confined HCFA-CFRP hybrid specimens. In addition, LCFA-CFRP hybrid specimens showed lower weight gain and therefore, the specimens confined by carbon FRP fabrics exhibited slightly better seawater resistance than the specimens wrapped by basalt FRP fabrics. LCFA matrix showed better resistance both confined and unconfined state, which can be attributed to both low CaO content by forming reduced amount of $Ca(OH)_2$ and higher fineness ratio by reducing the porosity. The moisture uptake due to chemical environment was also reported in the previous studies (Mohammed, 2007; Thokchom, 2014). The sulphate ions from the sea water were reacted with the Ca(OH)2 solution and formed delayed ettringite. As a result, concrete volume was raised by a factor of about two with a reduction in density (Soroka, 1979). Thus, weight gains of the specimens under chemical solution may be attributed to the rise in relative volume more than the reduction in relative density (Attiogbe and Rizkalla, 1988).

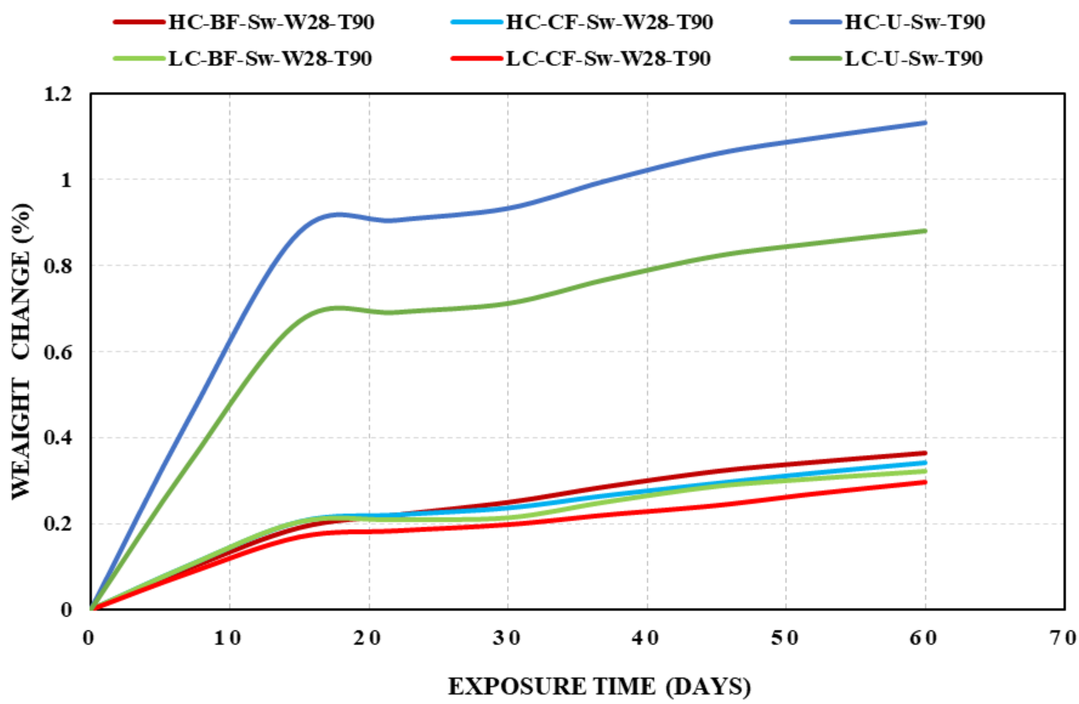

Figure 6.2 Weight change in ECC specimen exposed to seawater attack for duration 60 days

6.3 Compressive strength of the specimens

In general, the behaviors of ECC specimens confined by FRP fabrics under axial load were found to be consistent with the performance of conventional concrete confined by FRP in the literature. During early stages of the axial loading process, the noise related to the micro-cracking of ECC-concrete was clear, which indicate the beginning of the stress transfer from the expanded ECC specimen to the FRP fabrics. The cracking noises intensity could be heard pre-failure that achieved after the slow rupture of FRP fabrics with a violent and sudden noise. Failure initiated from an overlap place of the FRP fabrics at the middle height of specimen and moved to the bottom and top of the specimens. For the tested specimens, all failures happened as a result of the rupture of FRP fabrics followed by a ductile performance of ECC and failure due to de-bonding was not observed in confined specimens. Figure 6.3 represents the compressive strengths of specimens. Results showed that specimen confined by FRP indicated superior performance than unconfined specimens under both seawater and ambient environments.

6.3.1 Specimen nomenclature

Three types of specimens were obtained in the scope of the research; CFRP-ECC hybrid specimens (specimens confined by carbon FRP fabrics), BFRP-ECC hybrid specimens (specimens confined by basalt FRP fabrics) and control specimens (unwrapped specimens). In addition, two mixes; high calcium fly ash mix (HCFA mix) and low calcium fly ash mix (LCFA) mix were prepared. Specimens were subjected to two different environments; 3.5% seawater environment and control environment (unexposed specimens). Control specimens (unexposed specimens) were tested at the ages of 28 days and 90 days, while specimens subjected to seawater environment were tested at the age of 90 days (water curing was applied until 28 days and the remaining days specimens exposed to the seawater environment). In a total, 102 cylindrical specimens were cast and tested in the scope of the study. As shown in Table 6.1, eight test series (series A to H) were designed in this study as follows:

Series A: 9 LCFA-ECC control cylindrical samples (3 unconfined and 6 confined) were tested at 28 days. The FRP wrappings were also applied at 28 days.

Series B: 18 LCFA-ECC control cylindrical samples (6 unconfined and 12 confined) were tested at 90 days. The FRP wrappings were applied at 28 days.

Series C: 18 LCFA-ECC (6 unconfined and 12 confined) specimens were cured in a water tank until 28 days and FRP wrappings were applied. Then, these confined specimens immersed into 3.5% seawater solution at the age of 90 days.

Series D: 6 LCFA-ECC unconfined specimens were cured in a water tank until 28 days and these unconfined specimens subjected to 3.5% sea water solution at the age of 90 days. Then, sea water exposed specimens were confined at the age of 90 days to evaluate the influence of FRP confinement as a rehabilitation method.

Series E: 9 HCFA-ECC control cylindrical samples (3 unconfined and 6 confined) were tested at 28 days. The FRP wrappings were also applied at 28 days.

Series F: 18 HCFA-ECC control cylindrical samples (6 unconfined and 12 confined) were tested at 90 days. The FRP wrappings were applied at 28 days.

Series G: 18 HCFA-ECC (6 unconfined and 12 confined) specimens were cured in a water tank until 28 days and FRP wrappings were applied. Then, these confined specimens immersed into 3.5% seawater solution at the age of 90 days.

Series H: 6 HCFA-ECC unconfined specimens were cured in a water tank until 28 days and these unconfined specimens subjected to 3.5% sea water solution at the age of 90 days. Then, sea water exposed specimens were confined at the age of 90 days to evaluate the influence of FRP confinement as a rehabilitation method.

In total, 102 cylindrical specimens were cast and tested in the scope of study the effect of seawater attack.

As shown in Table 6.1, eight test series were designed in this study as follows:

Table 6.1 Details of test series conducted in this chapter

6	Type of concrete	No. of samples	Unconfined	Confined		Control sample	Seawater exposed	Wrapping age		Testing age		Specimen ID
				BFRP	CFRP			28-days	90-days	28-days	90-days	
A	LCFA	3	✓			✓				✓		LC-U-Co-T28
		3		✓		✓		✓		✓		LC-BF-Co-W28-T28
		3			✓	✓		✓		✓		LC-CF-Co-W28-T28
B		6_a	✓			✓		✓			✓	LC-U-Co-T90
		6_a		✓		✓		✓			✓	LC-BF-Co-W28-T90
		6_a			✓	✓		✓			✓	LC-CF-Co-W28-T90
C		6_a	✓				✓	✓			✓	LC-U-Sw-T90
		6_a		✓			✓	✓			✓	LC-BF-Sw-W28-T90
		6_a			✓		✓	✓			✓	LC-CF-Sw-W28-T90
D		3		✓			✓		✓		✓	LC-BF-Sw-W90-T90
		3			✓		✓		✓		✓	LC-CF-Sw-W90-T90
E	HCFA	3	✓			✓				✓		HC-U-Co-T28
		3		✓		✓		✓		✓		HC-BF-Co-W28-T28
		3			✓	✓		✓		✓		HC-CF-Co-W28-T28
F		6_a	✓			✓		✓			✓	HC-U-Co-T90
		6_a		✓		✓		✓			✓	HC-BF-Co-W28-T90
		6_a			✓	✓		✓			✓	HC-CF-Co-W28-T90
G		6_a	✓				✓	✓			✓	HC-U-Sw-T90
		6_a		✓			✓	✓			✓	HC-BF-Sw-W28-T90
		6_a			✓		✓	✓			✓	HC-CF-Sw-W28-T90
H		3		✓			✓		✓		✓	HC-BF-Sw-W90-T90
		3			✓		✓		✓		✓	HC-CF-Sw-W90-T90

Note: a Three specimens under static loading and three specimens under cyclic loading.

In the Table 6.1, HC and LC indicates the high calcium FA and low calcium FA, U, CF and BF points out unconfined, confined by carbon FRP and basalt FRP fabrics, Co and Sw represents the control and sea water environments, W28 and W90 shows the wrapping ages of 28 days and 90 days, T28 and T90 demonstrates the age of compressive strength at 28 days and 90 days, respectively.

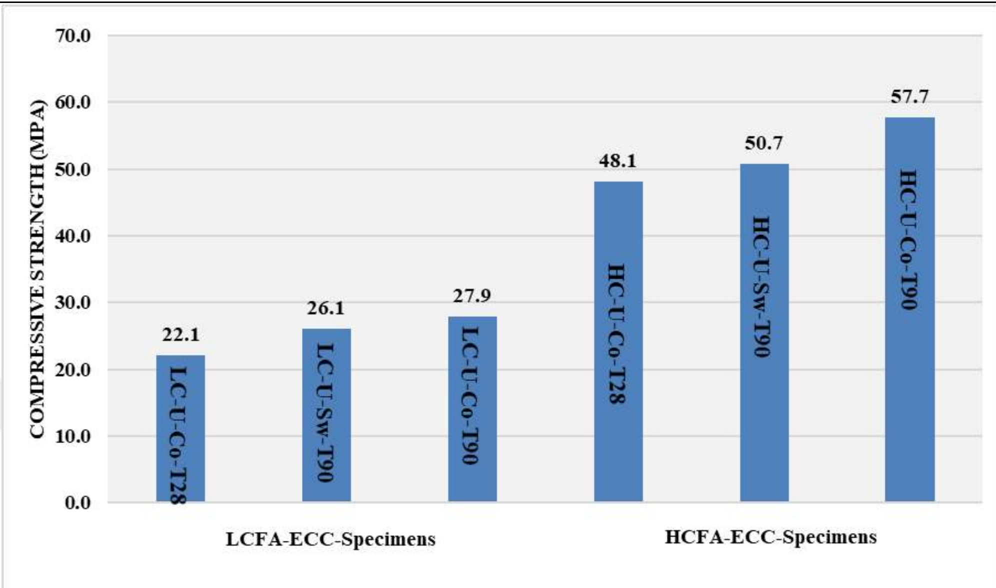

a) Unconfined ECC specimens

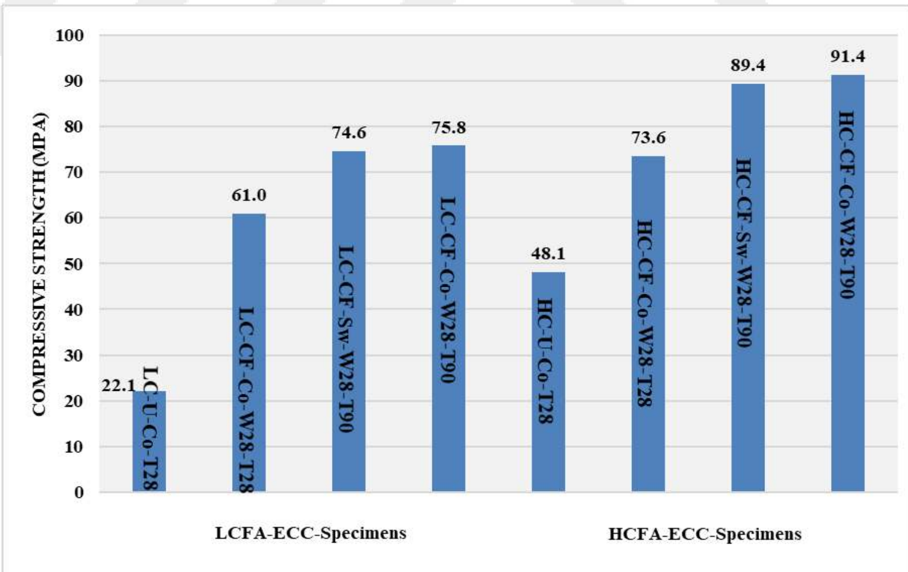

b) Unconfined ECC specimens and ECC specimens wrapped by CFRP

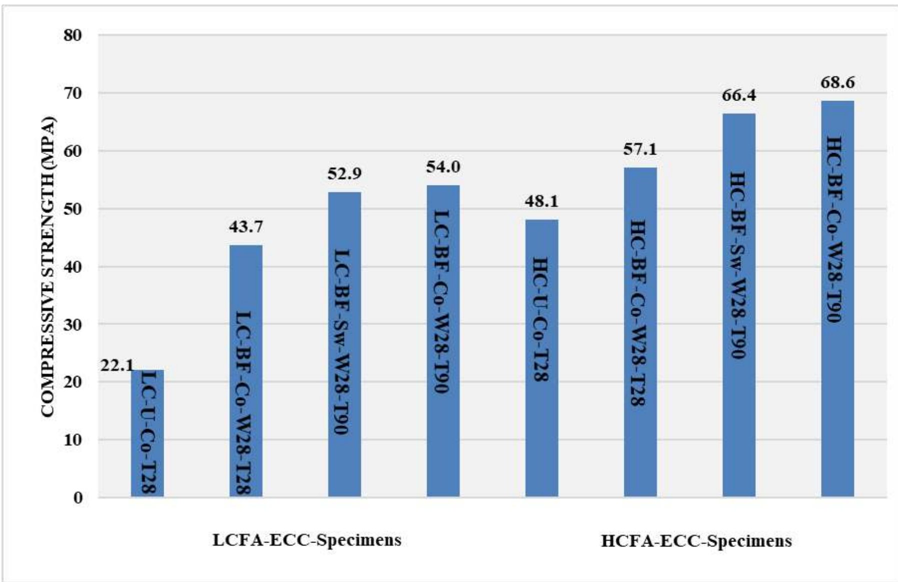

c) Unconfined ECC specimens and ECC specimens wrapped by BFRP

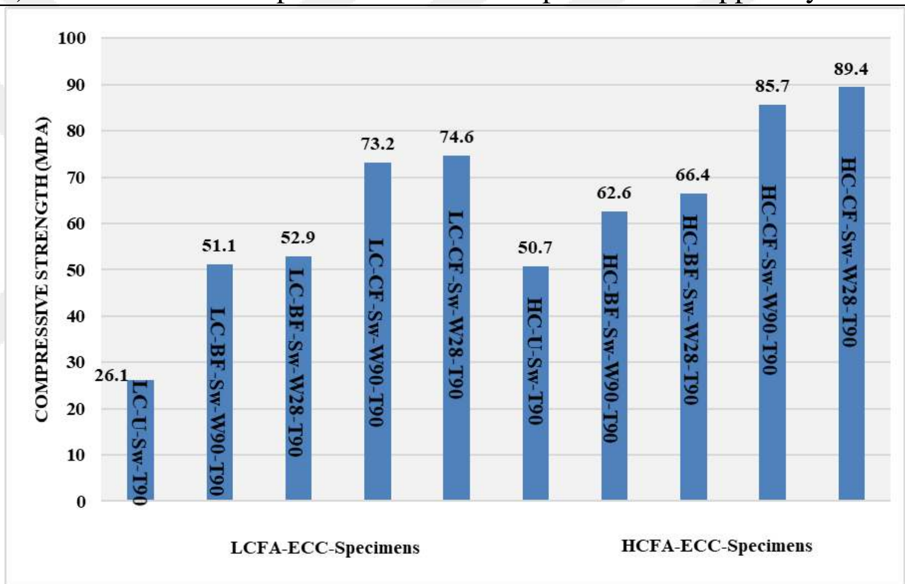

d) Unconfined ECC specimens and ECC specimens wrapped by both FRP exposed to seawater and exposure specimens wrapped by both FRP

Figure 6.3 Compressive strength of confined and unconfined ECC specimens

6.3.2 Compressive behavior of unwrapped specimens

Figure 6.4 shows stress-strain behaviour of the unconfined HCFA-ECC and LCFA-ECC specimens. Results indicated that compressive strength values of the specimens increased slightly up to 90 days, which may be attributed to the slow pozzolanic reaction of fly ash and the continuity of hydration reactions. Previous researchers were also reported similar outcomes (Choucha *et al.*, 2017; Liu *et al.*, 2017; Zhigang Zhang, 2017).

Compressive strength improvements due to additional 56 days of curing were 26.77% and 19.85 % for the unconfined LCFA-ECC and HCFA-ECC specimens, respectively. The higher strength increase was observed for the LCFA-ECC specimens, which can be attributed to slow rate of hydration reactions due to lower CaO amount in the low calcium fly ash (LCFA) specimens. The reduction in compressive strength due to 8 weeks of exposure to the sea water environments were 12% for HCFA-ECC specimens and 6.5% for LCFA-ECC specimens compared to ambient environment compressive strength results. The higher strength reduction for the HCFA-ECC specimens can be attributed to the high CaO content. Similar stress-strain behaviours for the PVA-ECC specimens were obtained in the ambient and sea water environments since sea water attack have not affected the mechanical behaviour of the PVA-ECC specimens effectively. One may argue that 8 weeks of sea water solution cannot be detrimental to structural performance. However, in the previous study, long term performance of ECC specimens under both sodium sulfate and combination solutions of sea water and sodium were also investigated by Liu *et al.* [17]. They revealed that ECC specimens maintained their initial conditions and showed superior durability performance after 420 days of exposure to sodium sulfate and combined sulfate-sea water solutions. Researchers also pointed out that mortar specimens exhibited remarkable deterioration, while no signs of deterioration were observed for the PVA-ECC specimens under 420 days of exposure to chemical attacks. In addition, they also found out that compressive strength change results became stabilized after 8 weeks of chemical exposure, and the difference in compressive strength values was found negligible for 8 weeks and 420 days of seawater exposure. Therefore, researchers proposed PVA-ECC concrete in hydraulic structure applications. In the scope of the study, further mechanical and durability improvements due to different type of FRP fabrics-ECC hybrid specimens were studied in details.

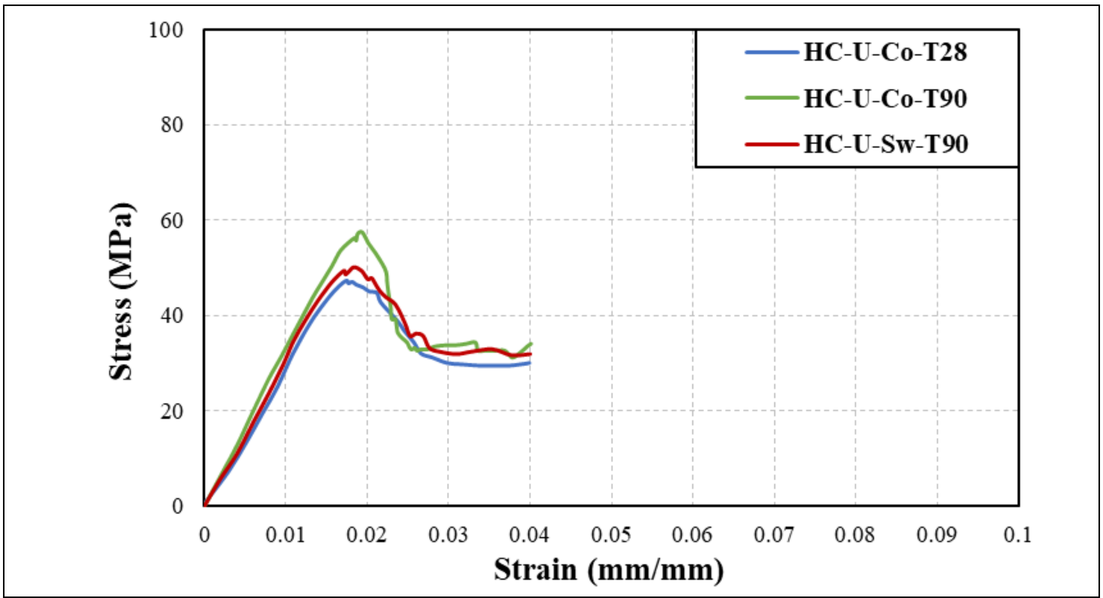

a) Unwrapped HCFA-ECC specimens

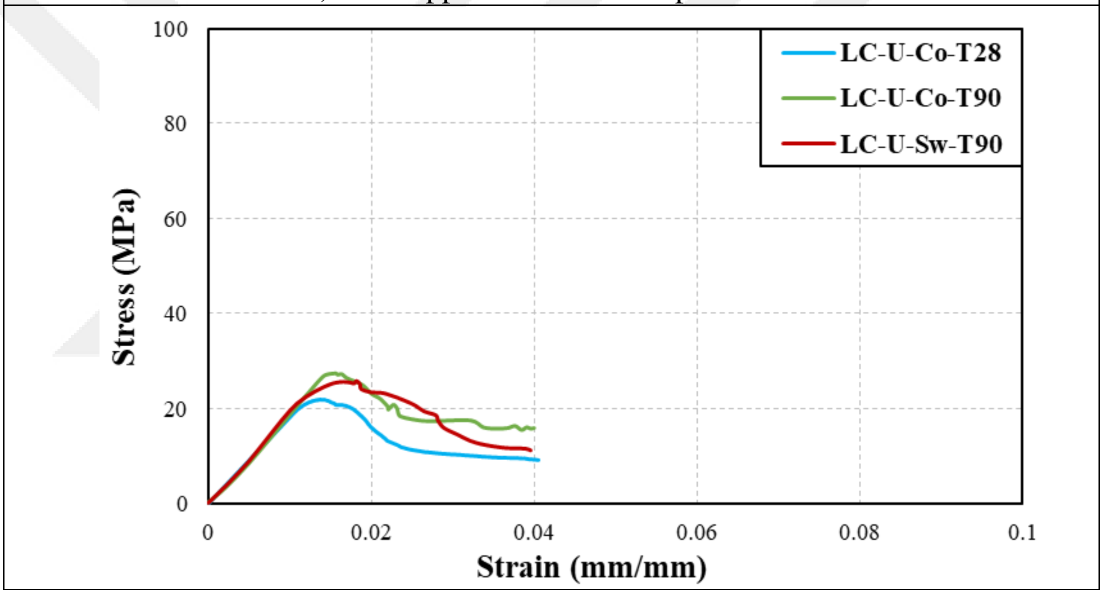

b) Unwrapped LCFA-ECC specimens

Figure 6.4 Stress-strain curves of unwrapped ECC specimens

6.3.3 Compressive behavior of wrapped specimens

Figure 6.5 illustrates the compressive strength and axial strain enhancement due to the FRP confinements. The favorable effect of confinement on compressive strength results was found to be slightly further on specimens tested at 28-days than specimens tested at 90-days. LC-CF-Co-W28-T28 and LC-BF-Co-W28-T28 specimens showed 2.76 (61 MPa) and 1.98 (43.7) times greater compressive strength values than LC-U-Co-T28 specimens (22.1 MPa), while LC-CF-Co-W28-T90 and LC-BF-Co-W28-T90 specimens exhibited 2.72 (75.81 MPa) and 1.93 (53.98 MPa) times higher compressive strength values than LC-U-Co-T90 specimens (27.9 MPa). This may be due to the effect of confinement becomes greater when compressive strength of matrix is low.

Similar observation was also observed for the HCFA specimens. HC-CF-Co-W28-T28 and HC-BF-Co-W28-T28 specimens showed 1.53 (73.6 MPa) and 1.19 (57.07 MPa) times greater compressive strength values than HC-U-Co-T28 specimens (48.1 MPa), while HC-CF-Co-W28-T90 and HC-BF-Co-W28-T90 specimens exhibited 1.58 (91.41 MPa) and 1.19 (68.55 MPa) times higher compressive strength values than HC-U-Co-T90 specimens (57.7 MPa). Results showed that the effect of confinement on compressive strength is strongly related to the matrix strength. When the compressive strength of the matrix is high, the effect of FRP confinement on compressive strength of the hybrid specimens becomes low, or vice versa.

For the specimens exposed to sea water environment, strength improvement due to FRP confinements was also found to compressive strength dependent. LC-CF-Sw-W28-T90 and LC-BF-Sw-W28-T90 specimens showed 2.86 (74.57 MPa) and 2.02 (52.85 MPa) times greater compressive strength values than LC-U-SW-T90 specimens (26.1 MPa), whereas HC-CF-Sw-W28-T90 and HC-BF-Sw-W28-T90 specimens exhibited 1.76 (89.39 MPa) and 1.31 (66.41 MPa) times higher compressive strength values than HC-U-SW-T90 specimens (50.7 MPa). Results also indicated that unconfined HCFA-ECC specimens deteriorated more than LCFA-ECC specimens, which can be attributed to high CaO content in the HCFA-ECC specimens. Therefore, the effect of confinement on compressive strength was found to be more for specimens exposed to seawater than specimens exposed to ambient environment.

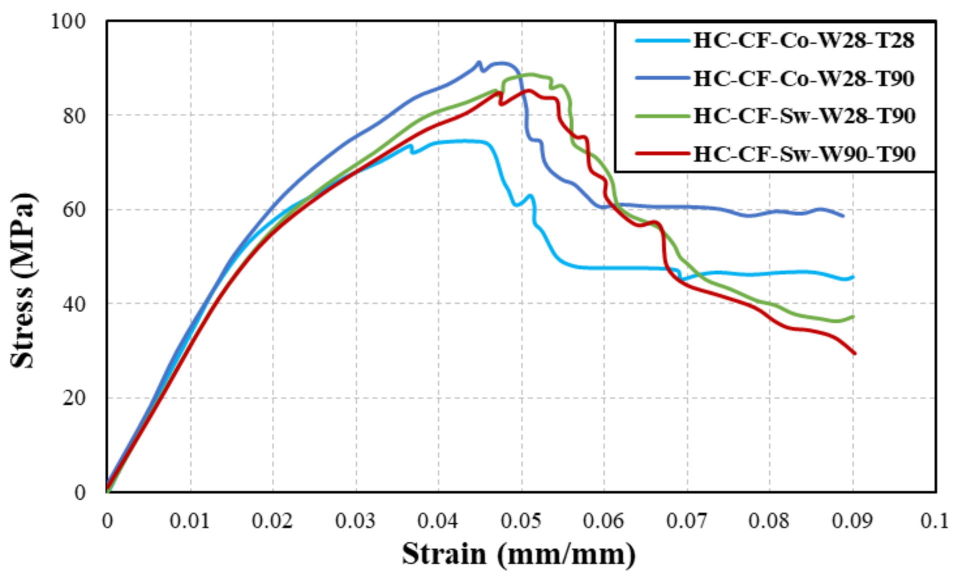

a) HCFA-ECC specimen wrapped by CFRP

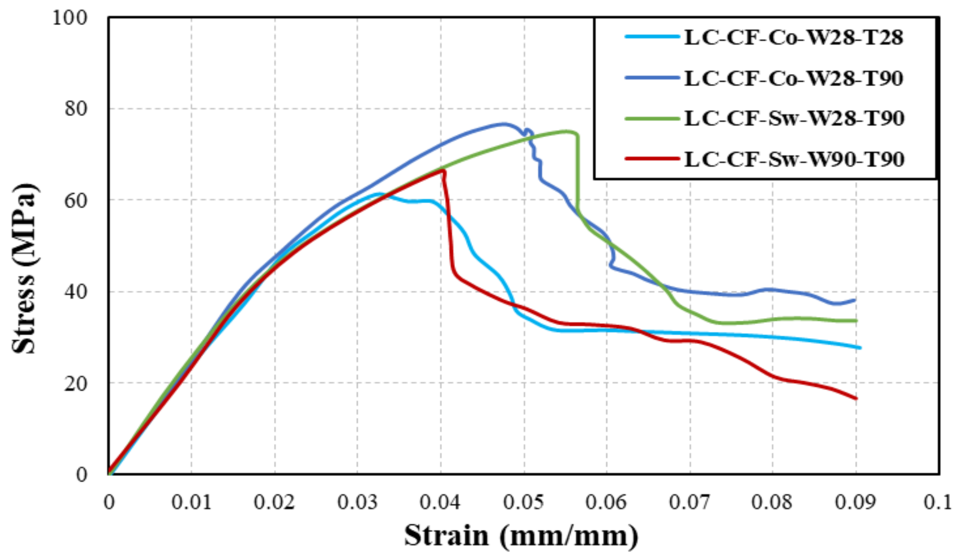

b) LCFA-ECC specimen wrapped by CFRP

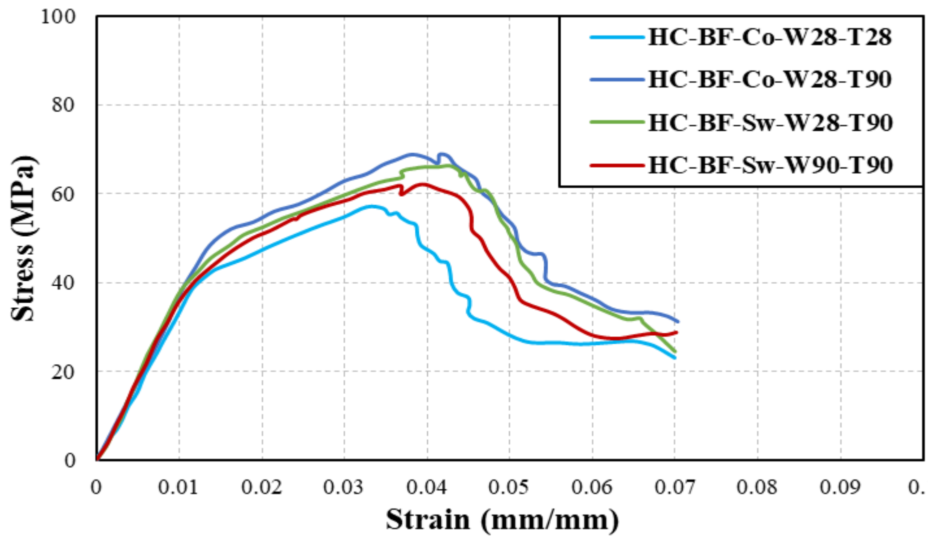

c) HCFA-ECC specimen wrapped by BFRP

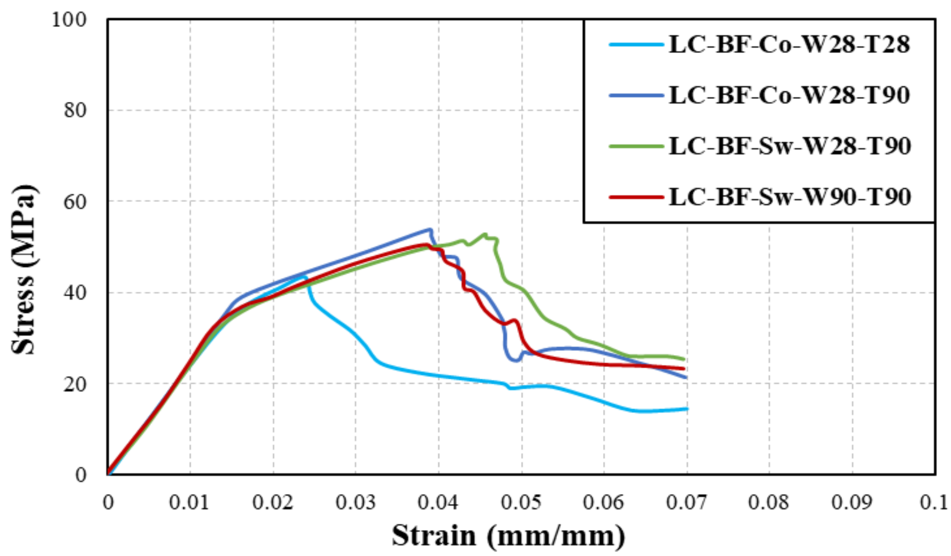

d) LCFA-ECC specimens wrapped by BFRP

Figure 6.5 Stress-strain curves of FRP confined ECC specimens

In addition to the enhancement of mechanical strength and durability, FRP fabrics also improve axial strain capability/ductility performance of the specimens. The ductility enhancement for ordinary concrete wrapped by FRP fabrics was stated in the literature (Photiou *et al.*, 2004). In general, PVA-ECC specimens had high toughness and ductility due to strain hardening behaviour. In addition to this, FRP-ECC hybrid materials yielded a very high lateral displacement capacity and toughness, especially after the initial rupture of FRP jacket (post-peak curve of the axial stress-strain curve). Therefore, FRP-ECC hybrid materials can be very significant in structural elements required high strength and ductility (especially structural column elements). In the study, strain capacity of the specimens increased from 0.04 (unconfined ECC) to 0.07 (for BFRP-ECC hybrid materials) and 0.09 (for CFRP-ECC hybrid materials) as shown in Figure 6.6. This increase can be attributed to the triaxle state of stress due to FRP confinement.

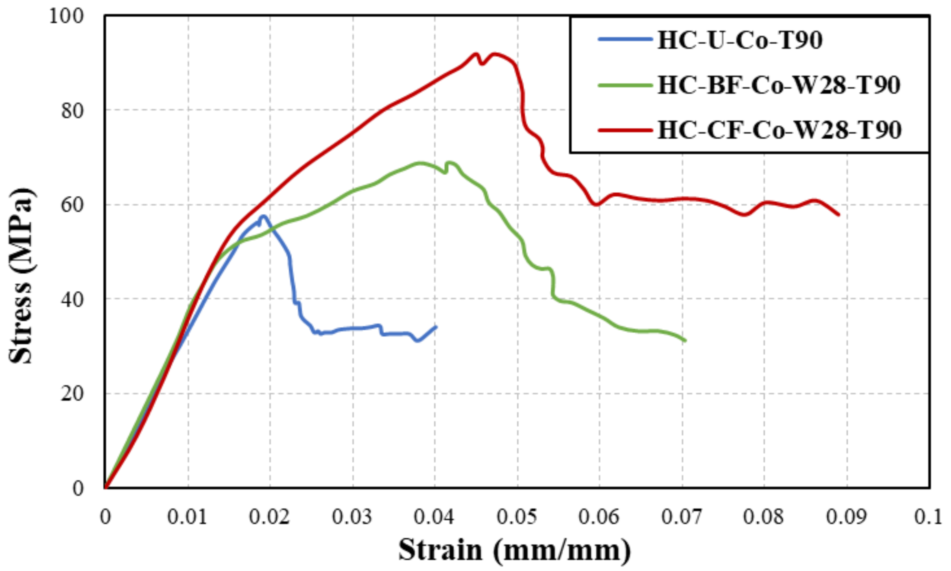

a) HCFA-ECC specimens

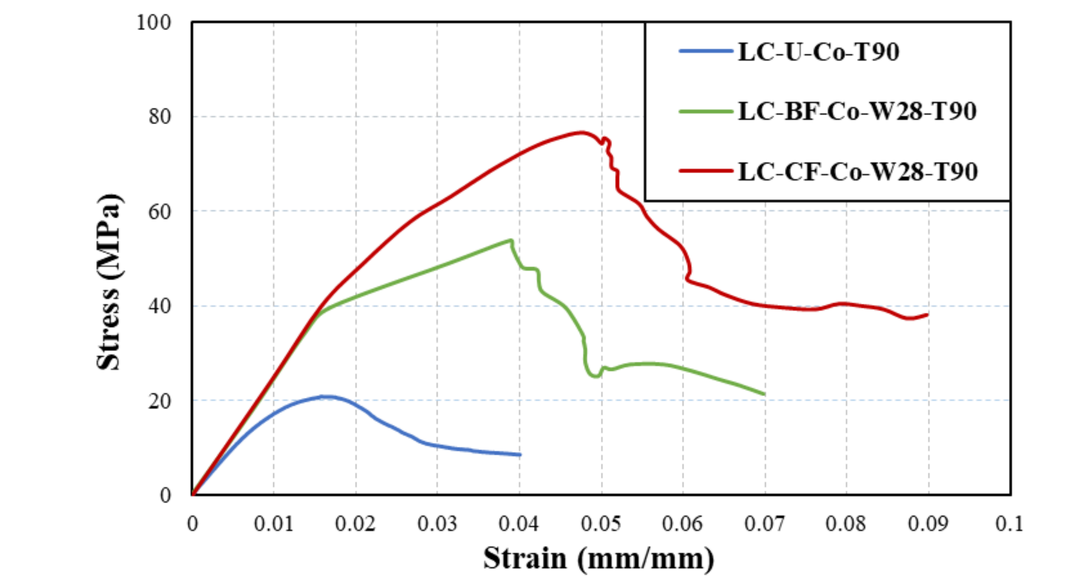

b) LCFA-ECC specimens

Figure 6.6 Stress-Strain Curves of wrapped and unwrapped ECC specimens

6.3.4 Failure modes of specimens under compression load

In general, ECC specimens confined by FRP fabrics exhibits similar behaviour with ordinary concrete wrapped with FRP fabrics under axial load. During axial loading, cylinder specimens start to expand and PVA-ECC and FRP fabrics show resistance to the expansion by creating confinement around the specimens. As tensile stresses due to axial load exceed the tensile strength of the ECC matrix composite, failure initiates from FRP rupture. The noise related to the micro-cracking of concrete was obvious during early periods of the loading process, showing the initiation of the stress transfer from concrete to the FRP jacket. The cracking noises intensity of expanded concrete could be heard prior to failure of FRP jacket with a sudden and violent noise. In the study, all failures realized due to the rupture of FRP jacket and then followed by failure of PVA-ECC matrix. No de-bonding failure was detected in FRP confined specimens. The failure due to FRP de-bonding had rarely been specified by some studies (Bradford, 1995; Demers and Neale, 1999).

Figure 6.7 shows the failure modes of the hybrid specimens due to compressive loading. For these specimens, crack generation started at the bottom or top regions of the cylinder specimen and crack progressing increased until the failure localizes at these regions due to high stress concentrations produced by the friction between the machine plates and the specimen. Since FRP sheet was applied uni-directional, the failure of the FRP fabrics occurs suddenly due to shearing off FRP jacket and then FRP fibers cannot be able to carry the load transfer. As stated in earlier, low popping noises during various periods of loading procedure were heard (Lau and Zhou, 2001; Taghia and Bakar, 2013). As the FRP jacket was removed, it was noticed clearly that the failure of most of the specimens occurred at the top or bottom region of the specimens due to the existence of PVA fibers that prevent the crack development into the mid-height of the ECC specimens (Li *et al.*, 2002). This performance may be attributed to the deterioration at outer surfaces (~ 1 cm) under seawater solution.

(a) U-LCFA (b) U-HCFA (c) BF-LCFA (d) CF-LCFA

(e) U-LCFA (f) U-HCFA (g) BF-LCFA (h) CF-LCFA

Figure 6.7 Failure mode of ECC specimens under seawater (a,b,c,d) and under ambient (e,f,g,h) environments

6.4 Cyclic Loading Behavior

Figures 6.8 and 6.9 give stress-strain curves of the specimens under static and cyclic loadings. Results indicated that pre-peak behaviour of unconfined and confined by FRP fabric samples as a result of static and reversed loading was found to be almost linear up to the maximum loads even for the specimens subjected to seawater environment. At the post-peak zone, a slight deviation is observed for the static and cyclic curve and the deviation was found to be further for the unconfined HCFA-ECC hybrid specimens, which may be due to the high deterioration resulted from high CaO content for the specimens.

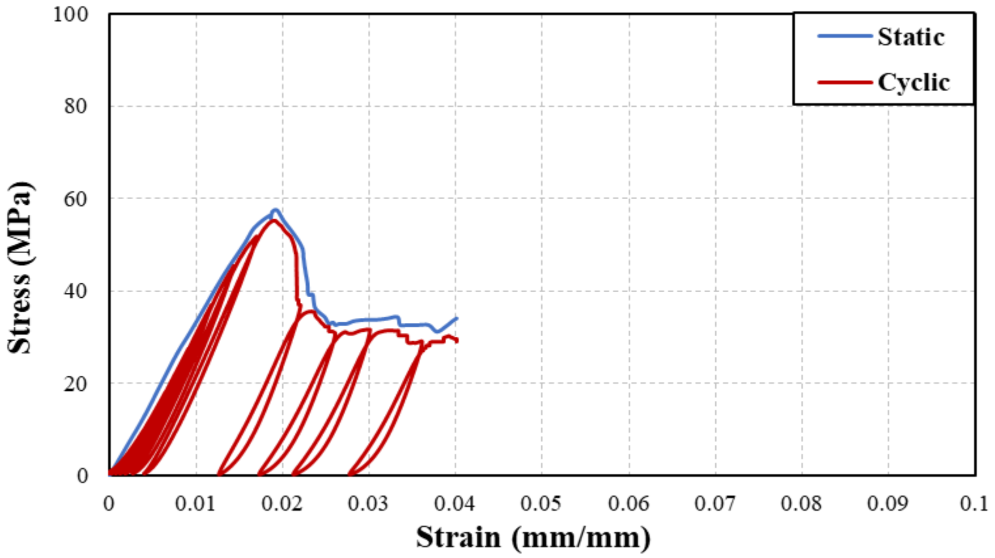

a) HCFA-ECC specimen exposed to ambient environment

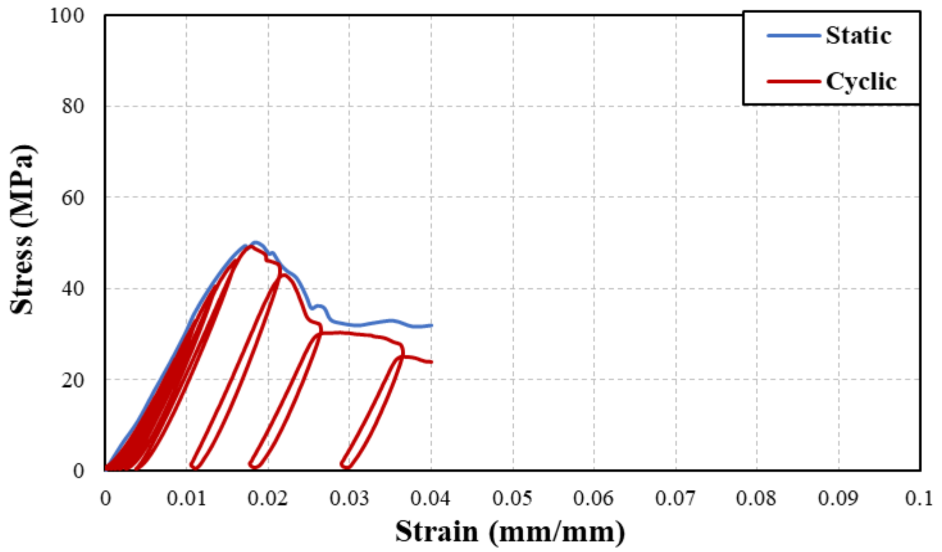

b) HCFA-ECC specimen exposed to seawater environment

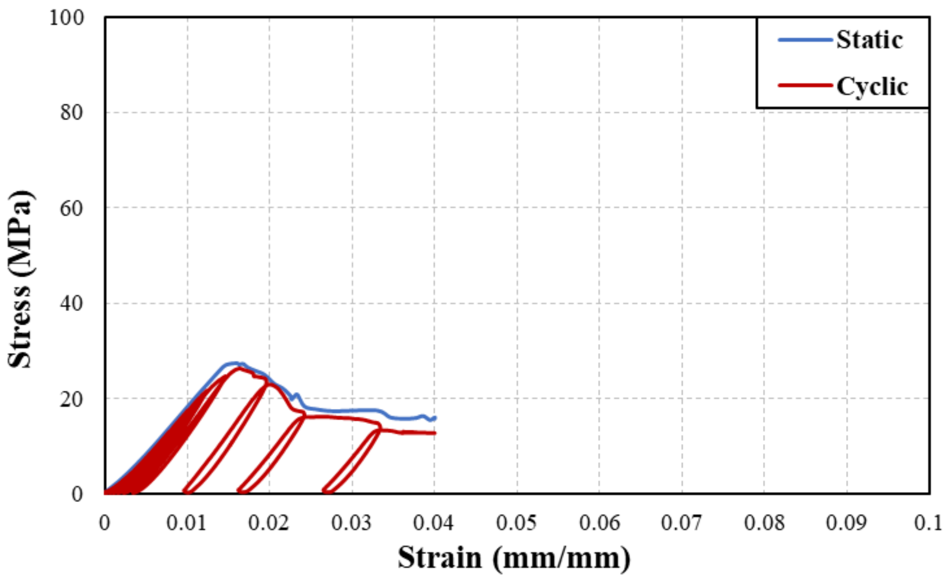

c) LCFA-ECC specimen exposed to ambient environment

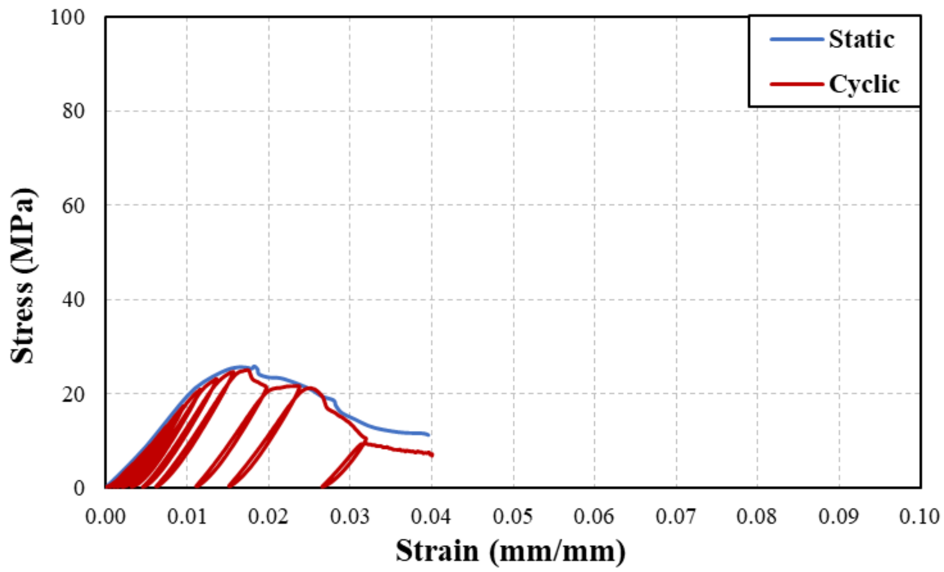

d) LCFA-ECC specimens exposed to seawater environment

Figure 6.8 Static and cyclic loading diagrams of unwrapped ECC specimens exposed to seawater and ambient environment

For the confined specimens, similar stress relaxation was obtained for the reversed and static loadings, which can be attributed the elastic behaviour of the FRP fabrics. The envelopes of stress-strain curves for wrapped and unwrapped samples under cyclic loading can achieve by bridging the peak points of the unloading cycles and the reached curve was mostly matches with the stress-strain curve under static loading. Lam et al. (Lam *et al.*, 2006) and Shah et al. (Shah *et al.*, 1983) were also reported similar investigations and they also stated that this behaviour is also suitable for FRP confined concretes. In this study, the static and cyclic loading curves of tested specimens wrapped by basalt and carbon FRP followed to each other as indicated in Figure 6.9. The similar outcomes were also obtained in the previous studies (Shah *et al.*, 1983; Theodoros, 2001; Lam *et al.*, 2006).

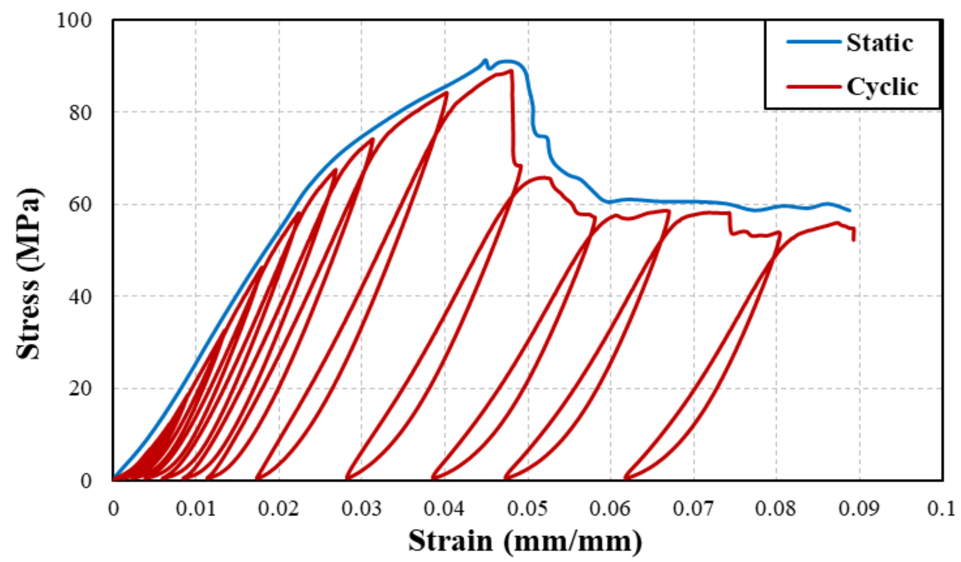

a) HCFA-ECC specimen wrapped by CFRP exposed to ambient environment

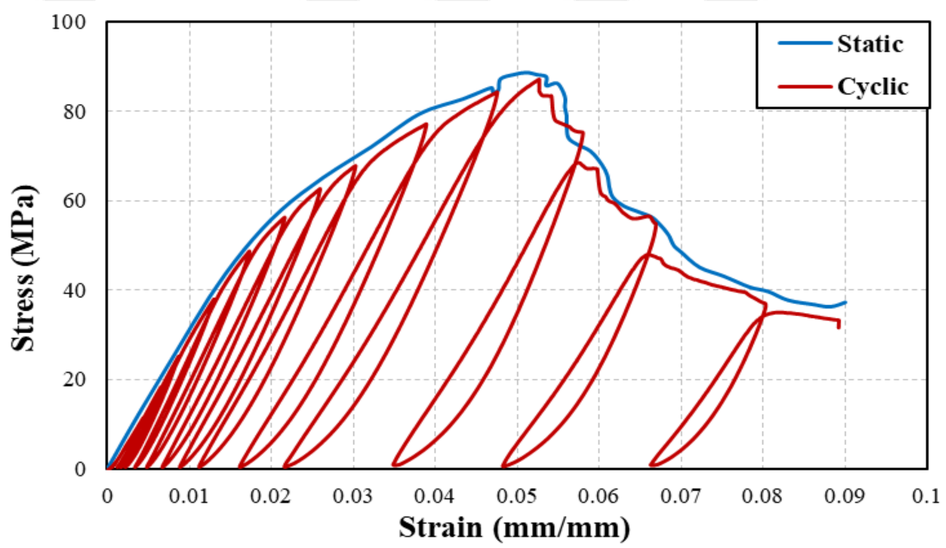

b) HCFA-ECC specimen wrapped by CFRP exposed to seawater environment

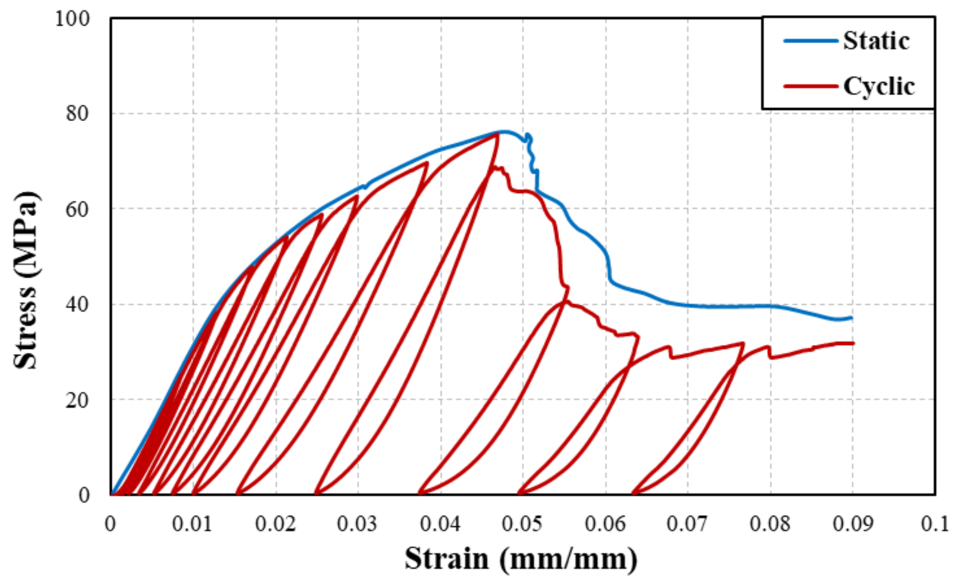

c) LCFA-ECC specimen wrapped by CFRP exposed to ambient environment

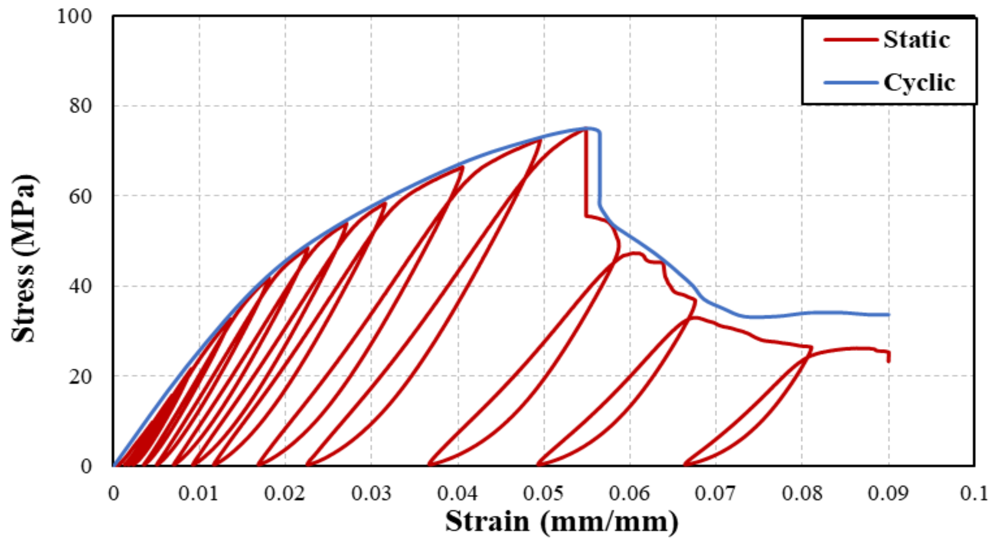

d) LCFA-ECC specimens wrapped by CFRP exposed to seawater environment

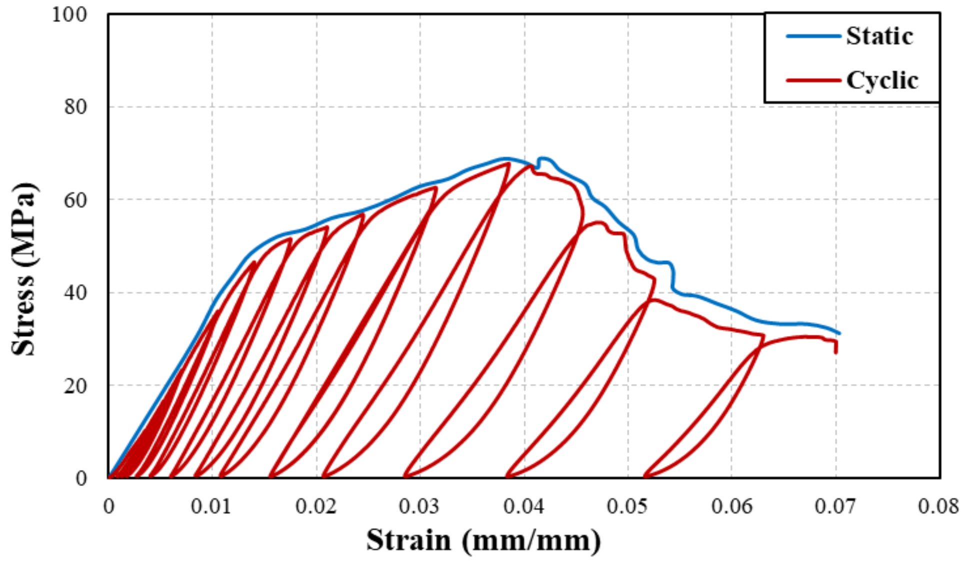

e) HCFA-ECC specimen wrapped by BFRP exposed to ambient environment

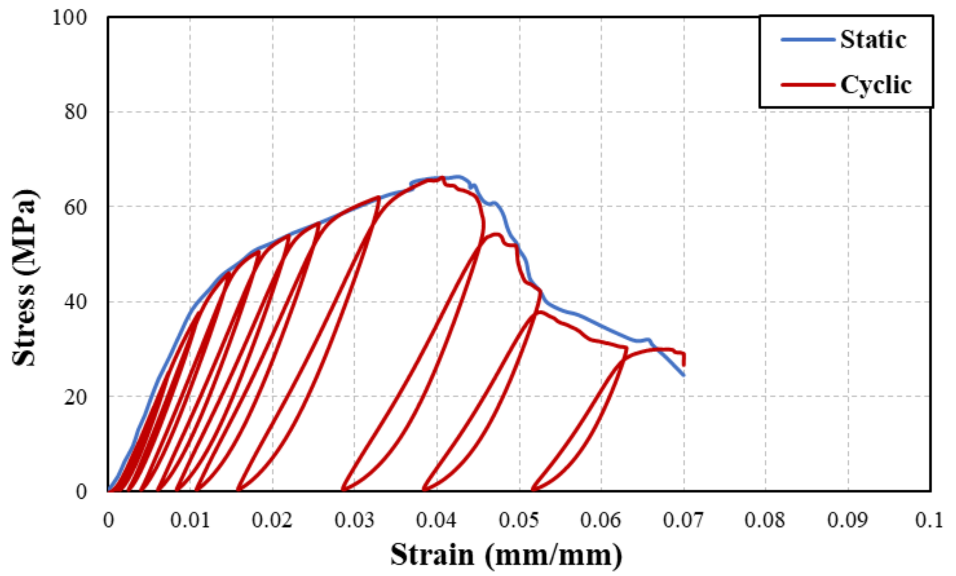

f) HCFA-ECC specimen wrapped by BFRP exposed to seawater environment

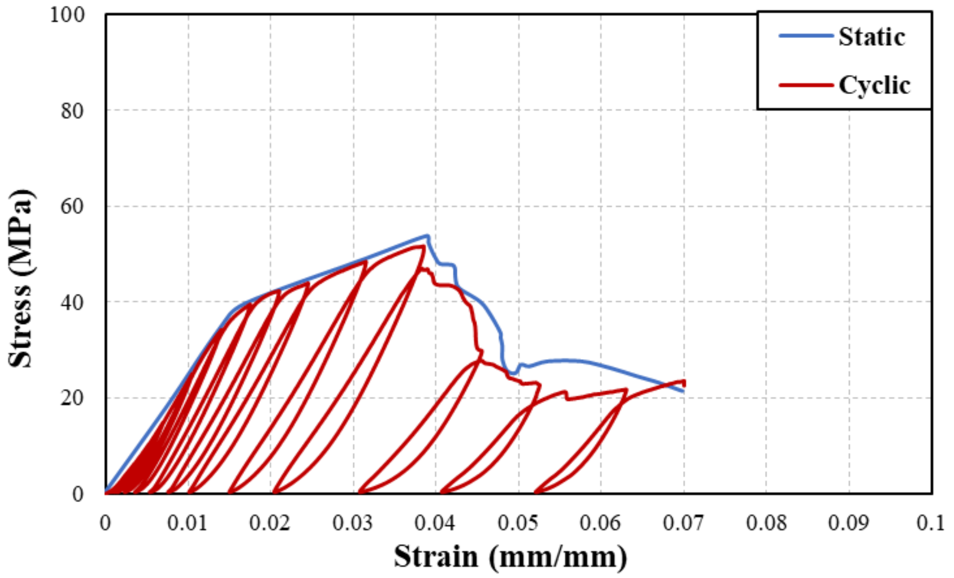

g) LCFA-ECC specimen wrapped by BFRP exposed to ambient environment

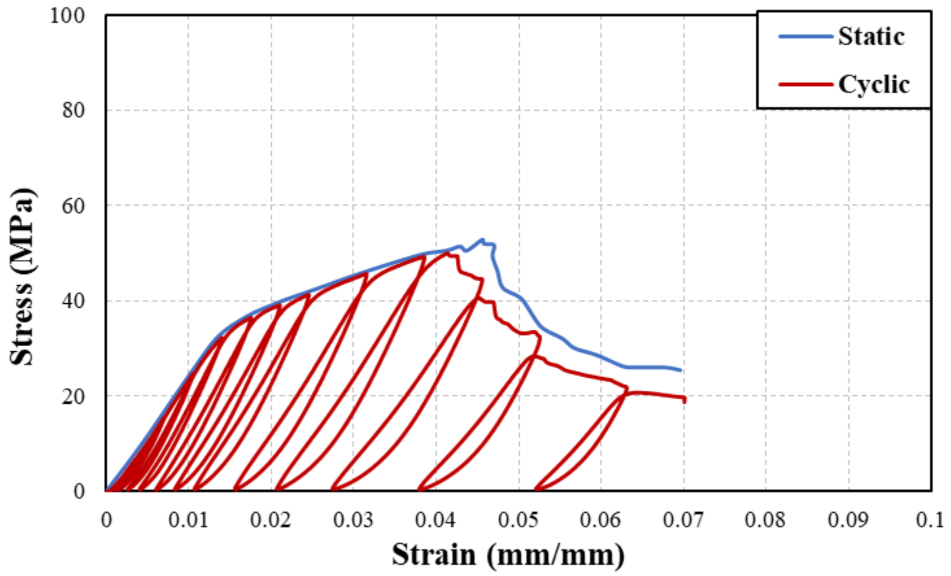

h) LCFA-ECC specimens wrapped by BFRP exposed to seawater environment

Figure 6.9 Static and cyclic loading diagrams for wrapped ECC specimens exposed to ambient and seawater environment

6.5 Scanning Electron Microscopy (SEM)

Scanning electron microscopy (SEM) was utilized to analyse confined and unconfined hybrid specimens in micro-scale to reveal the seawater effect on the surface of PVA fibers and the interfacial transition zone between the fibers and the matrix. In addition, the changes on basalt and carbon FRP fabrics were examined in microscale. In order to prepare SEM samples, one-inch (2.54 cm) slices were removed and discarded from both top and bottom parts of the specimens, and thick circular slice of 1 cm was used for SEM observations. The width of the seawater affected zone was about 8 mm from the outer surface of the cylinder specimen as observed in Figure 6.1. Thus, for each specimen two SEM samples were taken, one of them was taken inside the seawater effected region (0-1 cm from the outer surface) and the other one was taken from the not-effected region (close to the effected zone but out of the 1 cm from the outermost layer).

Figure 6.10 illustrates the SEM photos of the unconfined specimens under ambient and sea water conditions. Results indicated that white sediments/ettringite form on the surface of the PVA fibers and the number of sediments for HCFA specimens was much more than LCFA specimens. This may be attributed to the high content of CaO, higher ratio of Ca/Si and high amount of free calcium. Similar results were also obtained in the previous study (Ariffin *et al.*, 2013). Researchers investigated durability properties of the two types of fly ashes; FA1 (including low calcium) and FA2 (including high calcium) and found out that specimens containing low calcium fly ash showed less compressive strength decrease due to the low calcium content. The formation of gypsum and ettringite can create expansion, dimensional instability, cracking, spalling and at the end of the processes reduced mechanical properties were obtained (Bassuoni and Nehdi, 2007; Ariffin *et al.*, 2013). As mentioned previously, SEM images were also taken out of the seawater affected zone (specified after 1cm from the outer surface) and SEM photos of the second region (SEM_2) revealed that the number of white sediments on the surface of the PVA fibers was found to be low. Results proved that seawater attacks initiates from the outer layer and progresses to the inner side of the specimens. It was also pointed out that the adverse effect of seawater on HCFA-ECC hybrid specimens was higher than LCFA-ECC hybrid specimens at both seawaters affected and unaffected zone. The white sediments also noticed in the transition zone, which is the explanation of the reduced bond between PVA fibers and cement matrix.

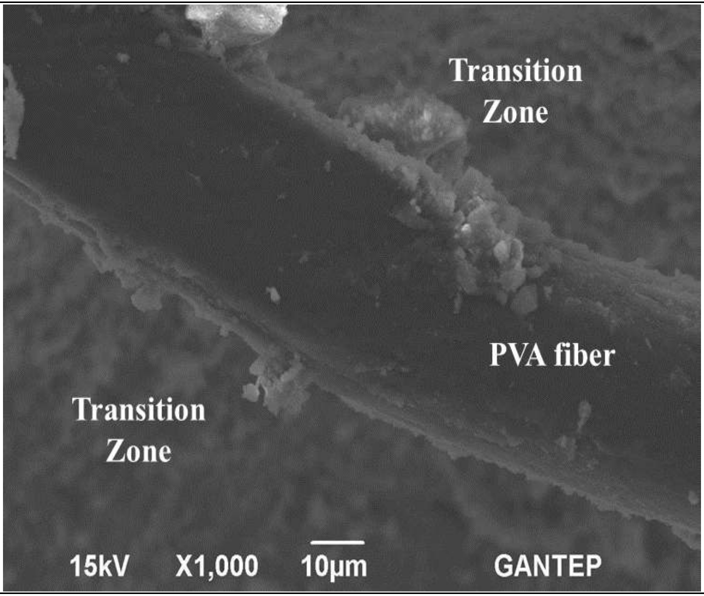

a) HCFA-ECC specimen exposed to ambient environment

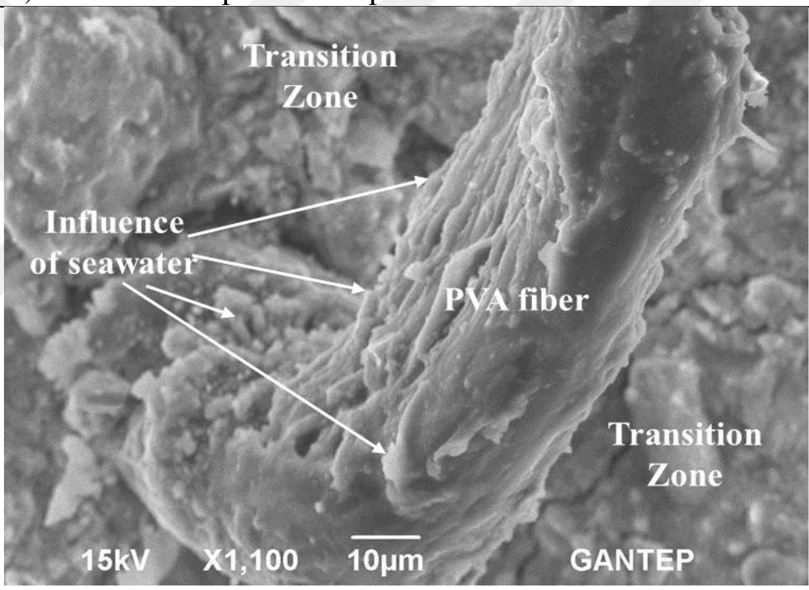

b) HCFA-ECC specimen exposed to seawater environment (at the outer part 0.8cm)

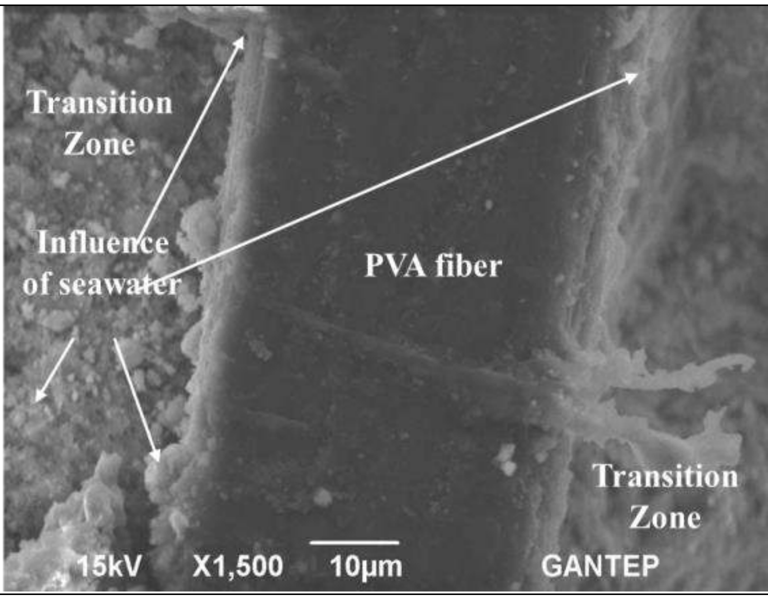
c) HCFA-ECC specimen exposed to seawater environment (after 1cm from the outer surface)
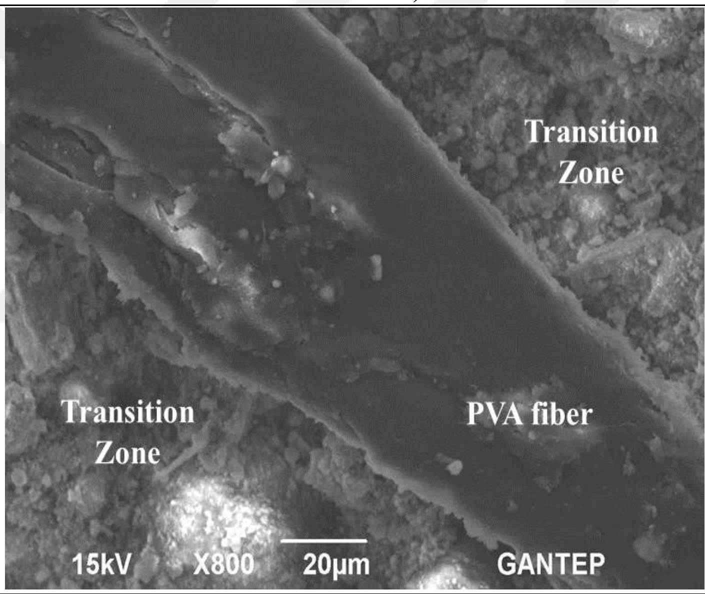
d) LCFA-ECC specimens exposed to ambient environment

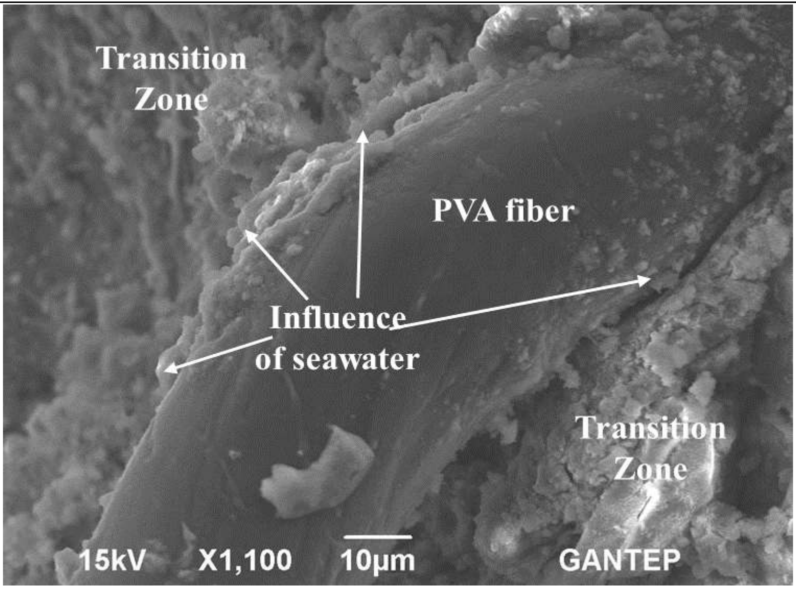

e) LCFA-ECC specimen exposed to seawater environment at the outer part (0-1 cm)

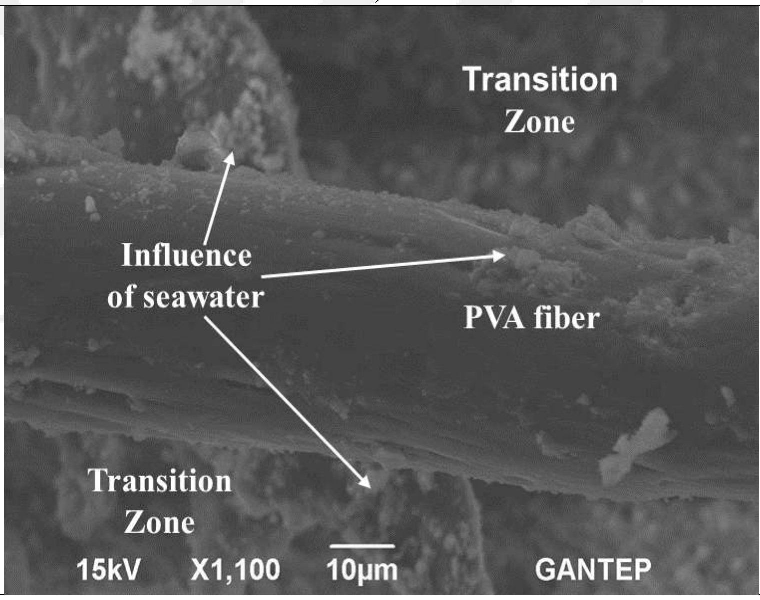

f) LCFA-ECC specimens exposed to seawater environment at the part after 1cm

Figure 6.10 SEM photos of unwrapped ECC specimens exposed to ambient and seawater environment

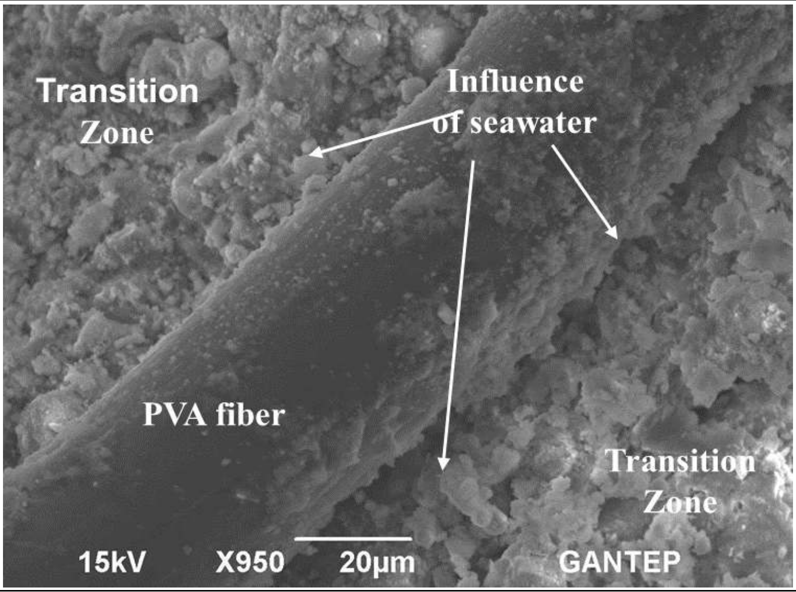

a) LCFA-ECC specimen wrapped by CFRP exposed to seawater environment at the outer part (0-1cm)

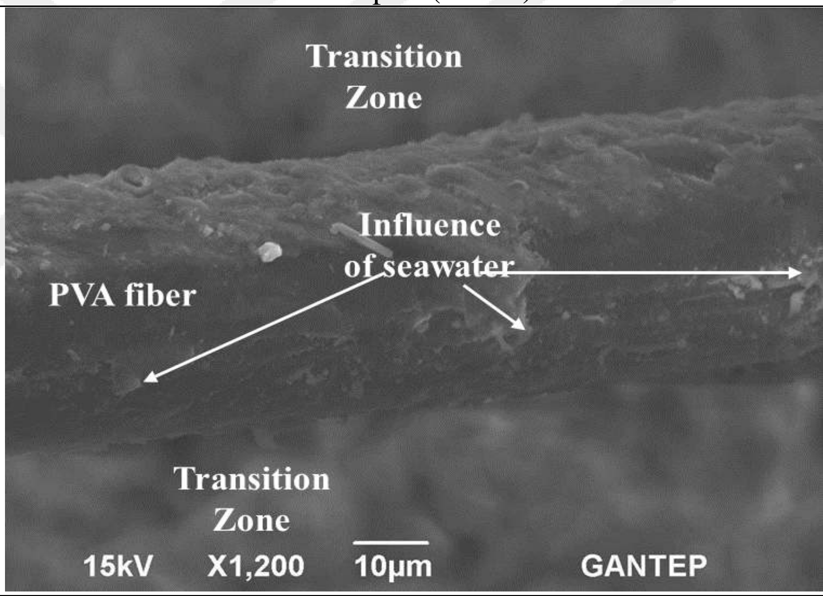

b) LCFA-ECC specimen wrapped by CFRP exposed to seawater environment at the part after 1cm

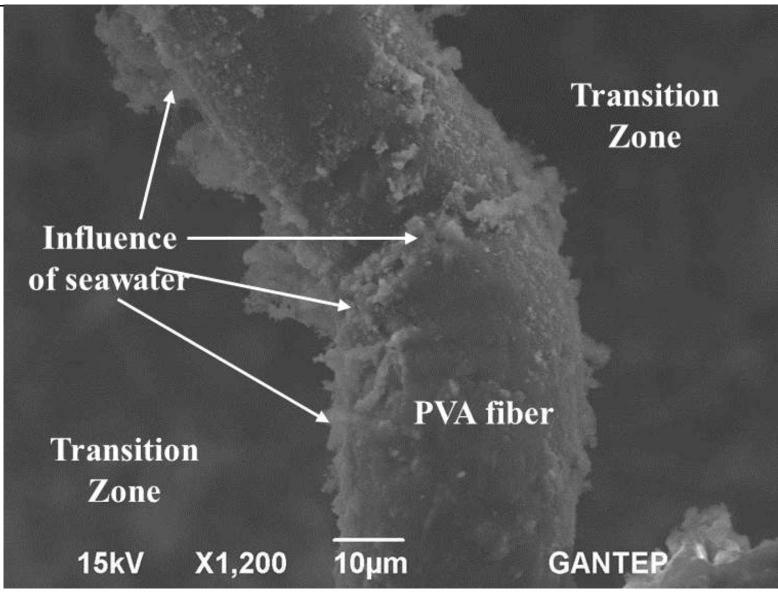

c) LCFA-ECC specimen wrapped by BFRP exposed to seawater environment at the outer part (0-1cm)

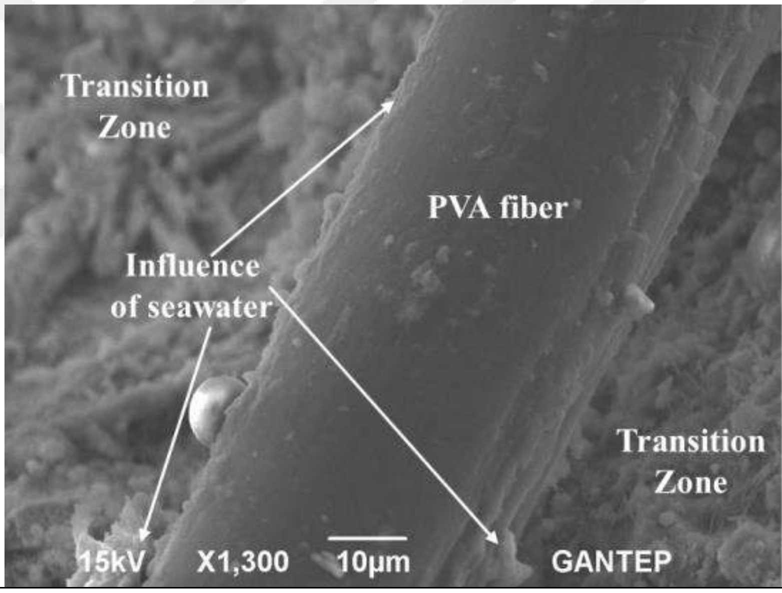

d) LCFA-ECC specimen wrapped by CFRP exposed to seawater environment at the part after 1cm

Figure 6.11 SEM photos of FRP wrapped ECC specimens exposed to ambient and seawater environment

Figure 6.11 illustrates SEM photos of HCFA-ECC specimens confined by basalt and carbon FRP fabrics. Outcomes showed that PVA-ECC specimens confined by carbon and basalt FRP were less deteriorated by seawater attack than unconfined ECC specimens. FRP materials sacrificed itself to protect ECC matrix from chemical solutions. In addition, carbon and basalt FRP fibers were also affected by the seawater attack. Due to the sensitivity of epoxy resin to alkaline solutions, CFRP and BFRP fabrics were also significantly affected by the seawater solutions. Furthermore, due to the higher bond between carbon FRP fabrics and the epoxy resin, specimens wrapped by CFRP fabrics were less affected by seawater compared to the specimens wrapped by BFRP fabrics as shown in Figure 6.12.

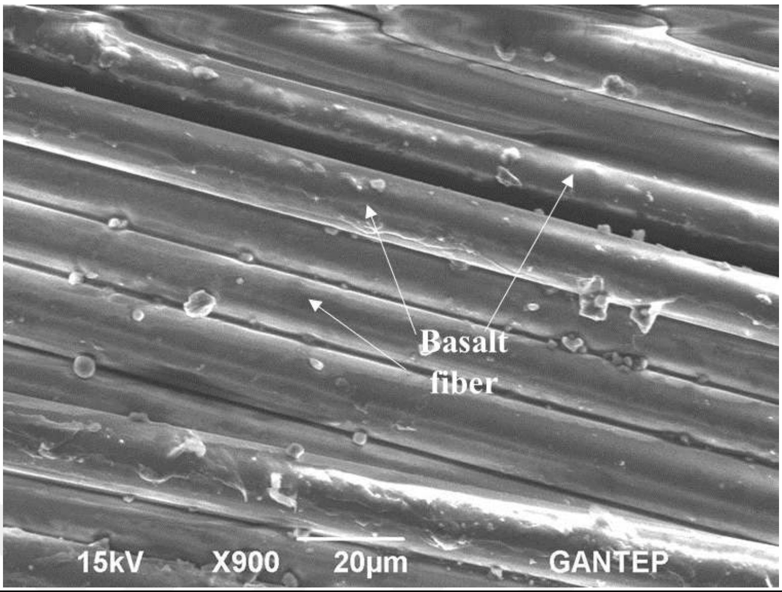

a) BFRP sheet without epoxy exposed to ambient environment

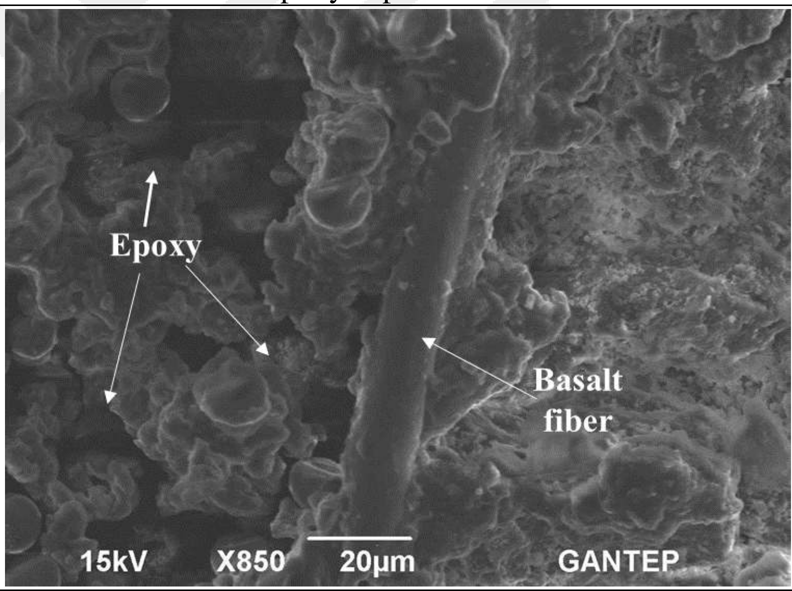

b) BFRP sheet with epoxy exposed to ambient environment

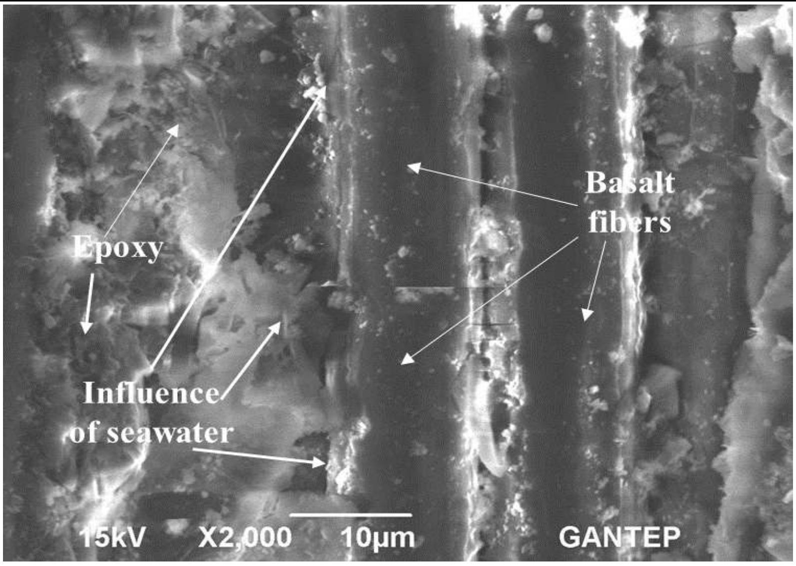

c) BFRP sheet with epoxy exposed to seawater environment

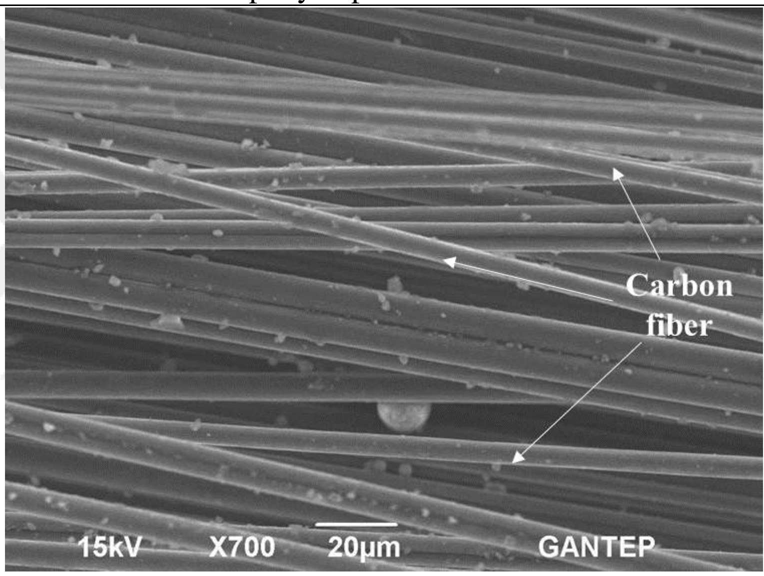

d) CFRP sheet without epoxy exposed to ambient environment

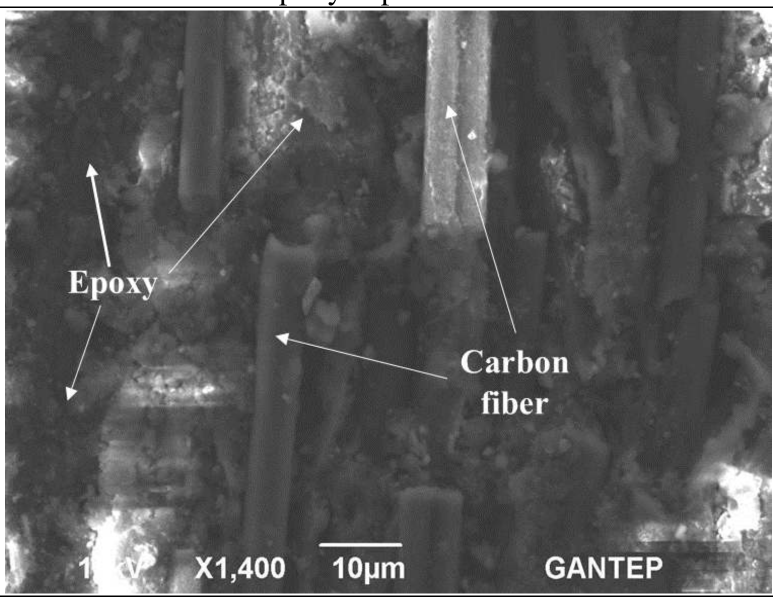

e) CFRP sheet with epoxy exposed to ambient environment

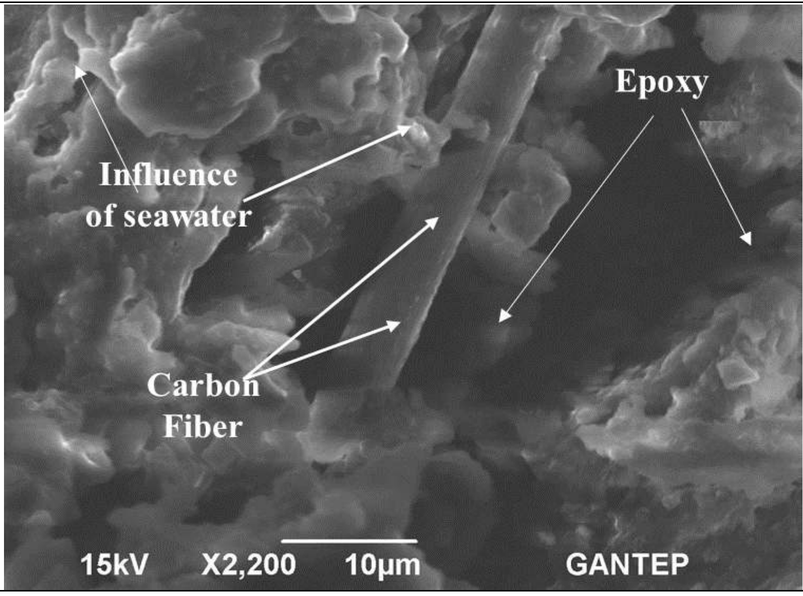

f) CFRP sheet with epoxy exposed to seawater environment

Figure 6.12 SEM photos of BFRP and CFRP fabric sheets exposed to ambient and seawater environment

CHAPTER 7
CONCLUSION AND RECOMMENDATIONS

7.1 Conclusion

In the study, mechanical performance (strength and ductility) and durability properties of ECC, CFRP-ECC and BFRP-ECC hybrid specimens produced with low calcium (LCFA) and high calcium fly ash (HCFA) based matrix were investigated under 3.5% seawater and ambient environments. Static and cyclic loadings were applied to the hybrid materials to observe any deterioration in the mechanical and ductility performance under reversed loadings (earthquake loading) in the sea water/marine environment. The study also focuses on the behaviour of the CFRP and BFRP fabric materials using different matrix types under seawater environment. In order to observe micro-scale changes due to sea water environment, SEM images were performed and evaluated on the hybrid specimens. In addition, FRP fabric material use as a retrofit material is also examined on the seawater influenced specimens. The main findings of the study can be summarized as follows:

- Visual inspection results indicated that surface color of the high lime containing fly ash (HCFA) specimens exposed to sulphuric acid changed from grey to white after 15 days of exposure, while the surface color of the low lime fly ash specimens (LCFA) exposed to sulphuric acid remained grey even after two months of exposure. In addition, more lateral expansion was observed for HCFA specimens.
- Visual inspections showed that specimens maintained their initial condition and there is no cracking and spalling observed in the specimens exposed to both sulfate and seawater. Only a small layer of efflorescence was observed on the specimen surfaces and the amount of surface erosion was found to be more for the unconfined ECC specimens at the end of the sulfate and seawater exposure. In addition, the surface of the PVA fibers and FRP fabric sheets were also slightly affected by sulfate and seawater solution.

- Mechanical strength results indicated that high calcium fly ash based concrete (HCFA) showed better compressive strength performance than the low calcium fly ash based concrete (LCFA) due to high CaO content. This enhanced performance is still valid when specimens were confined by FRP materials. When hybrid material performance was evaluated, specimens confined by carbon FRP performed outstanding performance than the basalt FRP and unconfined specimens, respectively.
- The degree of the enhancement in the mechanical performance also depends on the matrix type. When high strength concrete is used, the favorable effect of FRP confinement on compressive strength becomes less than the effect of normal strength concrete. In addition, HCFA-CFRP hybrid specimens showed the superior performance than the LCFA-ECC hybrid specimens. The compressive strength of the ECC specimens followed a trend: HCFA-CFRP hybrid specimens > HCFA-BFRP hybrid specimens > LCFA-CFRP hybrid specimens > LCFA-BFRP hybrid specimens. Under normal environment (no chemical exposure), HCFA-CFRP hybrid specimens should be used in structural elements when high strength and ductility is required.
- Ductility results indicated that specimens confined with CFRP showed highest axial strain capability of 0.09, specimens confined with BFRP showed moderate axial strain capability of 0.07 and unconfined specimens showed the lowest axial strain capability of 0.04. Therefore, CFRP fabrics materials performed highest ductility under both ambient and chemical attack environments.
- Specimens exposed to chemical attack indicated that the deterioration amount was found to be high for the HCFA matrix type due to the high CaO content and SEM images proved that white deposits were observed to be more for the HCFA specimens. When compared to FRP materials, carbon FRP materials affected less from the chemical attacks as compared to basalt FRP materials due to the higher bond between carbon FRP fabrics and the epoxy resin. SEM images also showed less amount white deposits for the specimens confined by carbon FRP fabrics.
- SEM images pointed out that deterioration due to chemical attack starts from the surface and progresses into the inner side of the specimens. Therefore,

white deposits were observed more at the outer side of the specimens. LCFA type of matrix with carbon FRP showed the least deterioration under chemical attack solutions. Therefore, LCFA-CFRP hybrid specimens should be used for structures required high strength and ductility under chemical environment.

- As a retrofit or rehabilitation materials, both type of FRP materials (carbon FRP and basalt FRP) can be utilized under both ambient and chemical attack environments. The highest strength enhancement was obtained for specimens confined by carbon FRP.
- The envelopes of stress-strain curves of confined and unconfined specimens obtained from static and cyclic loadings yielded similar stress-strain behavior under ambient condition. When specimens under chemical attack is evaluated, the pre-peak behavior part of the stress-strain curve is found similar for static and cyclic loading. However, for the unconfined specimens at the post-peak zone, static and cyclic curve separated from each other especially for the unconfined HCFA specimens, which may be attributed to the further reduction in elastic modulus due to softening upon continuous loading/unloading cycles. When confined specimens were evaluated, similar stress relaxation was obtained under static and cyclic loading, which may be due to the existence of the FRP materials that showed greatest resistance against reversed loadings.
- Due to the sensitivity of the epoxy to the chemical attack environment, CFRP and BFRP fabrics are also significantly affected by the chemical attack. However, due to the existence of the high bond between carbon FRP fabric and the epoxy, CFRP fabrics were less affected than BFRP fabrics by the chemical attack.

7.2 Recommendations

In the lights of this conclusions. I recommend the following investigations: -

1. Use of different pozolanic materials like (Ground Granulated Blast Furnace Slag (GGBFS), Meta-kaolin) with or instead of fly ash in the production of ECC concretes under chemical attacks.
2. Incorporate the nano-silica in the production of ECC concretes under chemical environments.
3. Microstructure analysis of different concretes under chemical attacks, to evaluate the influence of CaO contain on the mechanical and durability behavior under chemical environments.

- Use of various type of resin, to evaluate the strong and durable resins under chemical environments.

REFERENCES

ACI Committee 116R (1994). Cement and Concrete Terminology, *Detroit, Michigan: ACI manual of concrete practice*.

ACI Committee 224 (2001). Control of Cracking in Concrete Structures Reported (ACI Committee 224R-01), *American Concrete Institute, Farmington Hills, MI*, p. 46. doi: 0097-8515.

ACI Committee 440 (2002). Guide for the Design and Construction of Externally Bonded FRP Systems for Strengthening Concrete Structures (ACI 440.2R-02), *Farmington Hills, Mich: American Concrete Institute (ACI).*

Al-Tamimia, A., Abed, F. H. and Al-Rahmani, A. (2014). Effects of harsh environmental exposures on the bond capacity between concrete and GFRP reinforcing bars, *Advances in concrete construction*. Techno-Press, **2**(**1**), pp. 1–11.

Anwar Hossain, K. M. (2012). Lightweight concrete incorporating volcanic materials', *Proceedings of the ICE - Construction Materials*, **165**(**2**), pp. 111–120. doi: 10.1680/coma.900064.

Ariffin, M. A. M. *et al.* (2013). Sulfuric acid resistance of blended ash geopolymer concrete, *Construction and Building Materials*. Elsevier Ltd, **43**, pp. 80–86. doi: 10.1016/j.conbuildmat.2013.01.018.

ASTM C267 - 01 (2012). *Standard Test Methods for Chemical Resistance of Mortars, Grouts, and Monolithic Surfacings and Polymer Concretes*.

ASTM C39/C39M-12 (2012). *Standard test method for compressive strength of cylindrical concrete specimens*, *annual book of ASTM standard, Philadelphia*.

ASTM C618 (2012). *Standard Specification for Coal Fly Ash and Raw or Calcined Natural Pozzolan for Use in Concrete*, *West Conshohocken, PA: ASTM International*.

Attiogbe, E. K. and Rizkalla, S. H. (1988). Response of concrete to sulfuric acid attack', *ACI Materials Journal*, **85**(**6**), pp. 481–488.Bank, L. C. (2006). *Composite* *for construction: structural design with FRP materials*. John Wiley & Sons.

Baoying, D. *et al.* (1994). A Review on Causes of Cracking in Domestic Concrete Dams and Preventive Measures [J], *Water Resources and Hydropower Engineering*, **4**, pp. 12–18.

Bassuoni, M. T. and Nehdi, M. L. (2007). Resistance of self-consolidating concrete to sulfuric acid attack with consecutive pH reduction, **37**, pp. 1070–1084. doi: 10.1016/j.cemconres.2007.04.014.

Bisaillon, A., Rivest, M. and Malhotra, V. M. (1994). Performance of high-volume fly ash concrete in large experimental monoliths, *Materials Journal*, **91**(**2**), pp. 178–187.
Bo-Fang, Z. H. U. (2006). Current situation and prospect of temperature control and cracking prevention technology for concrete dam, *Journal of Hydraulic Engineering*, **12**(**32**), p. 1424–1432.

Bonen, D. (1992). Composition and Appearance of Magnesium-Silicate-Hydrate and it Relation to Deterioration of Cement-Based materials, *J. Am. Ceramic Soc.*, **75**(**10**), pp. 2904–2906.

Bonen, D. and Cohen, M. D. (1992). Magnesium sulfate attack on portland cement paste-I. Microstructural analysis, *Cement and Concrete Research*, **22**(**1**), pp. 169–180. doi: 10.1016/0008-8846(92)90147-N.

BP, B. (1968). Combating sulfate attack on concrete on bureau of reclamation projects, *Swenson EG, Editor. Performance of concrete: resistance of concrete to sulphate and other environmental conditions. Toronto (Canada): University of Toronto Press*, pp. 77–92.

Bradford, A. N. and N. M. (1995). FRP jacketed concrete under uniaxial compression, *Construction and Building Materials*, **9**, p. 115.

Brown, P. W. and Badger, S. (2000). The distributions of bound sulfates and chlorides in concrete subjected to mixed NaCl, MgSO4, Na2SO4 attack, *Cement and Concrete Research*. Elsevier, **30**(**10**), pp. 1535–1542.

Bryant, M. (1964). Effects of Seawater on Concrete, *U.S. Army Engineers, Waterways experiment station, Corps of Engineers, Vicks berg, Mississippi.*, p. Miscellaneous paper no 6-690.

Cai, J., Pan, J. and Zhou, X. (2017). Flexural behavior of basalt FRP reinforced ECC and concrete beams, *Construction and Building Materials*. Elsevier, **142**, pp. 423–430.

Ceroni, F., Cosenza, E., Gaetano, M. and Pecce, M. (2006). Durability issues of FRP rebars in reinforced concrete members, *Cement and Concrete Composites*, **28**(**10**), pp. 857–868. doi: 10.1016/j.cemconcomp.2006.07.004.

Chaallal, O., Hassan, M. and Shahawy, M. (2003). Confinement model for axially loaded short rectangular columns strengthened with fiber-reinforced polymer wrapping, *Structural Journal*, **100**(**2**), pp. 215–221.

Chakrabortty, A. and Khennane, A. (2014). Failure mechanisms of hybrid FRP-concrete beams with external filament-wound wrapping, *Advances in Concrete Construction*, **1**, pp. 57–75.

Choucha, S., Benyahia, A., Ghrici, M. and Mansour, M.S.. (2017). Effect of natural pozzolan content on the properties of engineered cementitious composites as repair material, *Frontiers of Structural and Civil Engineering*. Springer, pp. 1–9.

Cohen, M. D. (1983). Theories of expansion in sulfoaluminate-type expansive cements: schools of thought, *Cement and Concrete Research*. Elsevier, **13**(**6**), pp. 809–818.

Concrete Society (2004). Design guidance for strengthening concrete structures using fibre composite materials, *The Concrete Society, Wiltshire UK Technical Rep.*, 55.

Deb, P. S. (2013). School of Civil and Mechanical Engineering Department of Civil Engineering Durability of Fly Ash Based Geopolymer Concrete Partha Sarathi Deb.

Demers, M. and Neale, K. W. (1999). Confinement of reinforced concrete columns with fibre-reinforced composite sheets-an experimental study, *Canadian Journal of Civil Engineering*. NRC Research Press, **26**(**2**), pp. 226–241.

Diamond, S. (2004). The microstructure of cement paste and concrete----a visual primer, *Cement and Concrete Composites*. Elsevier, **26**(**8**), pp. 919–933.

Fardis, M. N. and Khalili, H. (1981). Concrete encased in fiberglass-reinforced plastic, in *Journal Proceedings*, pp. 440–446.

Fardis, M. N. and Khalili, H. H. (1982). FRP-encased concrete as a structural material, *Magazine of Concrete Research*. Thomas Telford Ltd, **34**(**121**), pp. 191–202.

FBI (2001). Externally bonded FRP reinforcement for RC structures, *International Federation for Structural Concrete, Lausanne, Switzerland*.

Fischer, G. and Li, V. C. (2002). Effect of matrix ductility on the performance of reinforced ECC column members under reversed cyclic loading conditions.

Friberg, E. and Olsson, J. (2014). Application of fibre reinforced polymer materials in road bridges – General requirements and design considerations, p. 359.

Guide, A. E. (2009). FRP Material Selection Guide.

Halliwell, S. (2010). FRPs The environmental agenda, *Advances in Structural Engineering*. SAGE Publications Sage UK: London, England, **13**(**5**), pp. 783–791.

Halstead, W. J. (1986). Use of fly ash in concrete. NCHRP 127 (October). Washington, *Transportation Research Board, National Research Council*.

Hamilton, H.R., Benmokrane, B., Dolan, C.W. and Sprinkel, M.M. (2009). Polymer materials to enhance performance of concrete in civil infrastructure, *Taylor & Francis*.

Han, T. S., Feenstra, P. H. and Billington, S. L. (2003). Simulation of Highly Ductile Fiber-Reinforced Cement-Based Composite Components Under Cyclic Loading, *ACI Structural Journal*, **100**(**6**), pp. 749–757. doi: 10.14359/12841.

Hognestad, E. (1951). A study on combined bending and axial load in reinforced concrete members, *Univ. of Illinois Engineering Experiment Station, Univ. of Illinois at Urbana-Champaign, IL*, pp. 43–46.

Hollaway, L. C. (2010). A review of the present and future utilisation of FRP composites in the civil infrastructure with reference to their important in-service properties, *Construction and Building Materials*. Elsevier Ltd, **24**(**12**), pp. 2419–2445. doi: 10.1016/j.conbuildmat.2010.04.062.

Hossain, K., Mak, C. and Ametrano, D. (2012). GFRP Reinforced UHPC Composites for Sustainable Bridge Construction, *Canadian Civil Engineer*, **29**(**1**), pp. 12–15.

Hossain, K. (2003). Effect of Volcanic Pumice on The Corrosion Resistance and Chloride Diffusivity of Blended Cement Mortars, *Journal of Advanced Concrete Technology*, **1**(**1**), pp. 54–62.

Hossain, K. M. A. (2005). Volcanic ash and pumice as cement additives: Pozzolanic, alkali-silica reaction and autoclave expansion characteristics, *Cement and Concrete Research*, **35**(**6**), pp. 1141–1144. doi: 10.1016/j.cemconres.2004.09.025.

Hossain, K. M. A. and Lachemi, M. (2004). Corrosion resistance and chloride diffusivity of volcanic ash blended cement mortar, *Cement and Concrete Research*, **34**(**4**), pp. 695–702. doi: 10.1016/j.cemconres.2003.10.021.

Hsu, T. T. C. *et al.* (1963). Microcracking of plain concrete and the shape of the stress-strain curve, in *Journal Proceedings*, pp. 209–224.

International Code Council-Evaluation Service (ICC-ES) (1997). Acceptance criteria for concrete and reinforced and unreinforced masonry strengthening using fiber-reinforced polymer (FRP) composite systems (AC125), *ICC Evaluation Service, Whittier, CA*.

Sim, J. and Park, C. (2005). Characteristics of basalt fiber as a strengthening material for concrete structures, *Composites Part B: Engineering*, **36**, p. 50.

Kabele, P., Novak, L., Nemecek, J. and Pekar, J. (2007). Multiscale experimental investigation of deterioration of fiber-cementitious composites in aggressive environment, *In Proc. MHM 2007: Modelling of Heterogeneous Materials, with Applications in Construction and Biomedical Engineering, M. Jirasek, Z. Bittnar and H. Mang, eds*, pp. 270–271.

Karahan, O., Hossain, K.M., Ozbay, E., Lachemi, M. and Sancak, E. (2012). Effect of metakaolin content on the properties self-consolidating lightweight concrete, *Construction and Building Materials*. Elsevier Ltd, **31**, pp. 320–325. doi: 10.1016/j.conbuildmat.2011.12.112.

Kent, D. C. and Park, R. (1971). Flexural members with confined concrete, *Journal of the Structural Division*.

Kim, Y. Y., Kong, H.-J. and Li, V. C. (2003). Design of engineered cementitious composite suitable for wet-mixture shotcreting, *Materials Journal*, **100**(**6**), pp. 511–518.

Kosmatka, S. H., Kerkhoff, B. and Panarese, W. C. (2011). Design and control of concrete mixtures. *Portland Cement Assoc*.

Kumar, S., Sharma, N. and Ray, B. C. (2007). Acidic degradation of FRP composites, in *Proc. the National Conference on Developments in Composites, India*.

Kuroda, M., Watanabe, T. and Terashi, N. (2000). Increase of bond strength at interfacial transition zone by the use of fly ash, *Cement and Concrete Research*, **30**(**2**), pp. 253–258. doi: 10.1016/S0008-8846(99)00241-0.

Lam, L., Teng, J.G., Cheung, C.H. and Xiao, Y. (2006). FRP-confined concrete under axial cyclic compression, *Cement and Concrete Composites*. Elsevier, **28**(**10**), pp. 949–958.

Lau, K. and Zhou, L. (2001). The mechanical behaviour of composite-wrapped concrete cylinders subjected to uniaxial compression load, *Composite Structures*. Elsevier, **52**(**2**), pp. 189–198.

Lepech, M. D. *et al.* (2008). Design of green engineered cementitious composites for improved sustainability, *ACI Materials Journal*. American Concrete Institute, **105**(**6**), p. 567.

Li, Mo, and V. C. L. (2011). Cracking and Healing of Engineered Cementitious Composites under Chloride Environment, *ACI Materials Journal*, **108**.**3**.

Li, K., Ma, M. and Wang, X. (2011). Experimental study of water flow behaviour in narrow fractures of cementitious materials, *Cement and Concrete Composites*. Elsevier, **33**(**10**), pp. 1009–1013.

Li, V. C. *et al.* (2001). Tensile strain-hardening behavior of polyvinyl alcohol engineered cementitious composite (PVA-ECC), *ACI Materials Journal-American Concrete Institute*. Detroit, Mich.: American Concrete Institute,[c1987-, **98**(**6**), pp. 483–492.

Li, V.C., Wu, C., Wang, S., Ogawa, A. and Saito, T. (2002). Interface tailoring for strain-hardening polyvinyl alcohol-engineered cementitious composite (PVA-ECC), *Materials Journal*, **99**(**5**), pp. 463–472.

Li, V. C. (2003). On engineered cementitious composites (ECC). A review of the material and its applications, *Journal of Advanced Concrete Technology*, **1**(**3**), pp. 215–230. doi: 10.3151/jact.1.215.

Li, V. C. and Kanda, T. (1998). Engineered Cementitious Composites for structural applications, *Journal of Materials in Civil Engineering*, **10**(**2**), pp. 66–69. doi: 10.1061/(ASCE)0899-1561(1998)10:2(66).

Li, V. C., Mishra, D. K. and Wu, H.-C. (1995). Matrix design for pseudo-strain-hardening fibre reinforced cementitious composites, *Materials and Structures*. Springer, **28**(**10**), pp. 586–595.

Li, V. C. and Stang, H. (2004). Elevating FRC material ductility to infrastrucure durability, *6th RILEM Symposium on Fiber-Reinforced Concretes*, (September), pp. 171–186.

Lin, Z., Kanda, T. and Li, V. C. (1999). On interface property characterization and performance of fiber reinforced cementitious composites.

Liu, H., Zhang, Q., Li, V., Su, H. and Gu, C. (2017). Durability study on engineered cementitious composites (ECC) under sulfate and chloride environment, *Construction and Building Materials*. Elsevier, **133**, pp. 171–181.

Mander, J. B., Priestley, M. J. N. and Park, R. (1988). Theoretical stress-strain model for confined concrete, *Journal of structural engineering*. American Society of Civil Engineers, **114**(**8**), pp. 1804–1826.

Marchand, J., Odler, I. and Skalny, J. P. (2003). Axial load behavior of large-scale columns confined with fiber-reinforced polymer composites, *ACI Structural Journal*. American Concrete Institute, **102**(**2**), p. 258.

Mehta, P. K. (2004). High-performance, high-volume fly ash concrete for sustainable development, in *Proceedings of the international workshop on sustainable development and concrete technology*, pp. 3–14.

Mesbah, H.-A. and Benzaid, R. (2017). Damage-based stress-strain model of RC cylinders wrapped with CFRP composites, *Advances in Concrete Construction*, **5**(**5**), pp. 539–561. doi: 10.12989/acc.2017.5.5.539.

Mohammed, M. (2007). Performance of plain and blended cements exposed to high sulphate concentrations, *Advances in Cement Research*.

Monteny, J., Vincke, E., Beeldens, A., De Belie, N., Taerwe, L., Van Gemert, D. and Verstraete, W. (2000). Chemical , microbiological , and in situ test methods for biogenic sulfuric acid corrosion of concrete, *Cement and Concrete Research*, **30**(**4**), pp.623-634.

Nanni, A. and Bradford, N. M. (1995). FRP jacketed concrete under uniaxial compression, *Construction and Building Materials*. Elsevier, **9**(**2**), pp. 115–124.

Neville, A. (2004). The confused world of sulfate attack on concrete, *Cement and Concrete Research*, **34**(**8**), pp. 1275–1296. doi: 10.1016/j.cemconres.2004.04.004.

Ning, L. (2004). Issues Related to Safety Management, Abandonment and Construction of Dams in 21st Century in China, *China Water Resources*, **23**, pp. 27–30.

Pan, Z., Wu, C., Liu, J., Wang, W. and Liu, J. (2015). Study on mechanical properties of cost-effective polyvinyl alcohol engineered cementitious composites (PVA-ECC), *Construction and Building Materials*. Elsevier, **78**, pp. 397–404.

Pessiki, S., Harries, K.A., Kestner, J.T., Sause, R. and Ricles, J.M. (2001). Axial behavior of reinforced concrete columns confined with FRP jackets, *Journal of Composites for Construction*. American Society of Civil Engineers, **5**(**4**), pp. 237–245.

Photiou, N., Hollaway, L. C. and Chryssanthopoulos, M. K. (2004). Strengthening of an artificially degraded steel beam utilising a carbon/glass composite system, in *Advanced Polymer Composites for Structural Applications in Construction*. Elsevier, pp. 274–283.

Prasad, J., Jain, D.K. and Ahuja, A.K. (2006). Factors Influencing The Sulphate Resistance of Cement Concrete and Mortar, *Asian Journal of Civil Engineering (Building and Housing)*, **7**(**3**), pp. 259–268.

Priestley, M.N., Seible, F., Calvi, G.M. and Calvi, G.M. (1996). *Seismic design and retrofit of bridges*. John Wiley & Sons.

Qiu, J. and Yang, E.-H. (2017). Micromechanics-based investigation of fatigue deterioration of engineered cementitious composite (ECC), *Cement and Concrete Research*. Elsevier, **95**, pp. 65–74.

Reis, J. M. L. and Ferreira, A. J. M. (2006). The effects of atmospheric exposure on the fracture properties of polymer concrete, *Building and Environment*. Elsevier, **41**(**3**), pp. 262–267.

Saadatmanesh, H., Ehsani, M. R. and Li, M.-W. (1994). Strength and ductility of concrete columns externally reinforced with fiber composite straps', *Structural Journal*, **91**(**4**), pp. 434–447.

Saatcioglu, M. and Grira, M. (1999). Confinement of Reinforced Concrete Columns with Welded, (**96**), pp. 29–39.

Sadeghian, P., Seracino, R., Das, B. and Lucier, G. (2018). Influence of geometry and fiber properties on rupture strain of cylindrical FRP jackets under internal ICE pressure, *Composite Structures*. Elsevier, **192**, pp. 173–183.

Sahmaran, M., Lachemi, M., Hossain, K.M., Ranade, R. and Li, V.C. (2009). Influence of aggregate type and size on ductility and mechanical properties of engineered cementitious composites, *Materials Journal*, **106**(**3**), pp. 308–316.

Sahmaran, M., Li, M. and Li, V. C. (2007). Transport properties of engineered cementitious composites under chloride exposure, *Materials Journal*, **104**(**6**), pp. 604–611.

Şahmaran, M. and Li, V. C. (2007). De-icing salt scaling resistance of mechanically loaded engineered cementitious composites, *Cement and Concrete Research*, **37**(**7**), pp. 1035–1046. doi: 10.1016/j.cemconres.2007.04.001.

Schleiss, A. J. and Boes, R. M. (2011). Dams and Reservoirs under Changing Challenges, p. 906. doi: 10.1201/b11669.

Sephaku Ash's facility. (2013). The process of producing of fly ash in a power plant.
Sethi, S. (2014). *Environmental Degradation Study of FRP Composites Through Evaluation of Mechanical Properties*.

Shah, S. P., Fafitis, A. and Arnold, R. (1983). Cyclic loading of spirally reinforced concrete, *Journal of Structural Engineering*. American Society of Civil Engineers, **109**(**7**), pp. 1695–1710.

Soroka, I. (1979). Portland Cement Paste and Concrete, *Macmillan Press, London*, pp. 151–152.

Stang, H. a. L. V. (1999). Extrusion of ECC-material, *In Proc. of High Performance Fiber Reinforced Cement Composites 3 (HPFRCC 3)*, pp. 203–212.

Sun, Y.M., Ma, Y.Q., Liu, Y.Q., Lin, Y.Y., Wang, Z.Y., Wang, Y., Di, C.A., Xiao, K., Chen, X.M., Qiu, W.F. and Zhang, B. (2006). High-performance and stable organic thin-film transistors based on fused thiophenes, *Advanced Functional Materials*. Wiley Online Library, **16**(**3**), pp. 426–432.

Taghia, P. and Bakar, S. A. (2013). Mechanical behaviour of confined reinforced concrete-CFRP short column-based on finite element analysis, *World Applied Sciences Journal*. Citeseer, **24**(**7**), pp. 960–970.

Theodoros R. (2001). Experimental Investigation of Concrete Cylinders Confined by Carbon FRP Sheets under Monotonic and Cyclic Axial Compression Load, *Research Report 01:2, Division of Building Technology, Chalmers University of Technology*.

Thokchom, S. (2014). Fly ash geopolymer pastes in sulphuric acid, *Int. J. Eng. Innovation Res*, **3**(**6**), pp. 943–947.

TR 55. (2004). Design guidance for stengthening concrete structures using fibre composite materials, *The Concrete Society, Camberley, Surrey, England*.

Tsukamoto, M. (1990). Tightness of fiber concrete, Darmstadt concrete, *Annual Journal on Concrete and Concrete Structures*, **5**, pp. 215–225.

Turgay, T., Polat, Z., Koksal, H.O., Doran, B. and Karakoç, C. (2010). Compressive behavior of large-scale square reinforced concrete columns confined with carbon fiber reinforced polymer jackets, *Materials & Design*. Elsevier, **31**(**1**), pp. 357–364.

Victor C Li and Fischer, G. (2002). Reinforced ECC-An evolution from materials to structures.

Visitanupong (2009). Durability of Fly ash Based Geopolymer Mortar, *thesis* *approval, Graduate school, Kasetsart university, Thailand.*

Wallah, S. E. and Rangan, B. V. (2006). Low-Calcium Fly Ash-Based Geopolymer Concrete: Long-Term Properties, *Concrete*.

Wang, S. and Li, V. C. (2007). Engineered cementitious composites with high-volume fly ash, *ACI Materials journal*. American Concrete Institute, **104**(**3**), p. 233.

Wischers, G. (1978). Aufnahme und Auswirkungen von Druckbeanspruchungen auf Beton, *Betontechnische Berichte*, **19**, pp. 31–56.

Wu, C. and Li, V. C. (2017). Thermal-mechanical behaviors of CFRP-ECC hybrid under elevated temperatures, *Composites Part B: Engineering*. Elsevier, **110**, pp. 255–266.

Wu, Y.-F. and Wang, L.-M. (2009). Unified strength model for square and circular concrete columns confined by external jacket, *Journal of Structural Engineering*. American Society of Civil Engineers, **135**(**3**), pp. 253–261.

Yang, E.-H. *et al.* (2009). Rheological control in production of engineered cementitious composites, *Materials Journal*, **106**(**4**), pp. 357–366.

Yao, J., Teng, J. G. and Chen, J. F. (2005). Experimental study on FRP-to-concrete bonded joints, *Composites Part B: Engineering*. Elsevier, **36**(**2**), pp. 99–113.

Zaman, A., Gutub, S. A. and Wafa, M. A. (2013). A review on FRP composites applications and durability concerns in the construction sector, *Journal of Reinforced Plastics and Composites*. SAGE Publications Sage UK: London, England, **32**(**24**), pp. 1966–1988.

Zhang, Z. and Zhang, Q. (2017). Self-healing ability of Engineered Cementitious Composites (ECC) under different exposure environments, *Construction and Building Materials*. Elsevier, **156**, pp. 142–151.

APPENDIX-A

Figure A1 Materials used in the production of ECC specimens

Figure A2 ECC mix vibrated to get proper compacting specimens

Figure A3 ECC fresh specimens covered by plastic sheet

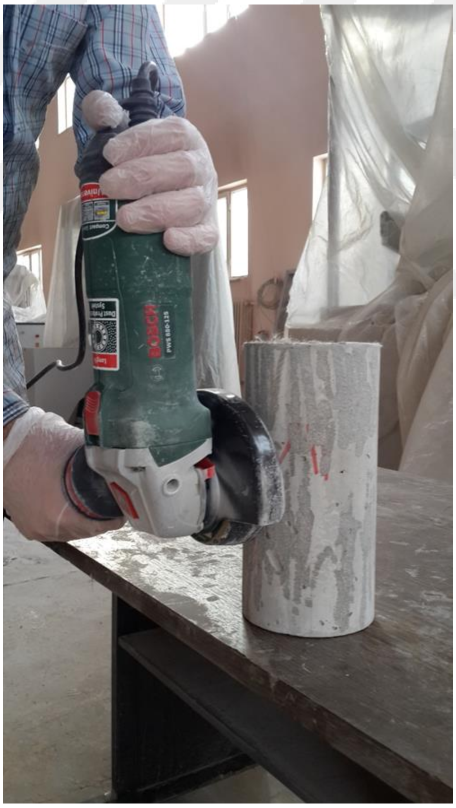

Figure A4 Preparing the surface of ECC specimens before wrapped by FRP fabrics

Figure A5 ECC surface prepared and non-prepared specimens

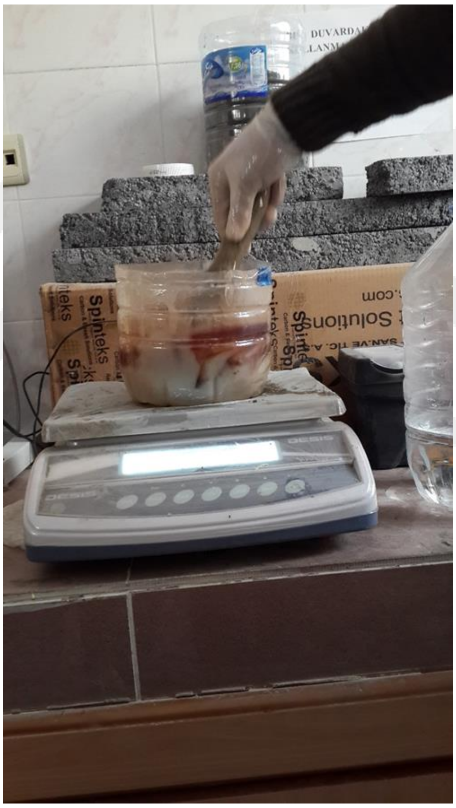

Figure A6 Preparing the adhesive epoxy

Figure A7 Coating the surface of ECC specimen by epoxy

Figure A8 Preparing the FRP sheet

Figure A9 Initial step of application the FRP fabrics

Figure A10 Continue the application of FRP fabrics

Figure A11 ECC specimens wrapped by FRP fabrics

APPENDIX-B

Figure B1 ECC specimens exposed to sulphuric acid environment

Figure B2 ECC specimens exposed to sulfate environment

Figure B3 ECC specimens exposed to seawater environment

Figure B4 ECC specimens wrapped by CFRP exposed to chemical environment

Figure B5 ECC specimens wrapped by BFRP exposed to chemical environment

APPENDIX-C

Figure C1 Preparing the ECC specimens for mechanical test

Figure C2 ECC wrapped specimens under axial compression test

Figure C3 Failure mode of unwrapped ECC specimens exposed to ambient environment

Figure C4 Failure mode of unwrapped ECC specimens exposed to acid environment

Figure C5 Failure mode of unwrapped ECC specimens exposed to sulfate environment

Figure C6 Failure mode of unwrapped ECC specimens exposed to seawater environment

Figure C7 Failure mode of ECC specimens wrapped by CFRP exposed to ambient environment

Figure C8 Failure mode of ECC specimens wrapped by CFRP exposed to sulfuric acid environment

Figure C9 Failure mode of ECC specimens wrapped by CFRP exposed to sulfate environment

Figure C10 Failure mode of ECC specimens wrapped by CFRP exposed to seawater environment

Figure C11 Failure mode of ECC specimens wrapped by BFRP exposed to ambient environment

Figure C12 Failure mode of ECC specimens wrapped by BFRP exposed to sulfuric acid environment

Figure C13 Failure mode of ECC specimens wrapped by BFRP exposed to sulfate environment

Figure C14 Failure mode of ECC specimens wrapped by BFRP exposed to seawater environment

APPENDIX-D

Figure D1 Preparing SEM samples by cutting wrapped and unwrapped ECC specimens

Figure D2 LCFA-ECC specimens exposed to ambient and acid environment

Figure D3 LCFA-ECC specimens exposed to ambient and sulfate environment

Figure D4 LCFA-ECC specimens exposed to ambient and seawater environment

Figure D5 HCFA-ECC specimens exposed to ambient and acid environment

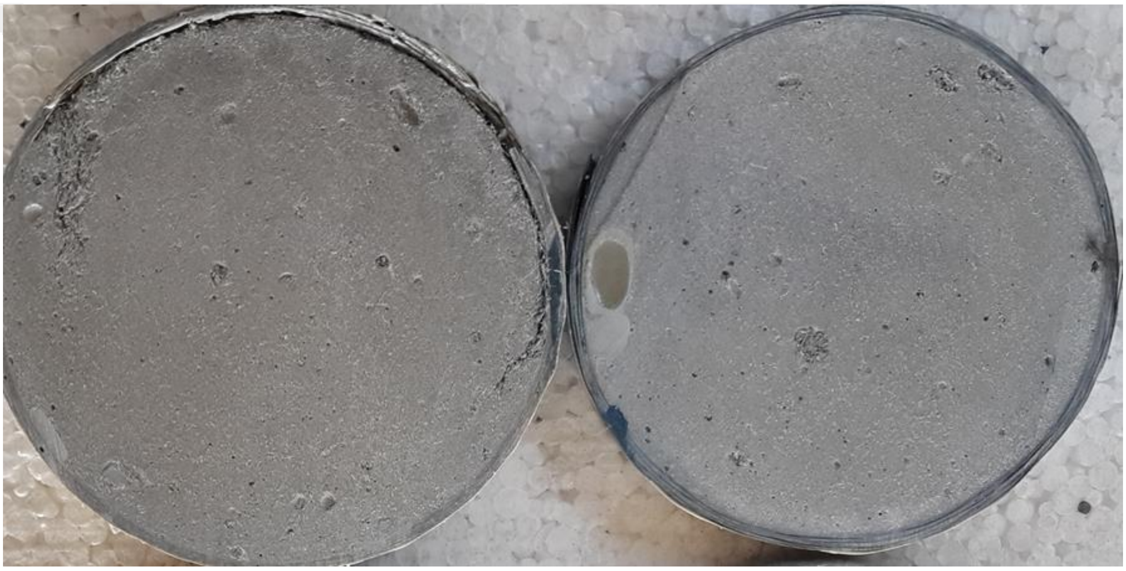

Figure D6 FRP wrapped ECC specimens exposed to acid environment

Figure D7 FRP wrapped ECC specimens exposed to sulfate environment

Figure D8 FRP wrapped ECC specimens exposed to seawater environment

PERSONAL INFORMATION

Name and Surname: Alaa A.

Mohammedameen

Nationality: Iraqi

Birth place and date: Iraq-Mosul/09-Auegest-1978

Marital status: married

Phone number: +90 538 068 7207

+964 750 4344090

Email: alaa.mohammedameen@dpu.edu.krd

alaa.mohammedameen@gmail.com

alaa.mohammedameen@yahoo.com

EDUCATION

Ph.D. Candidate /College of Eng./ Civil Engineering/ College of engineering

Master degree /College of Eng./ Civil Engineering/ College of Engineering

Bachelor's degree/ College of Eng./ Civil Eng./ College of Engineering

Work experience

	Place	**Enrollment**
2003-Present	Ministry of Higher Education	Lecturer

PUBLICATIONS

Published SCI& SCI-Expanded Articles:

1. Güneyisi, E., Gesoğlu, M., **Mohamadameen, A.**, Alzeebaree, R., Algın, Z. and Mermerdaş, K., 2014. Enhancement of shrinkage behavior of lightweight aggregate concretes by shrinkage reducing admixture and fiber reinforcement. Construction and Building Materials, 54, pp.91-98.
2. Gülşan, M.E., **Mohammedameen, A.**, Şahmaran, M., Niş, A., Alzeebaree, R. and Abdulkadir, Ç., 2018. Effects of sulphuric acid on mechanical and durability properties of ECC confined by FRP fabrics. Advances in Concrete Construction (**Accepted**).
3. **Mohammedameen**, A., Gülşan, M.E., Alzeebaree, R. and Abdulkadir, Ç., 2018. "Mechanical and Durability performance of FRP Confined and Unconfined Strain Hardening Cementitious Composite exposed to Sulfate Attack" Construction and Building Materials, (**Underreviw**).
4. **Mohammedameen**, A., Abdulkadir, Ç., Alzeebaree, R. and Gülşan, M.E., 2018. "Mechanical properties and Durability of Unconfined and Confined Engineered Cementitious Composite Exposed to Seawater" Composite Materials, (**Underreviw**).
5. Alzeebaree, R., Gülşan, M.E., Niş, A., **Mohammedameen, A.** and Abdulkadir, Ç., 2018. Performance of FRP Confined and Unconfined Geopolymer Concrete exposed to Sulfate Attacks. Steel and Composite Structures (**Accepted**)

FOREIGN LANGUAGE

Turkish

English

Kurdish

Arabic